A first assessment of nitrogen sources and biogeochemical processing in the speleothem record

Scott Oats Ambler

BSc (Hons)

January 2020

This dissertation is submitted in partial fulfilment of the requirements for the degree of Masters by Research.

Abstract

The most common groundwater contaminant is nitrogen, which presents a threat both to human health and the wider environment. Karstic aquifers are particularly vulnerable to contamination. As up to 25% of the world's population is reliant on karst groundwater as their source of potable drinking water, quantifying this nitrogen contamination is important for human health. Use of nitrate $\delta^{15}N$ and $\delta^{18}O$ to determine sources of nitrogen contamination is well established in the literature. 'Legacy N' – the poorly understood storage of nitrogen in the vadose zone - has been established through extensive groundwater modelling. However, there are very few reliable historic archives of nitrogen groundwater contamination that would assist in quantifying this nitrogen storage capacity. This project proposes the use of speleothem archives of nitrogen to create an historic record of nitrogen groundwater contamination.

Contemporary cave monitoring of Cueva-Cubío del Llanío in the Cantabria region of Northern Spain was undertaken to determine cave dynamics has classified the basic karst hydrology, cave ventilation and cave water chemistry that influence speleothem growth and the proxies preserved within the speleothem calcite. Nitrogen concentrations and isotopes in the major components of the nitrogen biogeochemical cycle were used to quantify the cycling of nitrogen through overlying environment and the impact on cave nitrogen. This included work on speleothem material.

Cueva-Cubío del Llanío was found to have a complex ventilation regime, with side chambers removed from the main density driven airflow. Drips were found to be a combination of matrix and fracture-fed flow, with drips in shallower chambers drying up during summer months. Seasonality was present in nitrogen concentrations within the cave waters, though was absent in isotope values, suggesting an as-yet-unidentified non-fractionating cause. A promising record of nitrogen has been preserved in the Cueva-Cubío del Llanío speleothem archive. The first successful extraction of speleothem nitrate isotopes was completed, with multiple speleothems from around the world all recording differing nitrate isotope compositions, and interpreted as reflection of nitrogen dynamics in the overlying environment. The record of nitrogen dynamics within speleothems establishes the potential for an historic record of groundwater nitrogen.

Declaration

I hereby declare that the work presented in this thesis is my own, except where acknowledged, and has not been submitted for the award of a higher degree or other qualification at this or any other institution.

Signed: Scott Oats Ambler

Date: 19/10/2020

Name: Scott Oats Ambler

Acknowledgements

To begin, I want to thank my supervisor Peter Wynn for his tireless support and advice throughout this project. His help has been invaluable, as has his patience with me over what has been a difficult year. Thank you, Peter, for answering all my questions, no matter how silly they seemed. Thank you also to Phil Barker, for his supervisory support. The support given by you both throughout my project has been instrumental in its completion.

Thank you to Imke Grefe for assisting me in the microbiology portion of the project – without her tireless work very few of my samples would have made it through to isotope analysis! Your instruction in lab work has made me more confident in my lab ability, considering I came into this project with very little laboratory experience.

Thank you to NERC Isotope Geoscience Laboratory, especially Andy Stott, for the many, many runs of samples that your funding and knowledge helped me analyse.

A huge thank you to the Matienzo Caving Community for their support, interest and fieldwork assistance. To Andy Quin, for letting me sleep in your basement and for the wonderful post-caving sandwiches. To Juan Corrin, for the infectious enthusiasm for my project and for the wonderful (and unflattering) photos of my field expedition. To Pete Smith, for collecting all that rainwater!

Thank you to my indomitable group of friends. To Beane – thank you for always being there for me and for your willingness to deal with my love of bad cinema and my general eccentricity. To Ella – for the relative stability in my (admittedly) kooky life. To Mioni – for being a bouncy and wholesome companion throughout the Masters experience! To Nick – for eating my cooking without complaint and listening to me complain.

Thank you to my parents for their support and patience through this journey. For always keeping their door open whenever I needed a break and for the love (and food!) they've provided me with along the way.

A massive thank you to the Liberation Forums on campus, especially the LGBTQ+ Forum. Monday evenings would be dull without you all – who else would be willing to listen to my nonsense?

Thank you to my crotchet crew – to Melanie at Ethel & Em for advising me with her extensive yarn-based knowledge, to Kate and Adrian for the cat photos.

To my family and friends – thank you for the endless support.

Table of Contents

Lists of Figures

List of Tables

1. Introduction

Groundwater is a vulnerable but essential resource for potable water, with 2.5 billion people relying solely on groundwater for their daily needs (WWAP, 2015). Karst groundwater is the source of potable drinking water for up to 25% of the world's population (Huebsch *et al*, 2013). Anthropogenic activity can lead to the contamination of groundwater resources, making them dangerous for human consumption. The most common groundwater contaminant is N, specifically NO_3^- (Exner *et al.*, 2014).

N groundwater contamination is a threat to both human health and the wider environment – the IARC (2010) classified nitrate and nitrite as Class 2A probable human carcinogens and consumption of water with N concentrations above WHO guidelines (nitrate concentrations > 3 mg/l) has been shown to lead to methemoglobinemia (Shukla and Saxena, 2008). Lower N concentrations in groundwater than the established guidelines are a risk to the environment with eutrophication of surface waters fed by contaminated groundwaters common.

Karst aquifers are particularly vulnerable to contamination – conduits, stream sinks and fracture flow allow for surface water and contamination to flow, relatively unimpeded by soil and overlying rock, into the groundwater (Huebsch *et al.*, 2013). Furthering karst aquifers' vulnerability to contamination it has been noted that karstic groundwaters have limited or no capacity for denitrification owing to the oxidising conditions within karst groundwater, thus making it difficult to remedy past contamination (Liu *et al*., 2006). There are multiple models that quantify a given catchment's N stores and transformations, with many noting the existence of a 'legacy N' - the long term and poorly understood store of N in the vadose zone (Ascott *et al*., 2017). Models such as Meter and Basu (2015), Meter *et al*. (2016) and Ascott *et al*. (2017) have begun to quantify legacy N but long-term historical N records that could be used to further validate these models are rare.

To understand the dynamics of N contamination it is important to understand the biogeochemical cycle that N undergoes. There are various stores, processes and transformations within the cycle which are important to consider when attempting to understand where N contamination is stored and in what form. A well-established method of tracing contaminant sources and transformations is using $\delta^{15}N$ values. Here the ratio between ^{15}N and ^{14}N is compared against a reference standard. As many organisms, chemical reactions and state changes preferentially use the lighter isotope over the heavier one, the isotopic composition of a product will be lighter than that of the reactant (Kendall, 1998). Thus, it can be a powerful tool in tracing N through the environment.

A potential record of N could be found in calcite speleothems. Speleothems have been used as archives of stable isotopes, trace elements and colloids and thus have been used extensively for their capacity to capture multiple paleoenvironmental proxies at once (Fairchild and Treble, 2009). If a record of N concentration and N isotopes is preserved within speleothem calcite, this would provide a valuable historical archive of changing groundwater chemistry over time.

To investigate the ability of speleothems to conserve information on N concentrations and isotopes, a cave site in northern Spain located under an intensively managed agricultural catchment will be monitored to provide background information on cave microclimate and thus on calcite deposition dynamics within the cave. A spatial and temporal survey of cave

drip waters will be undertaken to analyse the nature of N transfer through the karst system. Finally, speleothem calcite will be analysed for N concentration and isotope composition to investigate its suitability as an archive of groundwater N.

This dissertation will present a cave monitoring study and subsequent N concentration and isotope analysis from Cueva-Cubío del Llanío, Northern Spain. The primary aims are as follows:

- In the context of the agricultural activity over Cueva-Cubío del Llanío, use N isotopes and major ion chemistry to trace N sources and cycling into the speleothem record.
- To establish the cave microclimatic processes as a fundamental background to understanding the controls on cave system hydrology and speleothem growth.
- To determine the role of biogeochemistry and karst hydrology in controlling the delivery of N to cave drip waters.
- To pioneer the extraction of N isotopes from contemporary speleothem calcite in order to establish use of N isotopes in a paleoenvironmental context.

A cave monitoring programme has been undertaken within Cueva-Cubío del Llanío to determine the dynamics of the cave site and thus give insight into any processes that may modify the N signal. The results and discussion of the cave monitoring programme are presented in chapter 3.

Samples were taken from all key components of the N biogeochemical cycle and analysed for N content to characterise the biogeochemical cycling present at Cueva-Cubío del Llanío. The impact of biogeochemical cycling on cave N is presented in chapter 5.

The samples taken from the key components of the N biogeochemical cycle were also analysed for stable N and nitrate isotopes to identify sources and fractionations of N present at Cueva-Cubío del Llanío. The isotopic compositions of the various components and discussion of this are presented in chapter 6.

2. Literature Review

2.1. N Biogeochemistry

2.1.1. The N Cycle

The N cycle (Figure 2.1) is intertwined with many important biological processes (Jaffe, 1992), making it a complex but important biogeochemical cycle that can assist in understanding much of the biological activity on Earth. N, alongside being an important chemical in the growth of plants and in many microbiological processes, is also essential for understanding many of the anthropogenic impacts on the environment, whether this be in the atmosphere as photochemical smog or acid rain, or in the hydrosphere as the nitrate pollution of groundwater or eutrophication of waterways.

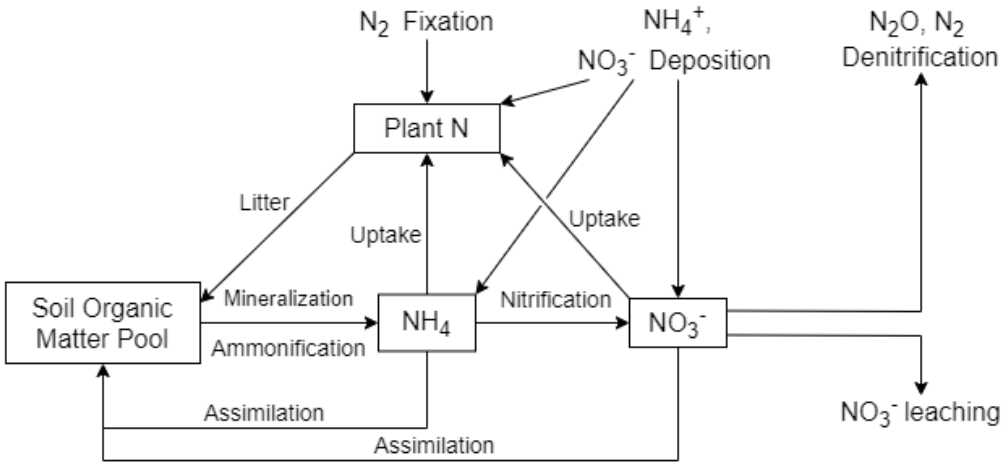

Figure 2.1. Diagram of N biogeochemical cycle taken from Kendall (1998).

The atmosphere is predominantly composed of N (Jaffe, 1992), thus to discuss the terrestrial N cycle the first step to understand is that of N_2 fixation, in which atmospheric N_2 is converted into organic N (Equation 2.1). The process of fixation is usually performed by symbiotic bacteria found in the roots of leguminous plants (Kendall, 1998) and requires an anaerobic environment as well as a large amount of input energy (Jaffe, 1992). Biotic N fixation is considered the primary source of reactive N on the continents, with Galloway *et al.* (1995) estimating that it provides about 90-130 Tg N yr^{-1}. Anthropogenic N fixation is also a significant source of terrestrial reactive N, with Galloway *et al.* (1995) estimating that a further 140 Tg N yr^{-1} is produced via anthropogenic fixation.

Anthropogenic fixation occurs in three major areas: energy production, in which NO_x is unintentionally produced via incomplete combustion (N_2 -> reactive NO); fertiliser production via the Haber-Bosch process (N_2 -> NH_3); and the cultivation of crops, specifically N fixing legume crops such as soy-beans, groundnuts, pulses and forage (Galloway *et al.*, 1995). All of these anthropogenic activities are increasing rapidly – fossil fuel combustion has increased by 1.5% yr^{-1} in the last decade (Le Quéré *et al.*, 2018) and the world fertiliser supply was predicted to have risen by 13.5% from 2013 to 2018 by the Food and Agriculture Organisation of the United Nations (2015) with N fertiliser providing more N input to agriculture than biological fixation (Connor, 2018). It is estimated that anthropogenic activities are responsible for half of all global N fixation annually, with the majority of this being terrestrial fixation (Fowler *et al.*, 2013).

Equation 2.1. N fixation

$$N_2 \rightarrow \text{organic N}$$

Once atmospheric N has been fixed by plants or microbes, it will eventually become part of the soil organic matter pool. Here, the next step of the N cycle will occur – ammonification. As can be seen in Equation 2.2, ammonification converts the N contained within organic matter to ammonium. Ammonification usually takes the form of the decay of organic matter, usually through microbial and enzymatic activities (Cai et al., 2017). As most plants

derive N from soil ammonium (Clark and Fritz, 1997), two popular forms of fertiliser add to soil NH_4^+ in either the form of anhydrous ammonia or urea fertilisers. In the United States, one of the leading producers of fixed N ammonia in the world, 88% of produced ammonia was used for fertiliser in 2014 (USGS, 2016), highlighting an anthropogenic input to reserves of soil NH_4^+ beyond the process of ammonification, which in turn affects the rate-limiting steps involved in the transformation of soil organic matter pool N to NH_4^+ and beyond.

Equation 2.2. Ammonification

$$\text{organic N} \rightarrow \text{NH}_4^+$$

If soil NH_4^+ does not undergo uptake by plants, the next step of the N cycle, nitrification, may take place. Nitrification is a two step process in which ammonium is first oxidised into nitrite, then further oxidised to nitrate (Equation 2.3.). As ammonia can bind to soil particles (sorption), a high nitrification rate can lead to increased loss of soil N via leaching or denitrification and as such can be seen as undesirable in agricultural settings, where inhibitors of nitrification are often used to reduce the losses of fertiliser N (Prosser, 2005).

Equation 2.3. Nitrification

$$\text{NH}_4^+ \rightarrow \text{NO}_2^- \rightarrow \text{NO}_3^-$$

It is occasionally the case that ammonification and nitrification are combined into a single step, referred to as mineralisation, which is the complete transferral of organic material N to N compounds.

Once organic N has been biologically transformed to nitrate, two further transformations may take place: dissimilatory nitrate reduction to ammonium (DNRA) or denitrification. DNRA can be seen as a process that conserves bioavailable N within the soil system as nitrate is returned to ammonia (Equation 2.4). However, denitrification is the principle process in soils that returns fixed N to the atmospheric reservoir, thus completing the N cycle (Equation 2.5). The control between DNRA and denitrification is primarily the availability of organic matter (specifically the availability of carbon) and the availability of NO_3^- (van de Berg *et al.*, 2017). In carbon rich systems where nitrate availability is limiting DNRA is the dominant process, whereas in carbon poor systems with excess nitrate, denitrification is the dominant process (van de Berg *et al.*, 2017).

Equation 2.4. Dissimilatory Nitrate Reduction to Ammonium (DNRA)

$$\text{NO}_3^- \rightarrow \text{NO}_2^- \rightarrow \text{NH}_4^+$$

Equation 2.5. Denitrification

$$\text{NO}_3^- \rightarrow \text{gaseous N species}$$

Denitrification is an important process when considering the impact of agriculture on global climate change, as nitrous oxide (a common gaseous N species produced by the process) is a potent greenhouse gas with a global-warming potential 320 times stronger than that of CO_2 – as the use of anthropomorphically fixed N for fertiliser continues to increase, it is understood by Martens (2005) that the production of nitrous oxide via denitrification will also increase.

Annamox should also be considered when discussing groundwater N (Equation 2.6.). As the anaerobic oxidation of NH_4^+ to N_2 (Nikolenko *et al*., 2018), it is theorised to play an

important role in the fate of N in groundwater systems (Robertson *et al*., 2012). While the role of anammox in marine systems is of high relevance on a global scale (Kumar *et al*., 2017), Nikolenko *et al.* (2018) report that anammox is generally only found in polluted groundwater systems contexts - it has been reported that up to 90% of N loss in such systems can be attributed to anammox (Kumar *et al.*, 2017). Anammox processes have been found to be favoured over denitrification under anoxic low organic carbon conditions, especially pristine limestone groundwater aquifers as detailed by Kumar *et al*. (2017), though at this time further literature detailing anammox processes in non-contaminated groundwater systems is sparse.

Equation 2.6. Anammox

$$NH_4^+ + NO_2^- \rightarrow N_2 + 2H_2O$$

2.1.2. N Isotopes

N isotopic composition is expressed as a ratio between ^{15}N and ^{14}N compared against a reference standard. The reference standard for N isotopes is N_{AIR}, or atmospheric N_2, which is considered globally uniform and has a ^{15}N abundance of 0.3663% (Heaton, 1986). Equation 2.7. shows the accepted notation for $\delta^{15}N$ – this is the standard notation for N isotopic composition.

Equation 2.7. the notation for the isotopic expression of $\delta^{15}N$, where R = atomic $^{15}N/^{14}N$ ratio (taken from Heaton, 1986).

$$\delta^{15}N(‰) = \left(\frac{R_{sample}}{R_{standard}} - 1\right) \times 10^3$$

When considering the differences in isotopic composition between product and reactant, the isotopic separation factor (ε) is shown in Equation 2.8. Sometimes ε is also referred to as the fractionation factor.

Equation 2.8. isotopic separation factor

$$\varepsilon_{product-reactant} \approx \delta^{15}N_{product} - \delta^{15}N_{reactant}$$

Organisms and many chemical reactions/state changes preferentially use the lighter isotope over the heavier isotope (i.e. ^{14}N is preferentially used over ^{15}N), thus the isotopic composition of a product will be isotopically lighter than that of the reactant (Kendall, 1998). Isotopic compositions in the environment are reliant on the fractionation factor and the size of the remaining reactant reservoir (Kendall, 1998).

Isotopic fractionation processes can be divided into two types: equilibrium and kinetic. In equilibrium fractionation, there is no net reaction in either direction but isotope exchange occurs. Isotopic equilibrium can be attained when the isotopic ratios no longer change with time (Tiwari *et al.*, 2015). Between two substances, A and B, an isotope fractionation factor can be expressed as shown in Equation 2.9 (Kendall and Caldwell, 1998). Kiwari *et al*. (2015) define the fractionation factor (α) as the ratio of isotopes in one phase to a coexisting phase. α tends to be heavily temperature dependent, with both magnitude and sign being controlled by temperature primarily amongst other factors (Kendall and Caldwell, 1998).

Equation 2.9: isotope fractionation factor, where R = the ratio of heavy isotope to light isotope in compounds A and B

$$\alpha_{A-B} = R_A/R_B$$

In kinetic fractionation, processes are incomplete and unidirectional, with no isotopic equilibrium attained (Kiwari *et al.*, 2015). Kendall and Caldwell (1998) state that bonds between lighter isotopes are more readily broken than those between heavier isotopes, thus lighter isotopes react faster and are more concentrated in the products, with the residual reactants becoming enriched in the heavier isotopes. Many biological processes are good examples of kinetic isotope fractionations. In such processes, magnitude of fractionation is often dependent on the rate-limiting step, as slower reaction steps show greater fractionation in biological processes as the organism has the time to be more selective in which bonds to break (Kendall and Caldwell, 1998).

A further isotopic fractionation can be defined - Rayleigh isotopic fractionation. An exponential relation describing the portioning of isotopes between two reservoirs as one decreases in size, Rayleigh isotopic fractionation can be expressed as Equation 2.10.

Equation 2.10: an example of a Rayleigh equation, where R_0 = original isotopic ratio, R = new isotopic ratio, α = fractionation factor, and f = ratio of present amount of reactant to initial total amount (taken from Kiwari et al., 2015)

$$R = R_0(f)^{\alpha-1}$$

2.1.3. N Sources and Associated Isotopic Signatures

When considering the sources of N in a given system, it can be helpful to identify the isotope composition of various sources.

A major source of N in terrestrial systems is fertiliser. Fertilisers can be split into inorganic/synthesised and organic varieties, with each having a particular isotope composition.

Inorganic fertiliser; such as urea, NH_4^+ and NO_3^-; can be easily distinguished from organic fertiliser due to the production method used to produce them. Most synthetic fertilisers are produced via the fixation of atmospheric N_2, which has $\delta^{15}N$ 0 ± 3‰ (Nikolenko *et al.,* 2018). The fixation process results in very little fractionation between atmospheric N_2 and the resulting product, thus the range of $\delta^{15}N$ in synthetic fertilisers remains low – Nikolenko *et al*. (2018) reports values such as -4 to +4‰, -8 to +7‰ and -6 to +6‰.

In contrast, organic fertiliser exhibits a heavier isotope composition: $\delta^{15}N$ +6 to +30‰ (Nikolenko *et al.,* 2018) or +10 to +20‰ (Heaton, 1986) are reported ranges in the literature. Nikolenko *et al*. (2018) note that organic fertilisers also exhibit a greater range of $\delta^{15}N$ compositions than inorganic fertilisers. As noted by Minagawa and Wada (1984), $\delta^{15}N$ becomes enriched as one moves up the trophic levels, thus manure and other excreta tend to display a level of isotopic enrichment. This concept also holds true for household sewage (Nikolenko *et al*., 2018), thus it can be difficult to distinguish whether an enriched $\delta^{15}N$ value in groundwater originates from the application of organic fertiliser or from a septic tank leak.

Soil organic N has an isotopic composition indicative of the mix of inputs in given system - Kendall (1998) reports it to be $\delta^{15}N$ 0 to +10 ‰. Thus, generally, when listing $\delta^{15}N$ values from highest to lowest a general order can be established: organic fertiliser and household waste are the most isotopically enriched, followed by NO_3^- from soil organic matter and then finally inorganic fertiliser. However, it can be noted that there is some overlap between certain sources – for instance it is impossible to distinguish between different forms of inorganic fertiliser such as NO_3^- and NH_4^+, which have the same range of $\delta^{15}N$ values (-5 to

+5‰, according to Kendall, 1998). Thus, it is standard to observe both $\delta^{15}N$ and $\delta^{18}O$ when looking at NO_3^- sources.

Figure 2.2 demonstrates the value of conducting dual stable isotope analysis when attempting to determine the source of nitrates found in groundwater. $\delta^{15}N$ values overlap for nitrate in precipitation, synthetic nitrate fertiliser, nitrate from reduced N fertiliser and nitrate from soil organic N very clearly but are separated once plotted against $\delta^{18}O$.

Biologically formed nitrate gains two oxygen atoms from H_2O rather than O_2, thus is more depleted in ^{18}O, whereas inorganically formed nitrate gains two oxygen atoms from atmospheric O_2, thus will demonstrate a $\delta^{18}O$ signature similar to that of atmospheric $\delta^{18}O$ (Clarke and Fritz, 1997). Indeed, the $\delta^{18}O\text{-}NO_3^-$ of synthetic fertiliser was found to be +18 to +22 ‰ by Kendall (1998), which is close to the atmospheric $\delta^{18}O$ value of +23‰.

It is also important to consider the contribution of NO_3^- of precipitation, which provides much of the water to terrestrial systems. Whilst it is difficult to give a single value or range of values for precipitation, as shifts as large as 20‰ in $\delta^{15}N$ between rainfall events have been observed (Kendall, 1998), there is a general seasonal trend in $\delta^{15}N$ values. Kendall (1998) notes that the $\delta^{15}N$ of precipitation in the spring/summer is more depleted than that in the winter as there is a release of depleted NO_x from soils during the warm and moist growing season and increased fossil fuel use in the winter. It is important to note, however, that there are large fractionations between NO_x and NO_3^-.

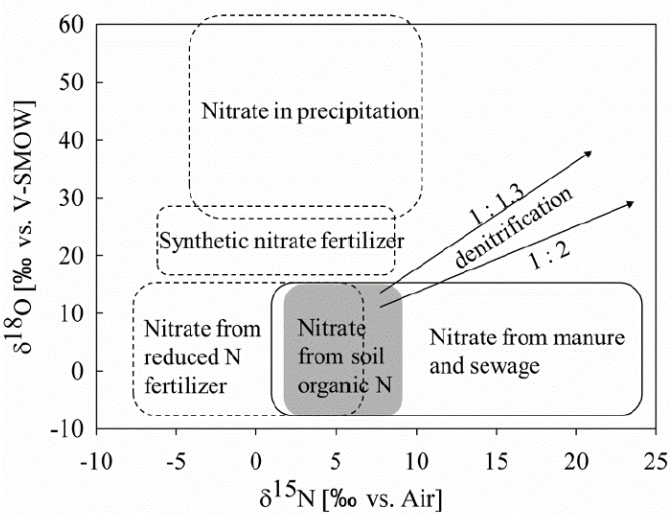

Figure 2.1: distribution of $\delta^{15}N\text{-}NO_3$ and $\delta^{18}O\text{-}NO_3$ from various potential nitrate sources, taken from Zhang et al. (2019).

2.1.4. N Isotope Fractionations

Both $\delta^{15}N\text{-}NO_3^-$ and $\delta^{15}N\text{-}NH_4^+$ have various sources, processes and factors that can influence the measured value. Figures 2.3 and 2.4 summarise these processes and factors and give examples of the enrichment and depletion from each process and source, thus giving a full understanding of what any $\delta^{15}N$ value could be indicative of.

2.1.4.1. $\delta^{15}N\text{-}NO_3$- Fractionating Processes and Factors

There are two main fractionating processes for $\delta^{15}N\text{-}NO_3^-$: nitrification and denitrification. Nitrification has been found to deplete $\delta^{15}N$ by 5 - 35‰ (Figure 2.3) with a preferential incorporation of ^{14}N into NO_3^-, whilst denitrification has been found to enrich $\delta^{15}N$ by 5-40‰

(Figure 2.3). Both are potentially strongly fractionating processes, though it is important to consider how various factors can affect the rate and magnitude of these processes.

The first factor to consider is the size of the substrate pool – in areas where NH_4^+ fertiliser is applied the substrate pool for nitrification will be large for example. In N-limited systems, the extent of fractionations will be limited, and vice versa (Kendall, 1998). For denitrification it is important to consider the concentrations of NO_3^- - under systems where NO_3^- is excessive it has been found that the denitrification process can be terminated at the formation of N_2O, thus the efficiency of the denitrification process reduced (Rivett *et al.*, 2008). It is also important to note than in low NO_3^- concentrations (when carbon concentrations are high) DNRA can be the main process for the depletion of NO_3^- in a system.

The next is the concentration of dissolved oxygen (DO), which can have a major influence on the prevalence of nitrification versus denitrification reactions. A general trend noted by Nikolenko *et al*. (2018) is that higher DO concentrations accompany increased nitrification and so lower $\delta^{15}N$ values, whereas lower DO concentrations accompany increased denitrification and so higher $\delta^{15}N$ values. Despite this trend, there are no defined values or ranges in which it can be determined if nitrification or denitrification is the more influential – Rivett *et al*. (2008) state that denitrification cannot occur when DO concentrations are over 2 mg/L but acknowledge that this is only an estimate and Stenstrom and Poduska (1980) give a range of between 0.3 and 4 mg/L for optimum nitrification rates to occur but conclude that the highest nitrification rates tend to occur when DO concentration is about 4 mg/L.

As both nitrification and denitrification are biological processes, pH and temperature are both potential controls on the degree of fractionation from either process. Whilst nitrification has a known optimum pH range of 6.5 to 8 (Nikolenko *et al.*, 2018), the optimum pH range for denitrification is site-specific due to localised adaptations of the microbiological ecosystems involved (Rivett *et al*., 2008). Water temperature is a control on microbiological activity and on DO concentrations in groundwater, thus there is potential for a seasonal change in $\delta^{15}N\text{-}NO_3^-$ values but Nikolenko *et al*. (2018) state that no conclusive evidence of a seasonal change has yet been found. Rivett *et al.* (2008) point out that the groundwater environment has relatively stable temperatures and that any true seasonal changes influenced by temperature may be masked by the seasonal flux of organic carbon, which has an impact on denitrification rates.

Land use can have a large impact on $\delta^{15}N\text{-}NO_3^-$, as agricultural practices or adjacent land use can have a major impact. Nikolenko *et al.* (2018) highlight the impact of leaving crop residue on fields over the winter months and the potential for this practice to affect the seasonality of $\delta^{15}N\text{-}NO_3^-$ values. Sebilo *et al.* (2013) identified that prior land use can also impact on $\delta^{15}N\text{-}NO_3^-$ values decades into the future, due to the incorporation of N fertilisers into the soil organic matter pool, so it is important to consider past land use as well as present.

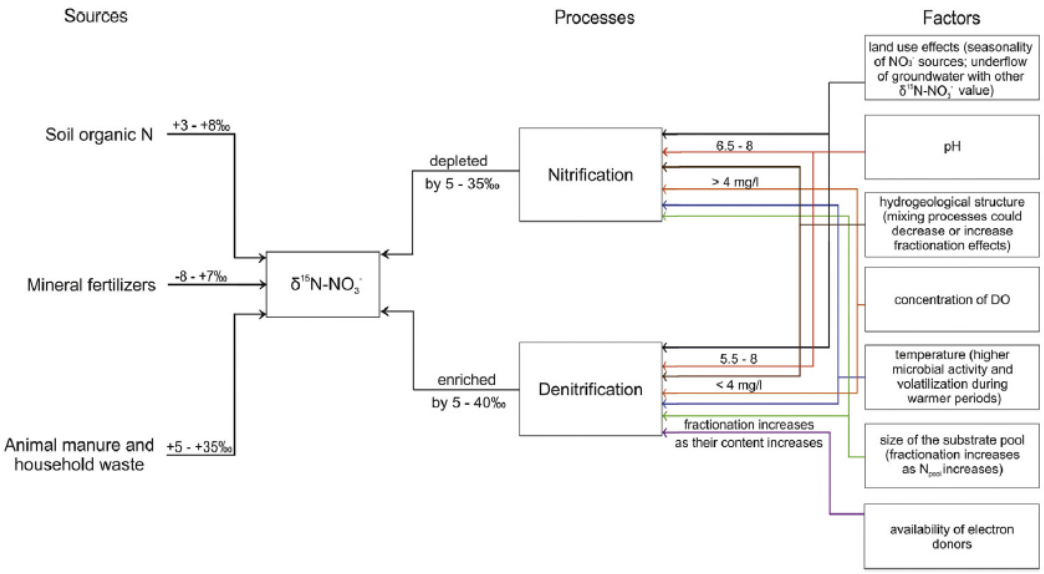

Figure 2.2. A summary of Influences on $\delta^{15}N\text{-}NO_3^-$ values. Arrow colours on arrows between factors and processes represent resulting fractionation effects: purple = availability of electron donors, green = size of substrate pool, blue = temperature, orange = concentration of DO, brown = hydrogeological structure, red = pH, and black = land use. Taken from Nikolenko et al. (2018).

2.1.4.2. 2$\delta^{15}N\text{-}NH_4^+$ Fractionating Processes and Factors

There are many more fractionating processes for $\delta^{15}N\text{-}NH_4^+$ than $\delta^{15}N\text{-}NO_3^-$, as there are more processes that involve ammonium than there are that involve nitrate, though the magnitude of fractionation for some of these processes is not as significant, though all are still important to note.

Sorption, in which NH_4^+ particles are drawn to and 'stick to' the surfaces of charged clay particles or other minerals, can deplete the $\delta^{15}N\text{-}NH_4^+$ of the remaining ammonia in solution by between 1-8‰ (Nikolenko *et al.*, 2018), though Kendall (1998) theorises that this fractionation factor could be dependent on depth in soil, as clay composition and water chemistry change with depth. Nevertheless, there is an opportunity for sorption processes to enrich or deplete ^{15}N in groundwater.

Volatilisation has the potential to be a highly fractionating process that can enrich remaining NH_4^+ in the system by approximately 25‰ (Bedard-Haughn *et al.*, 2003). Volatilisation provides good examples of both equilibrium and kinetic fractionation. Equilibrium fractionation is displayed between NH_4^+ and NH_3 in solution and between aqueous and gaseous NH_3. Kinetic fractionation is displayed in the diffusive loss of isotopically lighter NH_3. It is theorised, however, that the extent of fractionation by volatilisation could be dependent on pH and temperature (Nikolenko *et al.*, 2018). Nikolenko *et al.* (2018) note that volatilisation intensifies under alkaline soil pH, so soils with high carbonate content demonstrate higher rates of volatilisation and greater temperatures increase the rate of volatilisation also. Heaton (1986) gives the example of the impact of volatilisation on a field treated with organic manure, where the urea within the manure is hydrolysed and so increases soil pH, thus increasing the rate of volatilisation and enriching NH_4^+ in the soil as ^{14}N is preferentially lost via volatilisation. Volatilisation is also affected by localised factors such as wind-speed and moisture, making it difficult to give precise values of enrichment due to volatilisation in any given study area (Heaton, 1986).

As nitrification involves both NO_3^- and NH_4^+, it is important to note how this process fractionates NH_4^+ also. Increased nitrification will increase $\delta^{15}N\text{-}NH_4^+$ significantly, with total fractionation dependent on the rate-limiting step of the nitrification process, which is usually the oxidation of NH_4^+ to NO_2^- the slower of the two steps in most natural systems (Nikolenko *et al*., 2018). Substrate pool size is also influential, with N-limited systems having comparatively little fractionation due to nitrification (Nikolenko *et al.*, 2018).

DNRA can replace nitrification in N limiting systems with a high carbon to NO_3^- ratio (Figure 2.4), thus it is first important to understand whether DNRA or nitrification is reducing NO_3^- in any given system. Though there is no specific data in the literature demonstrating a particular depletion value for DNRA, Kendall *et al*. (2007) report that DNRA results in strongly depleted $\delta^{15}N\text{-}NH_4^+$ values.

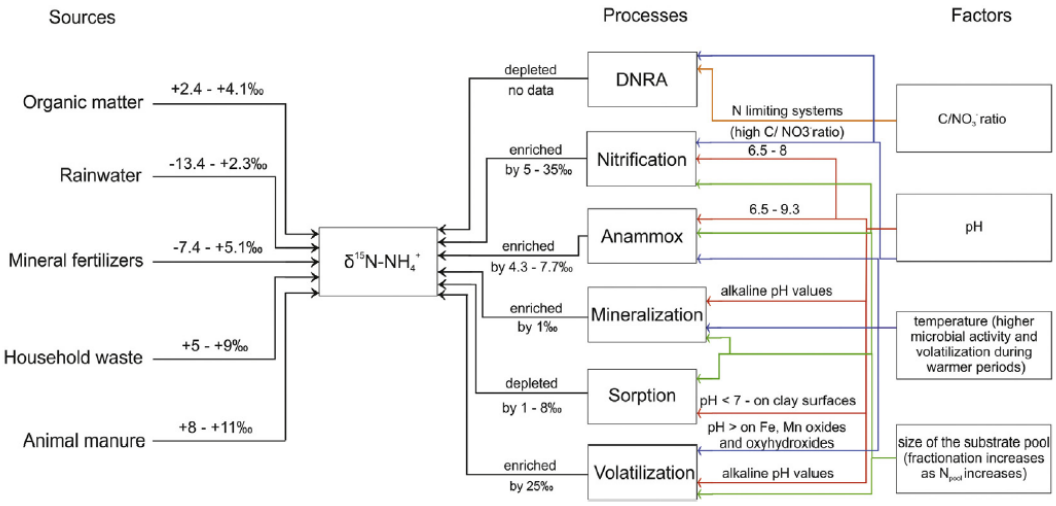

Figure 2.3. A summary of influences on $\delta^{15}N\text{-}NH_4^+$values. Arrow colours on arrows between factors and processes represent resulting fractionation effects: orange = C/NO_3^- ratio, red = pH, blue = temperature, and green = size of substrate pool. Taken from Nikolenko et al. (2018).

2.1.4. Geologic N

Geologic N is N currently stored in some form in rocks. There are various forms of geologic N but the following, taken from Holloway and Dahlgren (2002), are the most common: recalcitrant organic matter that accumulated during sedimentation, ammonium/nitrate salts or fixed ammonium in silicate minerals. Sedimentary, igneous and metamorphic rocks can all contain N in some form.

In igneous rocks, the most common form of N is as ammonium salts, likely originating from ammonium-rich thermal fluids (Holloway and Dahlgren, 2002). It is also theorised that extrusive igneous rocks, such as basalt or rhyolite, may contain N due to the emissions of volcanic gases and associated atmospheric deposition (Holloway and Dahlgren, 2002). Igneous rocks contain less than 100 mg kg^{-1} of N (Morford *et al*., 2016), thus are a minor source of N in most systems.

Sedimentary rocks often contain N in the form of organic matter accumulated during the sedimentation process, which then is incorporated as ammonium into clay minerals or organic matter during diagenesis (Holloway and Dahlgren, 2002). Sedimentary rocks are a long-term reservoir for 20% of global N (Holloway and Dahlgren, 2002; Dahlgren, 2006; Montross *et al*., 2013). Morford *et al.* (2016) report that fine-grained sedimentary rocks

contain the highest concentrations of N – 600-1000 mg kg^{-1} – and cover some 30% of the Earth's surface, whilst coarse-grained sedimentary rocks contain 200-400 mg kg^{-1} and cover ~40% of the Earth's surface. There is significant potential for systems with high N bedrocks to have a geologic N input.

Geologic N input is in the form of inorganic fixed N (Montross *et al*., 2013), as organic matter in rocks is mineralised during the weathering process to ammonium and then enters the soil N cycle via dissolution (Holloway and Dahlgren, 2002). Holloway and Dahlgreen (2002) note that denitrification in a system is critical to modifying the extent by which N derived from weathered bedrock is exported to surface and groundwaters.

As the input of geologic N into a given system is primarily controlled by weathering and denudation rates, it is thought that climatic factors establish a control on geologic N input

(Morford *et al*., 2016). Dahlgren (2006) notes that there is a pulse of N release from soils at the beginning of the wet season. Morford *et al*. (2016) note that their modelled N flux is highest in upland forest ecosystems where water is a limiting factor and controls the distribution of erosion rates and vegetation types – this may indicate that precipitation rates and patterns can have an effect on the magnitude input of geologic N in a given watershed.

Holloway and Dahlgren (2002) note that soil disturbance; such as construction, timber harvest or grazing; can allow for soil biota to access and accommodate further geologic N. Dahlgren (2006) describes the impact of the removal of oak trees for pasture improvement in California as a potential factor in the increase of geologic N to the system. The oak trees attenuated the deep leaching of N and then cycled it back into the soils as litterfall. Semi-frequent fire events also allowed for the volatilisation of soil N. This example demonstrates why modern land management practices in regions with high geologic N should be considered when tracing N through such systems (Holloway and Dahlgren, 2002) as there is a potential for further N exportation that can then be transferred into surface and ground waters.

In certain catchments, geologic N may be the main input of N into the system – Dahlgren's (2006) case study of geologic N found that, in a catchment in the northern Sierra Nevada Mountains in California, 90% of nitrate-N had originated from 10% of the watershed area having geologic N. Arid and semi-arid regions, where atmospheric deposition can accumulate due to lack of precipitation events to transport atmospherically deposited N, present a particularly significant pool of leachable N (Holloway and Dahlgren, 2002), thus systems in such regions have particularly large inputs of geologic N.

2.2. N Contamination in Groundwater

N, specifically nitrate is the most common contaminant in the world's aquifers (Exner *et al.*, 2014). Nitrate can enter groundwater systems both through natural and anthropogenic sources. The forms of N measured in groundwater include nitrate (NO_3^-), nitrite (NO_2^-) and ammonium (NH_4^+) as well as organic N (org-N). Nitrite is an intermediate product of nitrification and denitrification and thus relatively unstable in groundwater conditions so has a very limited occurrence (Burkart and Stoner, 2008). Organic N and NH_4^+ are both relatively rare in groundwater. Burkart and Stoner (2008) report that the generally accepted hypothesis for this rarity is that the required biological activity to produce both org-N and NH_4^+ is minimal in groundwater. Thus, the most commonly measured form of N in groundwater is nitrate.

2.2.1. Sources of N groundwater pollution

Both anthropogenic activity and natural processes can lead to an ingress of N into groundwater, though it is generally accepted that anthropogenic inputs are far greater than natural inputs in most systems (Harter *et al*., 2012).

2.2.1.1. Anthropogenic sources

The most common source of N pollution in groundwater is from agriculture, specifically the use of synthetic fertiliser on cropland (Shukla and Saxena, 2018). Over application of fertiliser beyond crop needs or improper timing of fertiliser application can lead to the leaching of N in groundwater. The most common fertiliser used is synthetic NO_3^- fertiliser, though this can be replaced in some regions by the use of animal manure, effluent and biosolids (Harter *et al*., 2012).

Human and animal waste can also lead to the leaching of N into groundwater – decentralised sewage treatments (such as the use of septic tanks and leaching pits/fields) can lead to point source contamination of groundwater when leaks occur. Open defecation and poor sanitation practices in low-income countries can be another source of groundwater N pollution (Shukla and Saxena, 2018). Waste from dairies and open feedlots is also a source of significant N pollution if managed poorly.

Industrial waste from dye manufacture, metal processing and explosives manufacture contains a significant proportion of N-containing compounds such as anhydrous ammonia, nitric acid and urea – all of which can be converted to nitrite or nitrate (Shukla and Saxena, 2018).

Urban and domestic activities can also lead to N leaching. Large expanses of turf such as golf courses can leach N as well as leaky sewerage systems or waste water treatment plants (WWTP) (Harter *et al*., 2012).

N can also enter the groundwater through the deposition of atmospheric N. Whilst atmospheric N can be sourced both from anthropogenic and natural sources, anthropogenic emissions of N_r are the dominant contribution to N deposition in a large proportion of regions (Liu *et al*., 2013). Goulding *et al*. (1998) note that in the SUNDIAL model deposited N comprised 10% of leached N in a fertilised agricultural plot – a significant contribution. N deposition can be either wet or dry, with wet deposition dominated by ammonium and dry deposition dominated by nitric acid and N dioxide (Goulding *et al*., 1998). Huang *et al.* (2016) reported that dry deposition contributed more to N deposition outside of precipitation-intensive months. While there is some evidence of N deposition affecting the water quality of surface waters such as lakes (Ti *et al.*, 2018; Chen *et al*., 2018), little has been done to investigate the impact such deposition has on groundwater quality, though the significant contribution deposited N makes to leached N (Goulding *et al.,* 1998) is likely to have an effect on N concentrations in groundwater.

2.2.1.2. Natural Sources

N can be introduced into groundwater via weathering of bedrock, as detailed in *2.1.4 Geologic N* or leached from soil-N through precipitation. Significant geologic N presence in a watershed can increase groundwater N concentrations but this elevated concentration usually remains below legal drinking water limits (Harter *et al*., 2012).

Cultivation of arid/semi-arid areas to irrigated cropland can mobilise stable organic N that built up in sediments over millennia and the recharge of irrigation water can mobilise nitrate

salts that accumulated over thousands of years in the unsaturated zone – however both of these N sources tend to be negligible compared to any of the above anthropogenic sources (Harter *et al*., 2012).

2.2.1.3. General Sources

Wells, whether they are in use, disused or poorly maintained, can be a source of N contamination in groundwater. Nitrate laden runoff can enter a well and thus infiltrate into the aquifer or allow for shallow nitrate groundwater pollution to be transmitted to deeper aquifer layers (Harter *et al*., 2012).

2.2.2. Issues with N Groundwater Pollution

N can enter groundwater in all forms (NO_3^-, NH_4^+, NO_2^-, org-N) with all sources of groundwater discharge – making it easy for N on the surface to be transferred into the groundwater through both diffuse and focused recharge (Harter *et al*., 2012). As nitrate, the most common form of N in groundwater, does not significantly adhere to or react with sediments it will move with groundwater flow (Harter *et al.*¸2012), increasing the risk of further aquifer contamination or surface contamination in groundwater dependent ecosystems such as wetlands, rivers and near-coastal areas (Hansen *et al.,* 2017). Van Meter and Basu (2015) report that 15% of fertiliser nitrate applied to agricultural land is present within the soil profile in organic form 30 years after application, indicating that in agricultural areas there is a constant leaching of N into the groundwater that changes in current management practices cannot reduce.

2.5 billion people worldwide rely solely on groundwater to satisfy their daily water needs (WWAP, 2015) – in the EU alone 75% of the population rely on groundwater for drinking water (Hansen *et al*., 2017). With this in consideration, it is important to note that N in groundwater can have major impacts on human health when above certain concentrations. WHO (2011) guidelines state that water should not contain nitrate levels above 100 mg/L and that caution should be employed when nitrate levels are between 50-100 mg/L. WHO (2011) also establish that nitrite should not be above 3 mg/L.

Consumption of water with N concentrations above WHO guidelines by infants has been shown to be a major cause of methemoglobinemia – the presence of methaemoglobin (metHb) in blood – leading to a reduction in oxygen carrying capacity in blood (Shukla and Saxena, 2008). Methemoglobinemia can cause cyanosis and even asphyxia (WHO, 2011). The IARC (2010) has classified ingested nitrate and nitrite as Class 2A probable human carcinogens, as both are precursors to the formation of nitrosamines, for which there is evidence that these can lead to colorectal cancer or bladder cancer (Hansen *et al*., 2017).

Nitrate is a goitrogenic substance – it disrupts the production of thyroid hormones by interfering with iodine uptake in the thyroid gland – and a 250-500 mg/L dosage of nitrate can lead to histomorphological changes in the thyroid (Shukla and Saxena, 2008), thus it is important that those susceptible to thyroid issues do not consume drinking water with high concentrations of nitrate.

Shukla and Saxena (2008) also report that at nitrate concentrations of between 100 and 200 mg/L in water livestock appetite has been shown to be reduced. Another risk is highlighted by Gao *et al*. (2012) - crops irrigated with groundwater with high N concentrations may pose a significant risk to human health and thus policy needs to be updated to take this risk into account in regions where valuable groundwater resources are heavily polluted with N.

2.3. Policy Implications of N in Groundwater

Anthropogenic use of reactive N in agriculture has been instrumental in feeding the growing world population (Galloway *et al*., 2008), even if the uneven distribution of the resource still leads to an unbalanced distribution of food resources across the globe. It is important to note that to continue to feed the world's growing population fertiliser N must continue to be used but its use balanced between sustainable use with minimal environmental damage and increased crop yields. With Pretty *et al*. (2000) estimating that some 80% of N in water resources as coming from agricultural sources, it is important to consider the ways in which policy can be implemented and how best to persuade farmers to follow governmental regulations on nitrate pollution.

Stigter *et al*. (2011) state that overfertilisation is a major issue in many agricultural areas, such as in the U.S. where one third of applied fertiliser is lost to the environment and thus not even effective in increasing crop yields. Unbalanced nutrition can also lead to an inefficient uptake of N by crops, as the presence of other macronutrients is essential for N recovery (Stigter *et al.*, 2011). With this taken into account, fertilisation practices in agriculture must be closely monitored and amended to ensure both high fertiliser N uptake and reduced fertiliser-N leaching. Boesch (2002) list some of the management practices that have had success in reducing losses of N from agricultural sources, with measures such as increasing efficiency of fertiliser application through a greater understanding of crop nutritional needs and application timings, crop rotation and specialised fertiliser application methods. Such changes in fertilisation practices reduce the traditional practice of overapplication to ensure maximum crop yields, which leads to increased nutrient leaching into surface and ground waters (Boesch, 2002). Landscape practices to reduce runoff of N into surface waters have also been effective – buffer strips between cultivated fields, moderating drainage from fertilised fields, maintenance of wooded riparian areas all reduce the leakage of N into surface waters (Boesch, 2002).

Goodchild (1998) provides an insight into the policy direction taken by the EU to reduce N pollution of water as well as implementation at the time of publishing – whilst the Nitrates Directive (the policy put into practice to reduce N pollution in water by the EU) was ambitious, implementation had been sluggish. Stitger *et* al. (2011) explain that the Directive aims to reduce water pollution by designating Nitrate Vulnerable Zones (NVZs), implementing monitoring programs, establishing action programs and publishing codes of good agricultural practices. Goodchild (1998) suggested that whilst some areas of the directive were imprecise in terms of whether action programmes were to be legally binding, it was likely that the power of the agricultural lobby was an important factor in the sluggish implementation. Buckley's (2012) analysis of farmer opinions of the EU Nitrates Directive regulations further examined the reluctance to implement better management practices. Many farmers in Buckley's (2012) study expressed scepticism to the improvements in agricultural practice that came from following regulations and felt that the implementations were equally spread across the agricultural community. It was reported that a lack of physical evidence led to reduced willingness and attempts to make changes (Buckley, 2012). With this in consideration, it is important that policy implication moving forward is as transparent as possible to ensure that farmers will abide by regulations put in place.

Despite sluggish implementation of the Nitrates Directive, it has been reported that rapidly responding aquifers in the UK have exhibited improvements following changes in agricultural practices (Stuart and Lapworth (2016). Improvements in regions with large unsaturated

zones, such as areas underlain with chalk, are not expected to seen for decades – as travel times are so long that improvements in practices are unlikely to have any measurable effect for decades (Stuart and Lapworth, 2016). Regions with low effective rainfall (and thus a reduced potential for dilution during recharge) and a large percentage of arable land were identified by Stuart and Lapworth (2016) as being of high risk for nitrate pollution – one of these areas being the Chalk of south Yorkshire and East Anglia. With farmers citing a lack of physical evidence of improvement (Buckley, 2012) this is problematic as such regions will not see improvements despite changes in practice, increasing farmer resentment in similar vulnerable regions.

Wang and Burke (2017) note that current environmental water management strategies rarely take this N time lag into consideration, even when it is clear that in some catchments it may take decades for leached nitrates to discharge into freshwaters. Current measures can seem ineffective at improving water resources in aquifers with large unsaturated zones. With the removal of N from drinking water costing water delivery companies upward of £16.4m per year - a cost that is often passed onto consumers (Pretty *et al*., 2000), it is important that such lag times be quantified and accounted for.

2.3.1. Modelling N in Groundwater

Models that consider the subsurface as a potential store for N are still being developed. Notable examples include the work of Van Meter and Basu (2015) who present one of the first frameworks for understanding the time lag between land use change and stream water quality improvements, with follow up work in Van Meter *et al*. (2016) providing further evidence of further subsurface stores of N not accounted for in older models, allowing for 'missing N' in the hydrological system to be accounted for. Wang and Burke (2017) also provide a useful catchment-scale model to account for subsurface 'legacy N' in the landscape, with considerations made for dual-porosity unsaturated zones that were not made in Van Meter and Basu (2015) and Van Meter *et al*. (2016). On a global scale, Ascott *et al*. (2017) model the nitrate stored within the vadose zone, again noting the issue of legacy N and the impact of considering the storage capacity of the subsurface when analysing the impact of anthropogenic activity on the N cycle. All models mentioned use either current average N concentrations or case study data to validate their models – it would beneficial for all cited models for a long-term historical record of groundwater N to be available for further validation, though at this time very few, if any, catchments have this kind of data available.

2.4. The Operation of Cave Systems and Karst Hydrogeology

Microclimatic conditions within caves control rates of speleothem growth and characteristics of the chemistry contained within (Spötl *et al*., 2005; Baker *et al.*, 2014, James *et al*., 2015; Wynn *et al*., 2014; Fairchild and Treble, 2009; Miorandi *et al*., 2010). The key parameters of concern are cave temperature dynamics and their accompanying effects on cave air CO_2 concentrations, and the hydrological dynamics of the overlying karst.

2.4.1. Cave Ventilation, Air Temperature and pCO2

Cave ventilation, the movement of air through caves, plays a critical role in modulating the pCO_2 of cave air and thus on the growth rates, trace element concentrations and stable isotope ratios of speleothems. Calcite precipitation relies on the outgassing of CO_2 from solution and thus a high cave air pCO_2 can inhibit speleothem growth significantly, whilst temperature can play a role in the incorporation of trace element ions into the speleothem calcite (Baker *et al*., 2014; Spötl *et al*, 2005; James *et al*., 2015; Wynn *et al*., 2014).

2.4.1.1. Temperature Dynamics and the Influence on Cave Air pCO2

Due to the key influence of CO2 on speleothem growth rates, it becomes important to understand the drivers behind CO2 levels in cave systems. At non-tropical latitudes, temperature is the most important control on cave air pCO2 levels (James *et al.,* 2015). Here, seasonal changes in average external temperatures, contrasted against a more stable internal cave temperature, drive a seasonal density-driven ventilation regime.

In the winter months, where external temperatures remain below internal cave air temperatures, the density of air outside the cave becomes greater than the density of the air within the cave. The cooler denser external air flows into the cave, displacing the warmer less dense air. Compared to the internal air mass, the external air mass has a comparatively low CO2 concentration, thus reducing cave air pCO2 (Vieten *et al.* 2016).

In summer months, where external temperatures remain above internal cave air temperatures, the density of the air outside the cave becomes less than that within the cave. The internal cave air is drawn out by this density difference, and air is drawn down through the soil and karst to replace the air drawn out of the cave. The air trapped within the soil and karst has a high pCO2 due to the microbial activity in the soil, thus the movement of air through the soil and karst into the cave results in a rise in cave air pCO2 (Vieten *et al.*, 2016).

Due to these seasonal cave ventilation regimes, many speleothems exhibit increased growth rates in the winter and inhibited growth rates in the summer. Global models of cave ventilation dynamics demonstrate a seasonal bias in temperate and boreal regions due to this seasonal ventilation dynamic (James *et al*., 2015).

2.4.1.2. Cave Carbon Dynamics and their in-cave influences

As detailed in 2.4.1.1., cave ventilation is a key control on cave air pCO2. CO2 concentrations in caves are not wholly derived from cave ventilation alone however. Root respiration and the decay of organic matter within the epikarst is a key source of CO2 in caves, especially during the summer months when microbial activity in the epikarst is at its highest. Another source that can influence cave air pCO2 is that of the degassing of dripwaters containing CO2 that have passed through the soil. Decaying organic matter within the cave can influence cave air pCO2, as can the respiration of living organisms within the cave – in Smith *et al.*, (2013), the effect of tourist groups on the cave air pCO2 in a show cave could be easily identified due to the sharp increase in pCO2 due to the effect of the groups' respiration of CO2 into the cave. In some caves, geothermal activity can also play a role (James, 1977; Baldini, 2010; Fairchild and Baker, 2012).

Spötl *et al*. (2006) provide a comprehensive suite pCO2 monitoring at Obir Cave, where a density-driven ventilation dynamic leads to increased cave air pCO2 in the summer and decreased in the winter. In the winter, this reduced pCO2 lead to the forced degassing of dripwaters entering the cave, increasing CaCO3 precipitation but also leading to kinetic fractionations in $\delta^{13}C$, highlighting the need to engage in a program of cave monitoring to determine the influences of cave microclimatic conditions on speleothem proxies in a given cave.

2.4.1.3. Pressure induced ventilation dynamics

Some specific caves may demonstrate a pressure induced ventilation dynamic that may occur alongside or overwrite the regular temperature-driven density ventilation dynamic seen in most temperate cave sites. Smith *et al.* (2016) reported that Asiul cave (N. Spain)

demonstrated a pressure-driven dynamic – ventilation was induced when external pressures were low (often brought on by storm activity), as this enhanced the pressure gradient between the internal cave and external atmospheric air. This replicated the same conditions as a normal summer ventilation regime, moving air out of the cave and resulting in air being drawn down through the karst and into the cave, thus increasing cave air pCO2.

2.4.2. Hydrological Dynamics

Water movement within the karst can be broadly divided into three main hydrological regimes which are differentiated by the size of the conduit through which the water flows (White, 2002; Smart and Friedrich, 1987).

1. True matrix flow is the flow of water through the intergranular permeability of the bedrock and thus is dictated by the bedrock primary porosity. For most Mesozoic limestones, such as those found in the Cantabrian region (Quin, 2010), this primary porosity is low (1-5%, as reported in Fairchild and Baker, 2012) – as such the amount of water that flows through the karst in this way is low. Thus, in karst literature, matrix flow is often used to instead describe water movement through microfractures in the karst (Smart and Friedrich, 1987). The karst is thought of a continuously permeable membrane (Fairchild and Baker, 2012), with flow often occurring via forced piston flow. This flow is characterised by the input of water at the 'top' of the system forcing water out of the 'bottom' of the system, often in the form of drip sites within caves. Such drip sites tend to have continual drips but with a low variation in drip rates, due to the low discharge of the hydrological pathway (Smart and Friedrich, 1987).
2. Fracture flow is a faster hydrological pathway than matrix flow and is characterised by the flow of water through joints and faults in the bedrock (Fairchild and Baker, 2012). Fracture flow exploits the expansion of microfractures caused by matrix flow and leads to the continual enlargement of the joints and bedding planes in the host bedrock (Miorandi *et al*., 2010).
3. Conduit flow is the flow of water through enlarged underground passages, with a flow regime that varies with rainfall intensity (Smart and Fredriech, 1987). At drip sites mainly fed by conduit flow, drips are found to be intermittent with a high variation in drip rates, due to high but non-constant discharge of the hydrological pathway (Smart and Fredriech, 1987). Conduit flow often acts as an overflow mechanism when both matrix and fracture flow pathways are fully saturated (Miorandi *et al*., 2010).

As these three hydrological pathways interact, theoretically a specific site hydrology is produced. In many cases, piston flow through the matrix flow pathway acts as a primary and continuous water movement mechanism, with fracture and conduit flow only occurring during wetter conditions (this is referred to as a piston overflow system) once the matrix flow mechanism is fully saturated.

Despite this, it is generally difficult to predict the water flow pathways due to the complex nature of karst (Baker and Brunson, 2003). Different antecedent conditions may lead to different drip sites sourcing water from different hydrological pathways or some combination of pathways at different times, thus making continual long term modelling the only viable method by which the general trends of drip site water source pathways can be understood (Miorandi *et al*., 2010; Fairchild and Treble, 2009).

2.4.2.1. Effect of karst hydrology on chemical signatures of drip waters

Understanding the hydrological regimes at play is important when considering a cave site suitable for use for speleothem proxy work, as changes in the hydrology can lead to changes in the interactions between the water and karst during infiltration.

Prior calcite precipitation (PCP) refers to the deposition of calcite within the karst above a cave site, removing Ca^{2+} ions and leaving the remaining solution comparatively enriched in other elements (Palmer, 2010; Fairchild and Treble, 2009). PCP can override many of the other factors that affect chemical concentration in speleothem calcite and can be considered indicative of dry phases in the overlying karst (McDonald *et al*., 2007) thus it becomes important to identify the role PCP plays in a given system.

Dry periods allow for an increased rock-water contact time and promote the dissolution of the bedrock and the chemical signals contained within (Lange *et al.,* 2010). Rapid infiltration of water into the system, in wetter conditions, lead to reduced rock-water contract time and can lead to a dilution effect on the chemical signatures contained within drip waters (Miorandi *et al*., 2010). However, a piston effect during a period of increased rainfall intensity can lead to the discharge of matrix flow water with a high solute load to a drip site (Fairchild *et al*., 2006), leading to an increase in the concentrations of chemical signals during wetter conditions (Miorandi *et al*., 2010). Thus, it is important to have an understanding of the hydrological conditions above a given cave site.

Karst storage can be inferred by comparing cave waters oxygen-deuterium isotopic signatures. Every rainfall event has a unique $\delta^{18}O - {}^{2}H$ signature that is imprinted by the evaporation and condensation processes occurring at their source (Clark and Fritz, 1997). Combining such rainfall signatures for a location provides a Local Meteoric Water Line (LMWL) (Craig, 1961), by which cave water oxygen isotopes can then be contrasted and compared. Those cave waters that correlate with the LMWL are considered to have been stored in the karst for less than a year (Carrasco *et al*., 2006), thus the resulting speleothems can be analysed at a higher resolution (Bradley *et al*., 2010). If there is evaporation within the soil and epikarst, water entering the cave can be depleted in ^{16}O and thus not correlate with the LMWL, thus this technique is not always appropriate.

2.5. N in Karst Aquifers

Karst aquifers provide an estimated 20-25% of the global population with potable water (Huebsch *et al*., 2013) yet are incredibly vulnerable to pollution due to the existence of solutional conduits that provide direct pathways for the flow of surface water into the aquifer (Katz *at al.*, 2004). Karst aquifers may have dual or even triple porosity through the caverns, fractures and matrix present (Katz *et al*., 2004) and there is a greater level of interactivity between surface and ground waters than found in other types of aquifer (Opsahl *et al*., 2017), making it difficult to monitor and analyse the movement and storage of N species. With the rapid transport of groundwater through conduit systems it can be difficult to limit the spread of contaminants through a karstic landscape (Huebsch *et al.,* 2013) and models such as Ascott *et al*. (2017) have had to account for this rapid transport through the vadose zone, making karst aquifers somewhat unique in their ability to transmit surface waters (and contaminants) into groundwater systems swiftly, as well as transport these waters swiftly through the groundwater (Huebsch *et al*., 2013), though it has been noted that vertical transport between younger shallow aquifer waters and older deep aquifer waters is less rapid (Katz *et al.*, 2004).

The behaviour of nitrate within karst groundwater systems is especially problematic when considering groundwater quality. Liu *et al.* (2006) and Mudarra *et al*. (2014) found that in the oxidising conditions within the karst medium denitrification is limited if not absent altogether, limiting the ability of karst groundwater to recover from N contamination. This makes karst aquifers vulnerable to being contaminated through conduit flow and surface/groundwater interaction and water quality difficult to improve once contaminated. Musgrove *et al*. (2016) also hypothesised that, within their studied aquifer, there may be nitrification occurring within the karst groundwater, providing a further source of nitrate to an already vulnerable aquifer.

Karst aquifers are influenced greatly by intense rainfall and recharge events due to the fast response of groundwater to such events (Liu *et al*., 2006), thus NO_3^- sources to groundwater vary seasonally. NO_3^- will leach into groundwater throughout the year at varying rates but the leaching is observed at maximum rates in the autumn season due to high infiltration rates (Madarra *et al*., 2014). Weather events are thus important to observe when considering the temporal patterns of NO_3^- concentrations in karst groundwater, as noted by Huebsch *et al*. (2013).

Madarra *et al*. (2014) noted that overlying soil, epikarst conditions and prevailing lithology can be crucial to consider when understanding the movement of NO_3^- into groundwater – if a karst system is overlain with an epikarst with a high sand content, NO_3^- is likely to increase in response to precipitation events but a high clay content epikarst may lead to a reduced NO_3^- concentration in response to the same precipitation events.

2.6. Speleothems as an Archive of N Dynamics

Calcite speleothems (such as stalagmites, stalactites and flowstones) are a potential archive of environmental change that can provide records of a seasonal to decadal resolution and often contain multiple environmental proxies simultaneously (such as stable isotope ratios, colloids and trace elements), making them a versatile source of paleoenvironmental data (Fairchild and Treble, 2009). Morellón *et al*. (2018) also note that many speleothems have robust age models, good preservation and allow for the combination of proxies to infer both regional and global patterns of change.

2.6.1. Speleothem Formation

Calcite speleothems are formed when rainwater (H_2O) reacts with carbon dioxide (CO_2) to produce carbonic acid (H_2CO_3) (Equation 2.11). The carbonic acid dissociates into hydrogen ions (H^+) and bicarbonate ions (HCO_3^-) (Equation 2.12) which then further dissociates into protons and carbonate ions (CO_3^{2-}) (Equation 2.13) (Newton *et al*., 2015).

Equation 2.11:

$$H_2O + CO_2 \leftrightarrow H_2CO_3$$

Equation 2.12:

$$H_2CO_3 \leftrightarrow HCO_3^- + H^+$$

Equation 2.13:

$$HCO_3^- + H^+ \leftrightarrow CO_3^{2-} + 2H^+$$

The acidic solution formed dissolves carbonate bedrock (usually limestone – $CaCO_3$) until an equilibrium is reached (Equation 2.14).

Equation 2.14:

$$2H^+ + CO_3^{2-} + CaCO_3 \leftrightarrow 2HCO_3^- + Ca^{2+}$$

Upon this solution reaching the cave system, CO_2 will be degassed from the solution until an equilibrium with the pCO_2 of the cave air is reached. This creates a solution supersaturated with calcite, which forces Equation 2.15 to occur to allow the solution to return to equilibrium, thus precipitating calcite and creating speleothems.

Equation 2.15:

$$2HCO_3^- + Ca^{2+} \leftrightarrow CaCO_3 + CO_2 + H_2O$$

2.6.2. Speleothem Proxies

There are many proxies found within speleothems, each which can be used to infer information about climatic, hydrological, biological or biogeochemical changes over time. For example: observations of Mg/Ca/Sr can be used to investigate changes in effective rainfall and paleohydrology (Treble *et al*., 2003); changes in the $^{87}Sr/^{86}Sr$ ratio can also be used to infer information about changes in effective rainfall (Verheyden *et al*., 2000), as well as potential changes in Aeolian activity (Frumkin and Stein, 2004); speleothem P can be used to infer changes in vegetation characteristics over time in the overlying ecosystem (Baldini *et al.*, 2002); sulphates can be investigated to understand changes in atmospheric pollution dynamics and better understand the extent and dating of past volcanic events (Borsato *et al.,* 2015); the stable isotope ratio of $\delta^{18}O$ can be indicative of changes in temperature and rainfall isotopic composition (Bar-Matthews *et al*., 1997); and $\delta^{13}C$ can be used to understand past vegetation cover and type (Denniston *et al*., 2000).

2.6.3. Potential for N Archive

There are very few long-term records of N concentration and isotopes currently. Lacustrine sediment cores such as that used in Talbot and Johannessen (1992) and Sun *et al*. (2016) are the most often used in literature, allowing for examinations of $\delta^{15}N$ over long periods. Borehole data is presented in rare occasions, such as the examination of N in desert vadose zone pore waters by Hartsough *et al.* (2001). As can be seen in Figure 2.5, cave drip waters and the resulting speleothems associated with them can give a new perspective of N in the hydrogeological system, especially with consideration to groundwater, which lacustrine sediments cannot provide insight into, and can complement and improve upon the scarce and situational borehole data available.

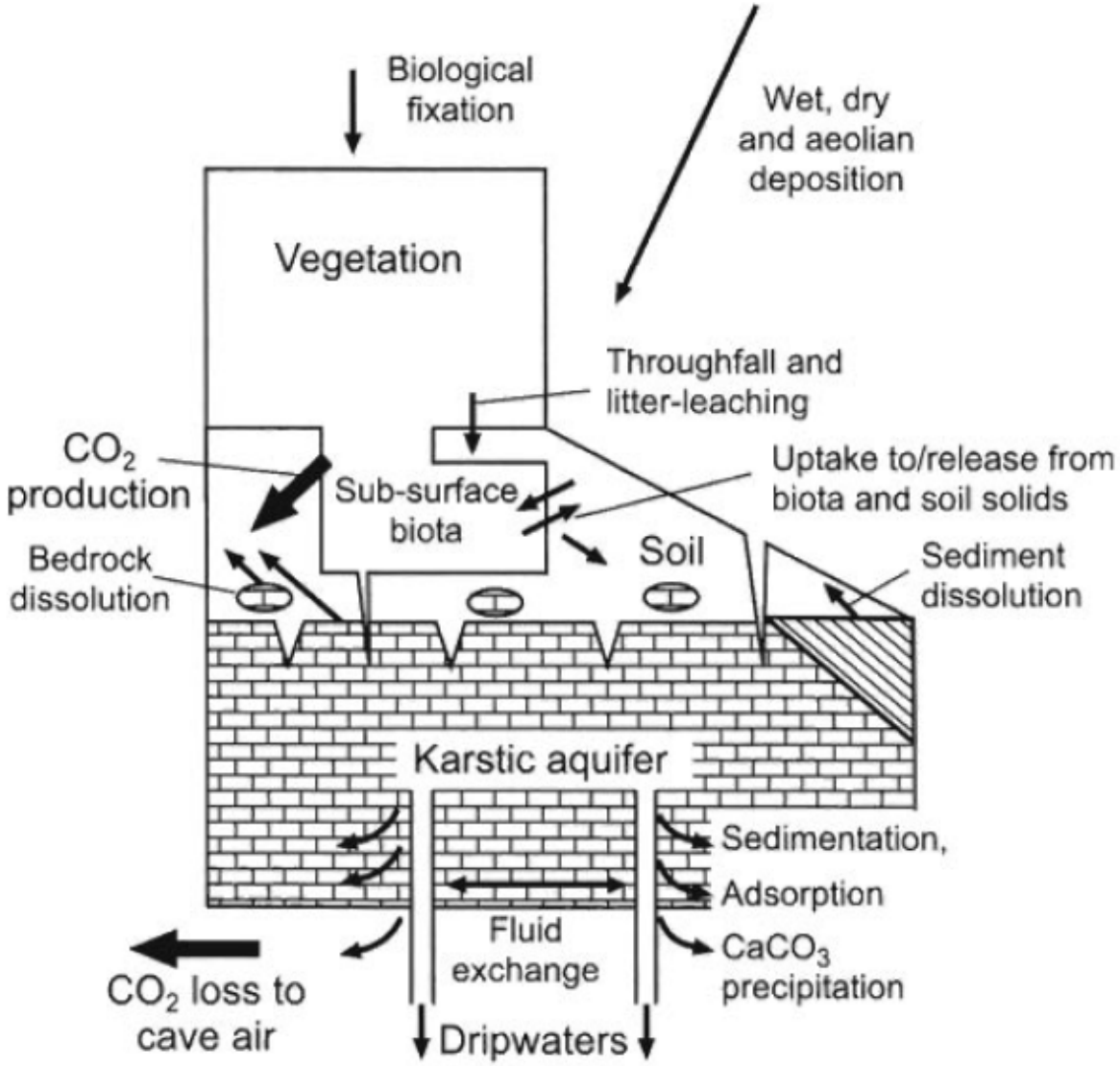

Figure 2.4: Schematic flow chart that indicates the sources of elements found in speleothem matrices and the processes involved in their transport and deposition in cave systems. Arrows represent element fluxes as particulates, colloids or solutes in aqueous solutions. (Taken from Fairchild and Treble, 2009).

2.7. Conclusion

N pollution is the most common form of groundwater pollution in the world (Exner *et al*., 2014) and karst aquifers are especially vulnerable to this form of contamination (Katz *et al*., 2004) despite being relied upon by a quarter of the population for potable water (Huebsch *et al*., 2013). $\delta^{15}N$ can be used to identify the sources of N pollution in groundwater as well as the processes acting upon groundwater N, allowing for a better understanding of the sources of contamination in a given catchment. Current regulations put in place to improve groundwater quality with respect to N are an important change but current models (used to enforce these regulations) are lacking historical data to assist in validating their predictions. Speleothems provide a versatile source of paleoenvironmental proxies and have been used to study changes in many different trace elements and stable isotope ratios in the past and thus could be a novel and useful source of historical groundwater N data, of which there is no current archive for.

3. Site Description and Methodology

3.1. Site Description

3.1.1. Location and regional geology

Cueva-Cubío del Llaníο (43°21’29.9”N, 003°35’53.8”W, 165 m a.s.l) is located in the Riaño valley, ~21km south east of Santander (Figure 3.1). The cave forms part of a connected network caves (The Four Valleys System) that link it to the caves of neighbouring Matienzo depression (Corrin, 2020). Developed in Lower Cretaceous (Aptian-Albian) carbonate of shallow water platform origin (Dewitt *et al*, 2014; Aranburu *et al*., 2015), the host bedrock of Cueva-Cubío del Llaníο comprises of a mixed calcite-dolomite composition interbedded with sandstones and marl (Gutíerrez, 2010).

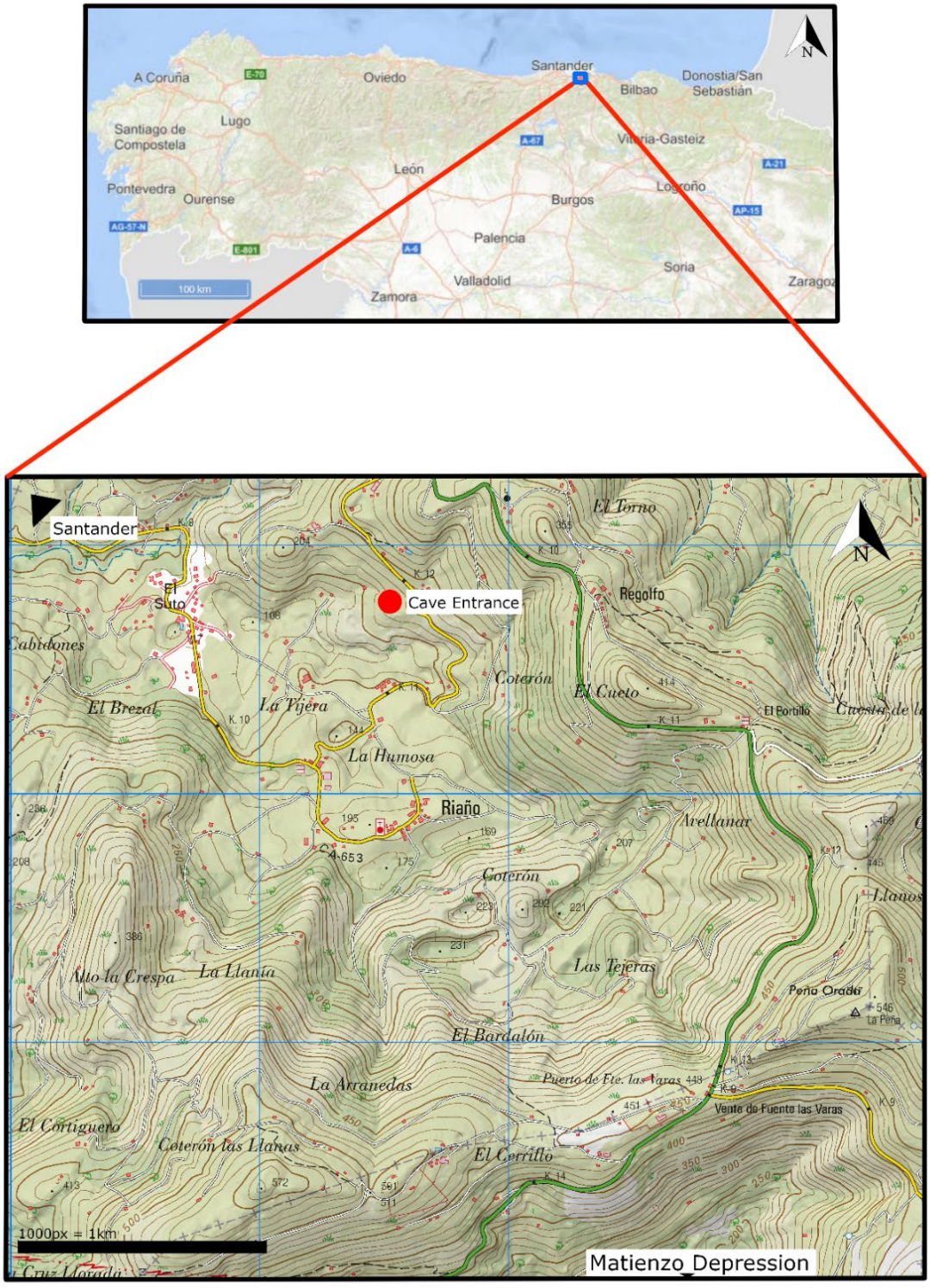

Figure 3.1: Maps demonstrating the location of the entrance to Cueva-Cub*í*o del Llan*í*o in relation to Santander and northern Spain. A section of the MTN25 map of Spain and Centro de Descargas overview map were used.

3. 1. 2. Modern environment

The general climate of the region is that of the damp temperate zone with an oceanic climate. An important feature of this oceanic climate is the intensity of the rainfall – mean rainfall is 1500mm throughout the year - with maximum rainfall experienced during the autumn and winter months. The mean temperature for the immediate area of Cueva-Cubío del Llaníο is 12°, as extrapolated from the nearby Arredondo weather station (Cobo, n.d.).

Land use above Cueva-Cubío del Llaníο is agricultural with a history of livestock grazing - many fields are delineated with drystone walls for this use, as can be seen in Figure 3.2. The region supports evidence of agricultural practices from the early Neolithic onward, thus it is likely this area has been used for agricultural practices at varying intensities since prehistory (Cubas *et al*., 2016). Current use of the land above the cave entrance is bee-keeping as of Apr-18 (Corrin, 2020). The overlying soil is often in excess of 50 cm depth and is organic rich with a loamy texture. Overlying vegetation is dominated by grasses, clover (*Trifolium sp.)*, dead-nettles (*Lamium sp.)* and dock (*Rumex obtusifolius)*, with sparse deciduous tree cover, thus supporting a clover-rich pasture of variable past grazing intensity.

Figure 3.2: Image of the field in which the entrance of Cueva-Cubío del Llaníο is located. (Photo: Mark Shinwell)

3.2. Cave description

Cueva-Cubío del Llaníο is a complex series of chambers and passages that has recently been linked to the extensive Four Valleys System – an extended cave system of 67,126m of passages. Cueva-Cubío del Llaníο itself makes up 7268m of these passages. The cave is dominated by phreatic passageways with large side chambers connected by fractures to the surface environment, and as such has a history of distinct phreatic history prior to drainage and the lowering of the water table. The current location of the cave places it high above the

water table to flood completely but from observation some chambers periodically dry on a seasonal basis.

The primary entrance used for this project was the original entrance discovered for Cueva-Cubío del Llanío - a crawl found at the back of a small stone-walled sheep enclosure at the base of the field pictured in Figure 3.2. A simplified cave survey can be seen in Figure 3.3, cropped to only include chambers where cave monitoring and sample collection was conducted.

These chambers are detailed below:

- **High Hopes Chamber:** A wide chamber characterised by the existence of an accessible overlying passage. The centre of the chamber contains a 1.5m column surrounded by a series of gour pools. The northeast section of this chamber contains a series of stalagmites and accompanying straw stalactites. This chamber is located approximately 14 m below managed pastureland with a history fertilisation by manure spreading (manure application ceased in 2017).
- **Whoopee Hall:** A tall chamber with a wide pool. A passage to the west leads to a small grotto with a selection of speleothems. Whoopee Hall is a shallower chamber approximately 5 m below a steeply sloping pasture with low intensity grazing and minimal manure application. Whoopee Hall has also been observed to dry on a seasonal basis.
- **The Hub:** A small chamber with a calcite floor over a prior cave collapse. Calcite floor covered with a thin even layer of mud that peels away from calcite floor in thick flakes.
- **Corner Series:** A standing-height series of sloping passages, characterised by the ~90° turn in the passage (the 'corner').
- **Aven Chamber:** A 32m high chamber characterised by the rift in the ceiling, which leads to further passages. Notable features include a large stalactite and corresponding stalagmite precipitating on a pile of collapsed cave material.

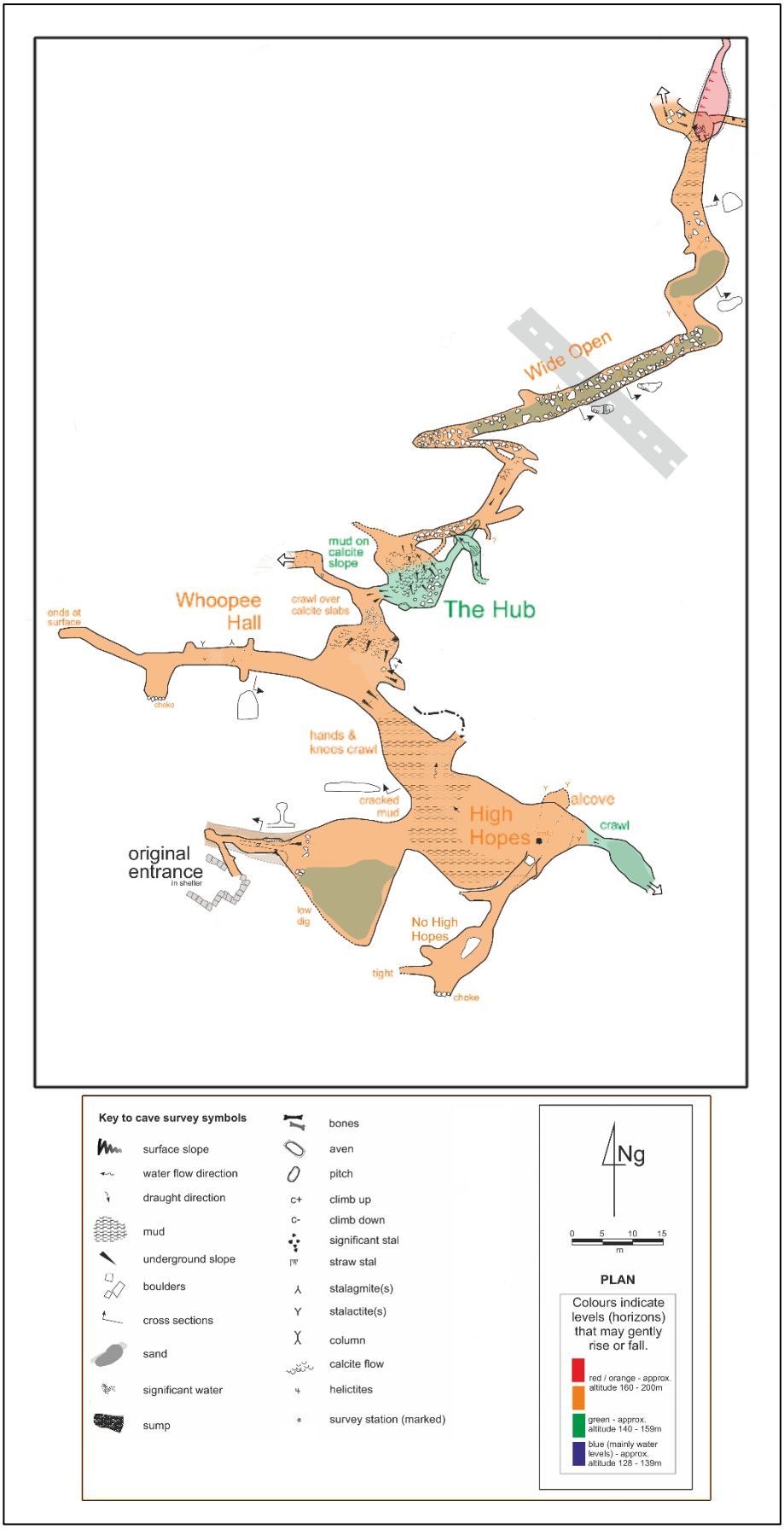

Figure 3.3 – Cave survey of Cueva-Cubío del Llanío adapted from Corrin (2018).

3.3. Climate, environment and cave monitoring

3.3.1. Overview

Climate and cave monitoring for this project began in Jan-18 and built off the work of Smith (2014) and Deeprose (2018). This monitoring was undertaken to gain an understanding into the dynamics of Cueva-Cubío del Llanío, investigating processes in the air, karst and cave that may influence the chemistry of the speleothems. Major field visits were made to Matienzo in Jan-18 and Jan-19 and further visits were made by members of the Matienzo Caving Community. Techniques and equipment used in the monitoring program will be detailed in the following section.

3.3.2. Temperature monitoring

3.3.2.1. External temperature

External temperatures were continuously logged at a location close to Cueva de las Perlas and Cueva de Asiul (43°19'00.1"N 003°35'40.1"W, 293m a.s.l) – caves in the region that has also undergone monitoring in the past – approximately 8.75km from Cueva-Cubío del Llanío. External temperatures were recorded Jan-18 to Jan-19 at this location.

External temperature data recorded beyond Jan-19 was recorded in the nearby village of Matienzo. All external temperature data recorded as part of this project was recorded using Tinytag Plus 2 – TGP-4017 or TGP-4500 data loggers. Measurements were logged at one-hour intervals and are accurate to within ±0.01°C. Further temperature data was taken from the work of Smith (2014) and Deeprose (2018) and methodology for this data can be found in their work.

3.3.2.2. Internal temperature

Internal cave air temperatures were recorded at various locations within Cueva-Cubío del Llanío, as detailed in Figure 3.4. The Entrance Shelter logger was concealed within the stones of the shelter, whilst the High Hopes and Whoopee Hall loggers were suspended from the cave ceiling. The Entrance Shelter and Whoopee Hall loggers recorded temperatures from Feb-18 onward. The High Hopes logger recorded temperatures from Jan-18 onward. A further temperature logger was placed in the cave in Jan-19 – the Junction logger. This logger was suspended from the cave ceiling in a similar manner to the High Hopes and Whoopee Hall loggers. All temperature loggers remain in the cave as of writing, to continue the cave monitoring work begun in this project.

All data were recorded using Tinytag Plus 2 TGP-4017 or TGP-4500 data loggers. Measurements were logged at 30-minute intervals and are accurate to within ±0.01°C.

-

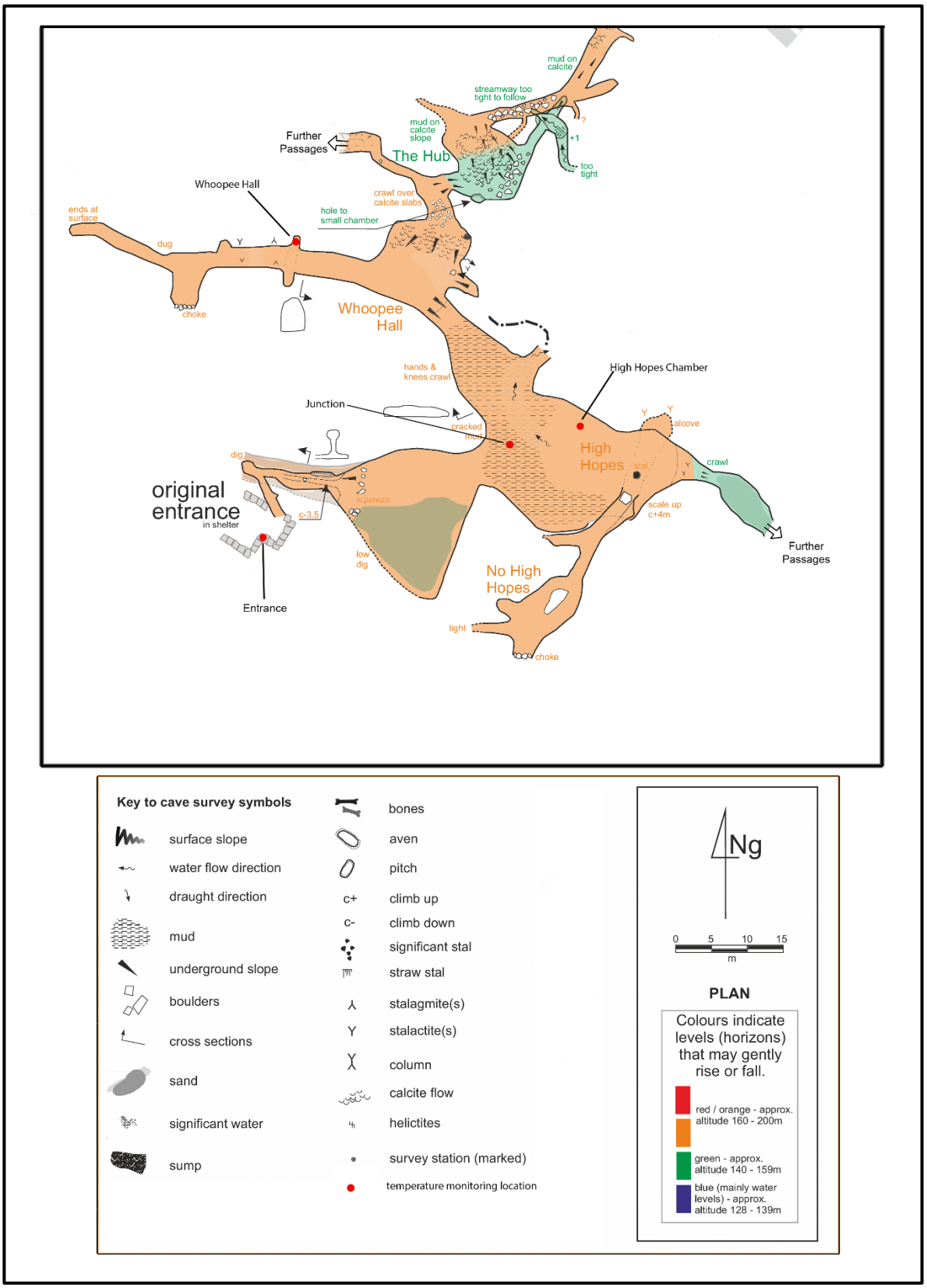

Figure 3.4 - Approximate temperature logger locations within Cueva-Cubío del Llanío. Survey adapted from Corrin, 2018.

3.3.3. CO_2 concentration logging

CO_2 concentrations were recorded in High Hopes chamber in Cueva-Cubío del Llanío for a month at a time. There were two month-long monitoring periods – from Jan-19 to Feb-19 and from Apr-19 to May-19.

A Vaisala GM70 Handheld Carbon Dioxide Meter was used to monitor air pCO_2. Unit measurement range is 0-10,000ppm with a measurement uncertainty of 2%. Measurements were taken at one-hour intervals. The CO_2 meter probe was hung from the cave ceiling to ensure the probe was measuring only the air pCO_2 and to reduce moisture build-up on the probe (Figure 3.5).

Figure 3.5 – A Vaisala GM70 CO_2 probe set up within High Hopes chamber. (Photo: Juan Corrin).

3.3.4. Rainfall Intensity Logging

Rainfall data was collected within Matienzo village, ~4.4 km from Cueva-Cubío del Llanío. A Pluvimate rain gauge was used to collect rainfall data from Feb-18 to Aug-18. All rainfall data was converted from drips/10 minutes to mL/day using Equation 3.1. The drip volume of 0.1ml in Equation 3.1 was derived using drip volumes from Mattey and Collister (2008) and Smith *et al.* (2015).

Equation 3.16:

$$0.1\text{ml} * \text{drips per day} = \text{mL/day}$$

3.3.5. Drip Rate Logging

Stalagmate acoustic drip loggers (Mattey and Collister, 2008) were used to collect drip rate data, with a logging interval of 10 minutes. Stalagmate factory settings record 0.15ml drops at a maximum drip rate of 5 drops per second.

Drip rates were collected throughout the cave site (see Figure 3.6 for locations of loggers). Stalagmate loggers were placed on top of two different stalagmites within the cave – one in the High Hopes Chamber (on stalagmite Hope 3) and one in Whoopee Hall (on the stalagmite Whoopee 1). The Whoopee 1 logger recorded drips from Feb-18 to Sep-18, whilst the Hope 3 logger recorded drips from Feb-18 to Aug-18.

All logging data ended around Aug/Sep-18 due to the loggers' memory capacities being exceeded, thus no more data was able to be captured past this point. During the Jan-19 field visit, drip loggers were restarted and replaced.

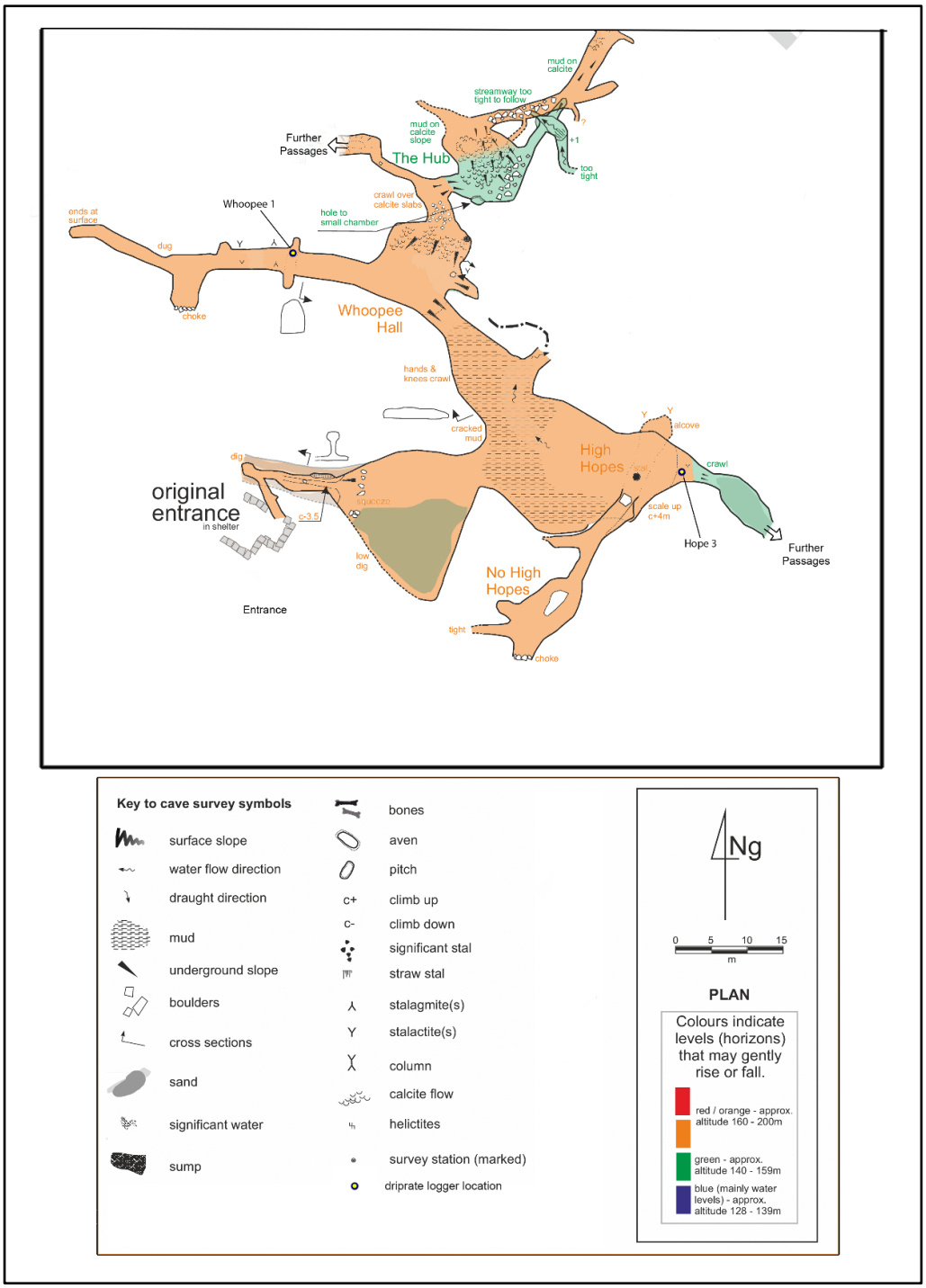

Figure 3.6: Approximate driprate logger locations within Cueva-Cubío del Llanío. Survey adapted from Corrin, 2018.

Cave Water Sampling

Cave waters were sampled throughout the cave monitoring period, with simultaneous samples taken in Jan-18, Feb-18, Aug-18, Jan-19, Apr-19, Aug-19 and Sep-19. Disposable plastic cups were placed underneath chosen drips to collect cave drip water. Cups were left for as long as was required for enough water to be collected for required analyses – the time required to collect a sample was

dependent on the drip rate of that particular drip. For most drips this was around 24 hours. Cave pools were directly sampled using a syringe.

60ml HDPE sample bottles were used to store water samples taken from the cave. If enough drip water was available two samples were taken: one unfiltered and one filtered through a 0.2 µm syringe filter to remove any particulate contaminants. Unless otherwise stated, all water samples were tested for pH, EC and water temperature in the field – this field analysis can be seen in Figure 3.7. Some water samples were also titrated in the field if enough water was collected. Further water samples were placed within brown glass 2ml autosampler vials for D/O isotope analysis. Samples were frozen soon after removal from the cave and transported to Lancaster University for further analysis.

Figure 3.7 – Field measurement of pH values. (Photo credit: Juan Corrin).

Figure 3.8 shows the locations of the drips and pools sampled – multiple locations throughout the cave were sampled. Table 3.1 contains a brief description of each sampling location.

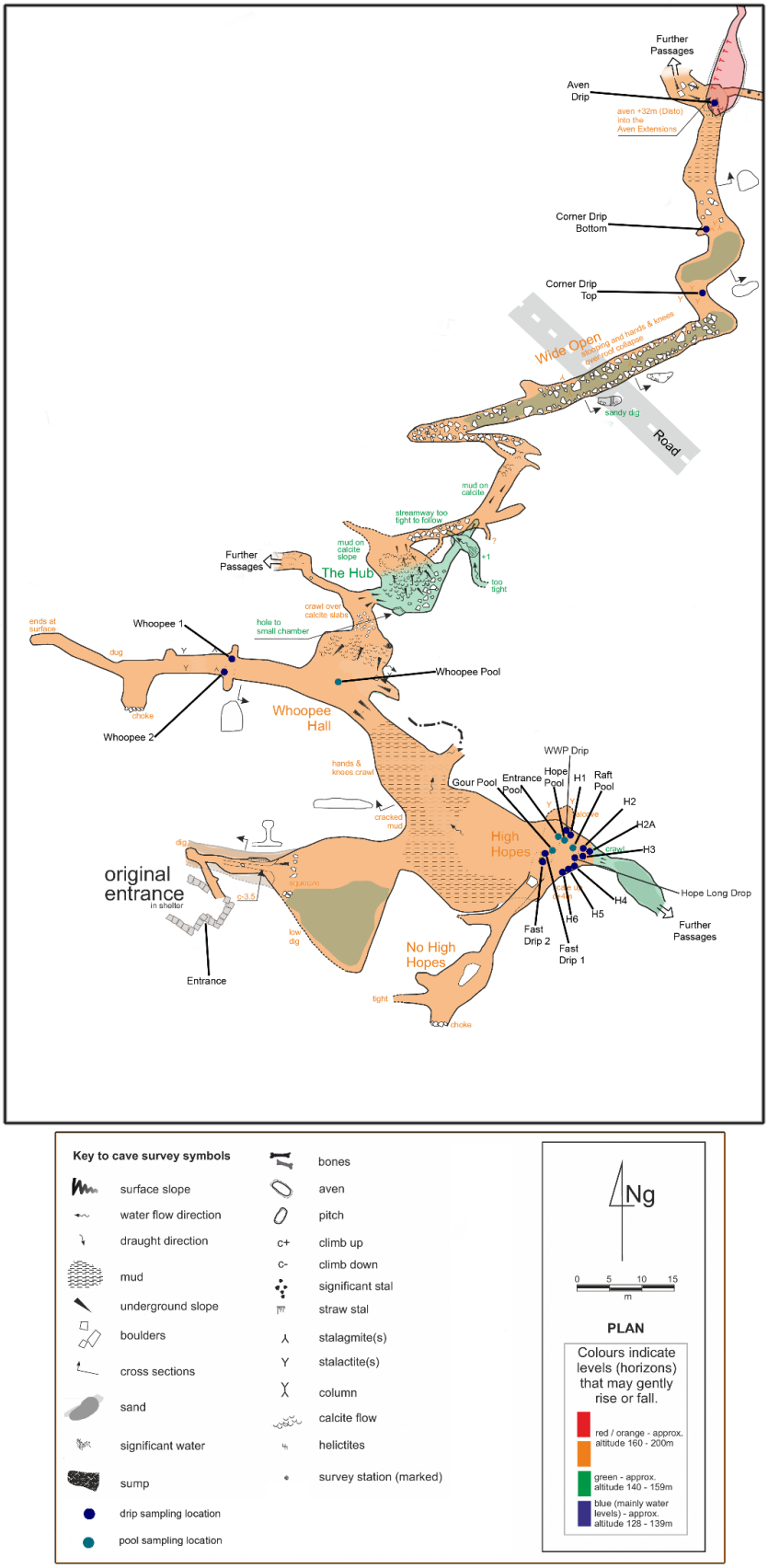

Figure 3.8: Water sampling locations within Cueva-Cubío del Llanío. 'H' refers to 'Hope'. Survey adapted from Corrin (2018)

Table 3.1: Descriptions of water sampling locations.

Sampling Location	Description
Fast Drip 1	One of the fast flowing drips above the large stalagmite in the centre of High Hopes Chamber. Dries up only under very dry surface conditions.
Fast Drip 2	One of the fast flowing drips above the large stalagmite in the centre of High Hopes Chamber. Dries up only under very dry surface conditions.
Hope 1	Slow but constant drip above the stalagmite Hope 1.
Hope 2	Above Hope 2 stalagmite. Dries up in summer.
Hope 2A	Above Hope 2A stalagmite, located behind Hope 2 and Hope 3. Dries up in summer.
Hope 3	Above Hope 3 stalagmite. Dries up in summer.
Hope 4	Above Hope 4 stalagmite. Dries up in summer.
Hope 5	Above Hope 5 stalagmite. Dries up in summer.
Hope 6	Above Hope 6 stalagmite. Dries up in summer.
Hope Long Drop	Drip from the chamber above High Hopes (No High Hopes Chamber) that drips through into High Hopes.
WWP Drip	Drip on a stalagmite above the 'Waste Water Pool' – a depression in High Hopes Chamber used to discard unused water samples.
Gour Pool	A series of gours below the large stalagmite fed by Fast Drips 1 and 2.
Entrance Pool	A pool close to the entrance of High Hopes Chamber.
Hope Pool	A pool further into the High Hopes Chamber than Entrance Pool.
Raft Pool	A pool in High Hopes Chamber characterised by a raft of calcite on the surface of the water.
Whoopee Pool	A large pool at the entrance of Whoopee Hall chamber.
Whoopee 1	A drip above a small stalagmite in Whoopee Hall.
Whoopee 2	A drip below a large hollow stalactite in Whoopee Hall.
Corner Drip Top	A drip at the top of the slope within the Corner Series.
Corner Drip Bottom	A drip at the bottom of the slope within the Corner Series.
Aven Drip	A fast dripping drip above the large stalactite in Aven chamber.

3.3.6. Vegetation and Soil Sampling

Figure 3.9 shows the sampling locations for soil and vegetation samples.

Figure 3.9 – Surface sampling locations for soil and vegetation samples. Aerial photography © Google.

Vegetation was taken from each of the four sites shown in Figure 3.9. At Entrance, three samples were taken: Entrance Vegetation Mixed, Entrance Vegetation Nettle and Entrance Vegetation Dock. The Mixed sample was a mixture of the vegetation found at the cave entrance. The Nettle sample was comprised only of dead-nettles (*Lamium sp.)* and the Dock sample was comprised only of dock leaves (*Rumex obtusifolius).* Vegetation samples taken from the Bottom Tree, Middle Tree and Top Tree were all mixed vegetation samples.

Soil samples were taken at the Bottom, Middle and Top Tree locations shown in Figure 3.9.

3.3.7. Cave Sediment Sampling

Figure 3.10 shows the sampling locations chosen for sediments from Cueva-Cubío del Llanío. S1, S2 and S4 were taken from the dry cave floor substrate, close to the cave walls but excluding larger rubble pieces. S3 was taken from the mud at the bottom of Gour Pool. S5 was a sample of a layer of geomorphically distinct mud atop further distinct layers – this layer was of a uniform thickness and came away as large sticky flakes of mud. Cave sediments were split into two sub-groups: modern and ancient. Modern sediments (S3 and S5) were both collected wet and were located underneath active drips, and thus were likely to contain modern in-washed sediments. Ancient sediments (S1, S2 and S4) were collected dry and above the active floor of the cave thus ensuring that they could not contain any recently in-washed sediments. Modern sediments were composed of soil and karst breakdown products in-washed into the cave via fracture flow, whereas ancient sediments were composite sediments comprised of aerosols, dust and drip splash alongside breakdown material from the cave chamber walls.

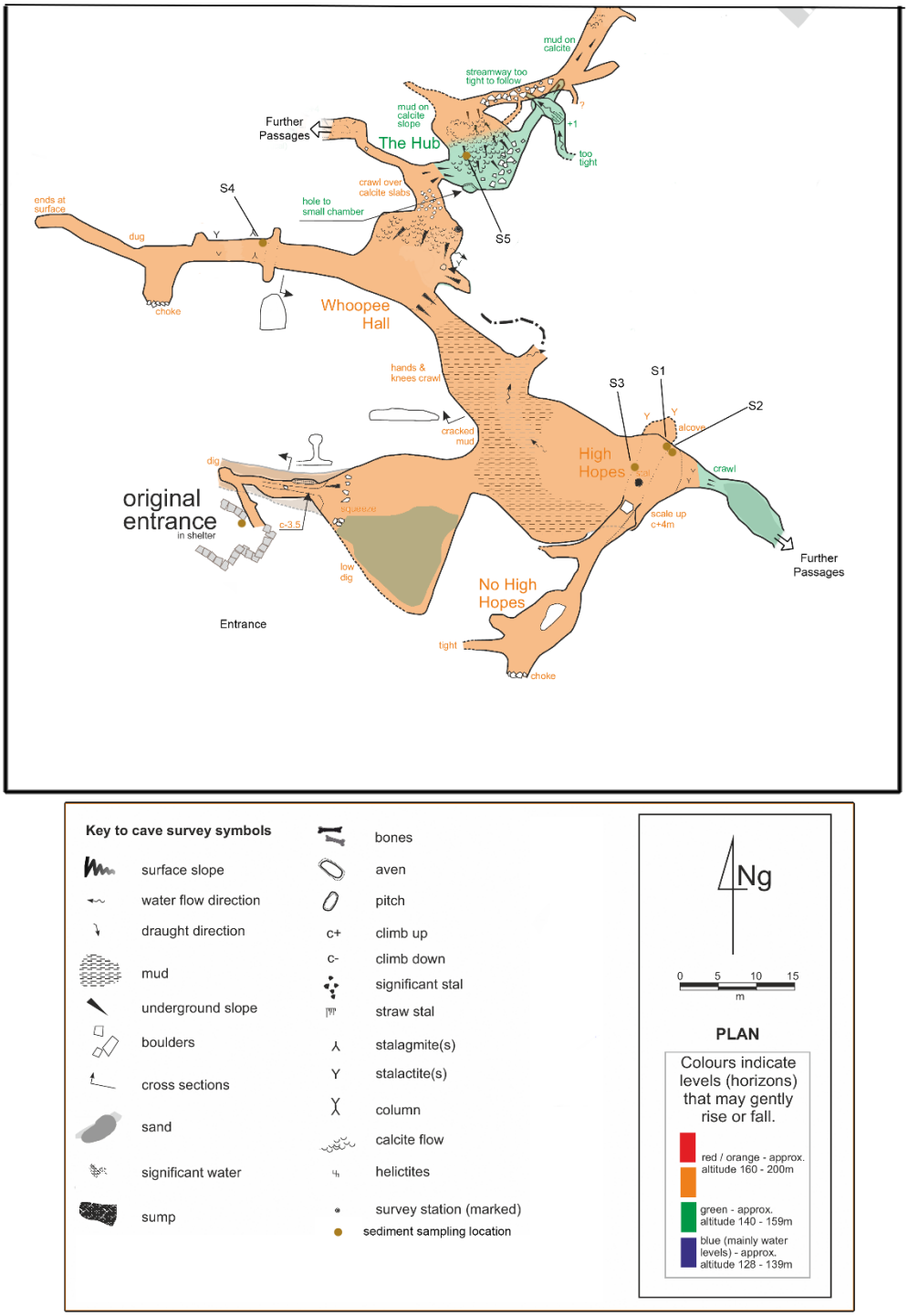

Figure 3.10 – Cave sediment sampling locations. Survey adapted from Corrin (2018).

3.3.8. Speleothem and bedrock samples

Speleothem material was collected on calcite plates and on Stalagmate loggers. Precipitated calcite was scraped off and weighed. Stalagmates left in the cave from Feb-18 to Jan-19 and calcite material was removed from these loggers in Jan-19. Calcite plates were left in the cave Jan-19 to Aug-19. Whoopee 1 was removed from the cave Jan-19. Speleothems are named after their corresponding drips – as such Figure 3.8 provides the location for each of

the speleothem samples. Bedrock samples were removed at outcrops close to the entrance of Cueva-Cubío del Llanío.

3.4. Laboratory Work

3.4.1. Sample Preparation

3.4.1.1. Soil, vegetation and cave sediments

Vegetation samples were sorted to remove any N-fixing clover and non-vegetative matter before drying. All samples were dried at 50°C – vegetation was dried for 24 hours, soil and sediments for 48 hours. Sediment and soil samples had any visible organic material removed and were sieved through a 2mm sieve to remove any larger rock particles prior to crushing. All samples were crushed using a ball mill until samples were a fine powder.

3.4.1.2. Speleothem and bedrock material

The Stalagmate loggers left in the cave had a significant amount of calcite precipitated over the time they were left over the Jan-18 to Jan-19 and Jan-19 to Aug-19 periods. Precipitated calcite was removed from the surface of the Stalagmate loggers, weighed and crushed in a pestle and mortar.

Glass plates were left in the cave following the Jan-19 visit, placed on Hope 3, 4 and 6. These glass plates were removed during the Aug-19 visit. Calcite was also removed from these plates, weighed and crushed in a pestle and mortar. Each plate yielded ~100mg of calcite.

Whoopee 1 was removed from Cueva-Cubío del Llanío and cut in half at the BGS Environmental Science Centre in Keyworth, Nottingham, UK. Samples were taken over adjacent 2.5mm transects as in Figure 3.11. Note that the two deepest samples (7.5-10.00mm and 10.0-12.5mm) are close to and/or overlap with a previous deposit not related to the current Whoopee 1 drip, thus were considered 'contaminated' by older non-contemporary material.

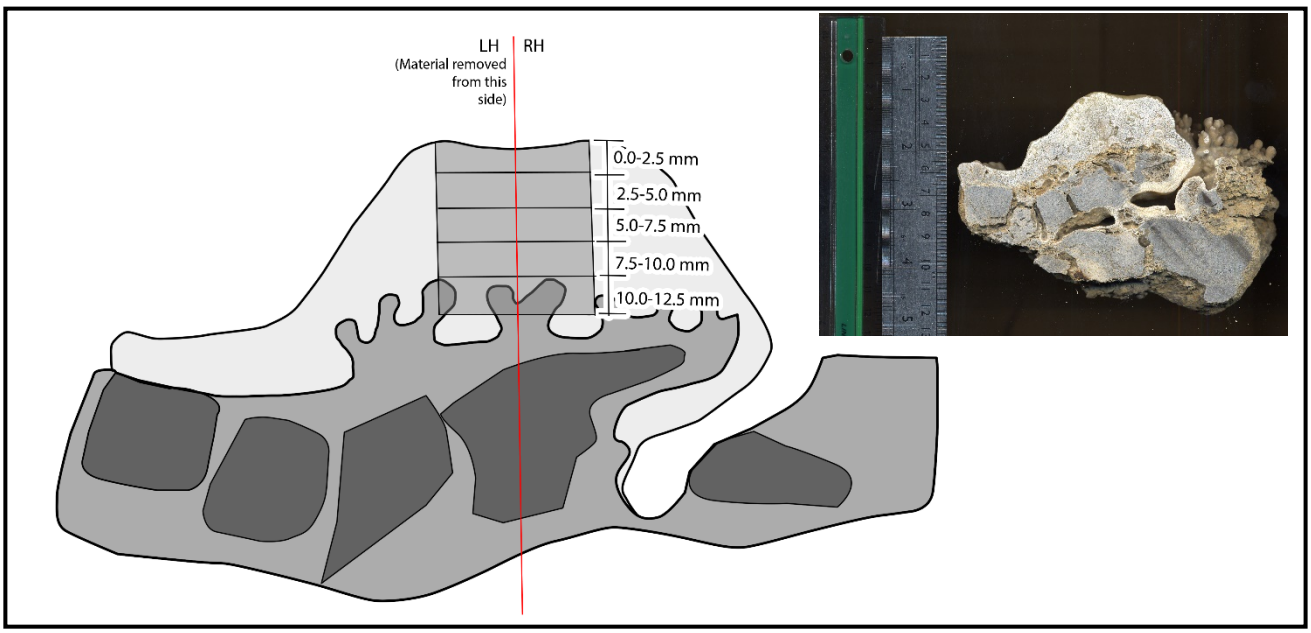

Figure 3.11 – Sampling of Whoopee 1 stalagmite from Cueva-Cubío del Llanío. Diagram not to scale. A photo of sample before sampling is presented inset for context.

Further speleothems were sampled: Browns Folley Mine (BFM) 96-2, Midlands, UK; CC-Bil, Crag Cave, Ireland; MERC-1, Rukiesa Cave, Ethiopia; and Easegill-1, Yorkshire Dales, UK. All speleothems (excluding Easegill-1) grew throughout the 20th Century and have a well constrained chronology. BFM 96-2 and CC-Bil both grew under natural vegetation and MERC-1 under cultivated land. This provides a good range of surface vegetation and overlying land management types. Easegill-1 was chosen to provide a contrast with a definite pre-anthropogenic signal.

Speleothems were first lightly scraped to remove material from the surface before samples were taken to ensure any surface contamination had been removed. Following this, 2-3 100mg samples were drilled using a COMO Drill with a diamond tipped drill bit from the scraped region of the speleothem sample. The drill bit was dipped in 1M HCl and then deionised water between samples to remove any contamination between samples. For all but Easegill-1, samples were taken from the outer growth layers of the speleothems. For Easegill-1, material was drilled from the base of the speleothem.

For nitrate concentration analysis 20mg of sample was digested in 1M HCl and diluted up to 1ml with deionised water. For nitrate isotope analysis 100mg of sample was digested in 1M HCl and diluted up to 5ml with deionised water.

3.4.2. δD and $\delta^{18}O$ Water Isotope Analysis

Continuous flow isotope ratio mass spectrometry was used to determine water sample D/H and $^{18}O/^{16}O$ ratios – an Elementar pyrocube elemental analyser coupled with an Isoprime 100 mass spectrometer were used. For D/H, sample injection aliquots of 0.3µl were used, which were reduced to hydrogen at 1050°C over chromium metal catalyst. $\delta^{18}O$ was determined using pyrolysis mode with sample injection of 0.4µl over glassy carbon chips at 1450°C. δD and $\delta^{18}O$ values were corrected against laboratory calibration standards relative to V-SMOW. Within-run standard replication (1SD) was better than +/- 0.06‰ for $\delta^{18}O$ and +/- 0.4‰ for δD.

3.4.3. Trace Element Analysis

Inductively coupled plasma optical emission spectrometry (ICP-OES) analysis was performed on filtered (0.2µm filter) water samples using a Thermo Scientific iCAP 600 series. Before analysis, all water samples were acidified within their 60ml collection bottles using ultra-pure (Primar grade) HNO_3 to create a 0.1M nitric acid solution, thus enabling matrix matching of samples and standards. HNO_3 also enabled desorption of cations from the sidewalls of the HDPE sample bottles.

Standard solutions were made using 1000ppm elemental standards which were diluted to predicted cave and rain water concentrations as seen in Table 3.2. A five-point calibration curve was created from the standards, from which trace element concentrations for the unknown samples were derived. A check standard made to 1000ppb for all elements was run every 10 samples to ensure machine stability. Limits of detection (LOD) were calculated – three times the standard deviation of the blanks run alongside the batch if the mean blank value was negative, mean blank value + 3 * stand deviation when the mean blank value was positive. Precision was better than 95% based on repeat analysis of internal standard materials.

Table 3.2: Cation standard information. Calibration standard ranges and limits of detection for elements analysed using ICP-OES.

Element	Calibration standard range	LOD
Calcium	0-100 ppm	0.036 ppm
Magnesium	0-10 ppm	0.001 ppm

3.4.4. N Concentration Analysis

3.4.4.1. Drip waters, bedrock and speleothem material

1ml of sample was pipetted into an Eppendorf tube and analysed by auto-colorimetry using a SEAL AQ2 analyser. The colorimetry reaction was based on the cadmium reduction of nitrate to nitrite to produce a pink colouration, which was measured at a wavelength of 520 nm. As there was very little nitrite in samples and this analysis measures nitrate + nitrite concentration, values are reported as nitrate-N.

Within run standards of similar concentration to samples (between 0.25 to 1ppm of nitrate N) were analysed in all run sequences and reported to within ±5% of reported values. The precision of this check standard was ±5%.

3.4.4.2. Soil, vegetation and cave sediments

Prepared samples were weighed into tin capsules. Weighed samples were combusted in an Elemental Analyser at 1100°C, converting all available constituent N into N_2 gas which was then analysed by a mass spectrometer for ^{15}N and ^{14}N ratios. Concentrations were calculated using the '% each' data provided as part of the analysis.

3.4.5. Isotope Analysis

3.4.5.1. Bacterial method for rainfall, cave drip water, bedrock and speleothem material

Bacterial denitrification was used to analyse samples for the N isotope analysis of nitrate in water and dissolved and neutralised rock/speleothem material samples. *Pseudomonas aureofaciens* was chosen as the denitrifier strain for bacterial denitrification of samples, as this strain allows for the determination of the oxygen isotopic composition of nitrate as well as the N isotopic composition (Sigman *et al*., 2001). NO_3 in samples are converted to N_2O gas without isotopic fractionation and the N_2O gas can then be analysed by mass spectrometer.

3.4.5.1.1. Preparation of Denitrifier Cultures

3.4.5.1.1.1. Media

800 ml of deionised water was mixed with 1.8g KNO_3, 0.45g $(NH_4)_2SO_4$, 11.7g K_2HPO_4 and 54g Triptych Soy broth granules in a 2L glass beaker. 445 ml of this medium was transferred into 500ml media bottles. Stoppers and bottle tops were wrapped with foil. Filled 500 ml media bottles were then autoclaved for 1 ½ hours and left to cool within the autoclave. Media bottles were stoppered and crimp sealed immediately after removal from autoclave. This media can be kept in the dark at room temperature for a year but were discarded if the bottles became cloudy at any point.

3.4.5.1.1.2. Plates

30g Tryptic Soy Agar granules were added to 500ml of freshly made media then autoclaved for 30 minutes. Controlled cooling was achieved in an oven. Agar was poured while still warm. Plates were filled ¾ full and left to dry overnight with lids on and then sealed with

parafilm. Plates were preferentially stored at room temperature, to avoid the condensation produced by fridge storage.

3.4.5.1.1.3. Nitrate free media (NFM)

Using a 2L glass beaker, 2000ml of deionised water was mixed with 0.5g $(NH_4)_2SO_4$, 13g K_2HPO_4 and 60g Triptych Soy broth granules. This was decanted into 250ml Duran bottles and autoclaved for 30 minutes. NFM was stored at room temperature and discarded if cloudy.

3.4.5.1.1.4. Revival of bacterial culture from stock

A sterile 100µL pipette tip was used to remove frozen cells from the frozen 2.5ml Eppendorf tubes used to store frozen cultures. Eppendorf tubes were only removed from the freezer for this process and were returned immediately following its completion. Plates were then streaked and sealed with parafilm. Loop was flamed between streaks.

Plates were incubated in the dark at room temperature for 3-4 days. Further plates were inoculated every 3-4 days.

3.4.5.1.1.5. Inoculation of *Pseudomonas aureofaciens*

A single colony was transferred to a 9ml media tube, which was capped and sealed with parafilm. This was done twice. Both media tubes were incubated overnight at room temperature on a shaker – tube was in a horizontal position.

Media from 2 tubes was mixed into a larger tube. This larger tube was used to inoculate the media bottles. 2.7ml of the bacterial media was injected into each media bottle by injecting through the crimp seal. Bottles were then placed, covered, on a shaker table for 6-10 days.

3.4.5.1.1.6. Concentrating the bacteria

Culture was divided evenly between 250ml pre-autoclaved centrifuge bottles. Bottles were centrifuged for 10 minutes at 4950 rpm. Liquid was poured off centrifuge bottles carefully, with cells left at bottom of bottle. Bottles were kept upside down. NFM was added to one centrifuge bottle (0.15ml of NFM per 1ml of original medium). NFM was poured back and forth between all centrifuge bottles until all cells were resuspended in one bottle. Antifoam was added to this bottle and swirled to mix. Amount added depended on number of media bottles used for this step.

3.4.5.1.1.7. Preparation of sample vials

3ml of cell concentrate was pipetted into 20ml headspace vials. Vials were crimp sealed and then purged with helium gas.

3.4.5.1.2. Sample injection

Sample was injected into prepared vials through seal using an airtight syringe with a 25 gauge needle. Sample injection volume was pre-calculated to give 20 nM of NO_3. For speleothem digests, all 5ml of the digest was injected.

Vials were then incubated at room temperature for a few hours in inverted position to prevent gas leakage. Following this incubation period 0.1-0.2 ml of 6M NaOH was injected into each vial to lyse the bacteria.

3.4.5.2. Isotope analysis following bacterial method

Within a few days of sample injection, the N_2O headspace vials produced by the bacterial method were analysed for $\delta^{15}N$ and $\delta^{18}O$ isotope ratios using an Isoprime trace gas analyser

linked to a controlled flow GV-Isoprime mass spectrometer. Standard precision was better than +/- 0.08‰ for $\delta^{15}N$ and +/- 0.27‰ for $\delta^{18}O$ for international standards. Internal standards, used for drift correction, had standard precisions better than +/- 0.18‰ for $\delta^{15}N$ and +/- 0.32‰ for $\delta^{18}O$. $\delta^{15}N$ values were corrected against laboratory calibration standards relative to N_{AIR} and $\delta^{18}O$ values were corrected relative to V-SMOW.

3.4.5.3. Isotope analysis of soil, vegetation and cave sediment samples

Prepared samples were weighed into tin capsules. Weighed samples were combusted in an Elemental Analyser at 1100°C, converting all available constituent N into N_2 gas which was then analysed by a mass spectrometer for ^{15}N and ^{14}N ratios. Standard precision in international standards was better than +/- 0.03‰ for $\delta^{15}N$ for the vegetation sample run and +/- 0.15‰ for $\delta^{15}N$ for soil and sediment sample run. $\delta^{15}N$ values were corrected against laboratory calibration standards relative to N_{AIR}.

3.5. Summary

This section has provided a description of the field and laboratory methods used in this thesis. A summary of laboratory methods can be seen in Table 3.3.

Table 3.3: Summary of laboratory methods.

Sample Type		Analysis	Method
Soil		$\delta^{15}N$	Isoprime100 IMRS coupled with a VARIO PYROcube Elemental Analyser
Sediment		$\delta^{15}N$	Isoprime100 IMRS coupled with a VARIO PYROcube Elemental Analyser
Vegetation		$\delta^{15}N$	Isoprime100 IMRS coupled with a VARIO PYROcube Elemental Analyser
Water		Cations	ICP-OES
		$\delta^{18}O\text{-}H_2O$	Isoprime100 IMRS coupled with a VARIO PYROcube Elemental Analyser
		$\delta D\text{-}H_2O$	Isoprime100 IMRS coupled with a VARIO PYROcube Elemental Analyser
		$\delta^{15}N\text{-}NO_3$	Isoprime trace gas analyser linked to a controlled flow GV-Isoprime mass spectrometer
		$\delta^{18}O\text{-}NO_3$	Isoprime trace gas analyser linked to a controlled flow GV-Isoprime mass spectrometer
Carbonates	Speleothem Material and Modern Calcite	$\delta^{18}O\text{-}NO_3$	Isoprime trace gas analyser linked to a controlled flow GV-Isoprime mass spectrometer
		$\delta^{15}N\text{-}NO_3$	Isoprime trace gas analyser linked to a controlled flow GV-Isoprime mass spectrometer
	Bedrock	$\delta^{18}O\text{-}NO_3$	Isoprime trace gas analyser linked to a controlled flow GV-Isoprime mass spectrometer
		$\delta^{15}N\text{-}NO_3$	Isoprime trace gas analyser linked to a controlled flow GV-Isoprime mass spectrometer

4. Cave Monitoring

4.1. Temperature Dynamics

4.1.1. External Atmospheric Temperature

The average temperature over the Jan-18 to Jan-19 logging period was 14.4°C. Temperatures rarely fell below freezing whilst maximum temperatures were over 20°C for almost all months in the long-term record (Figure 4.1). There is evidence of a seasonal cycle in the long-term record (Figure 4.1), with the warmest months occurring in June, July, August (average monthly temperatures exceed 20°C) and the coldest months occurring in December, January, February (average monthly temperatures below 10°C). Table 4.1 shows the monthly average, minimum, maximum and range for the Jan-18 to Jan-19 record – displaying what seems to be a typical year for the local area.

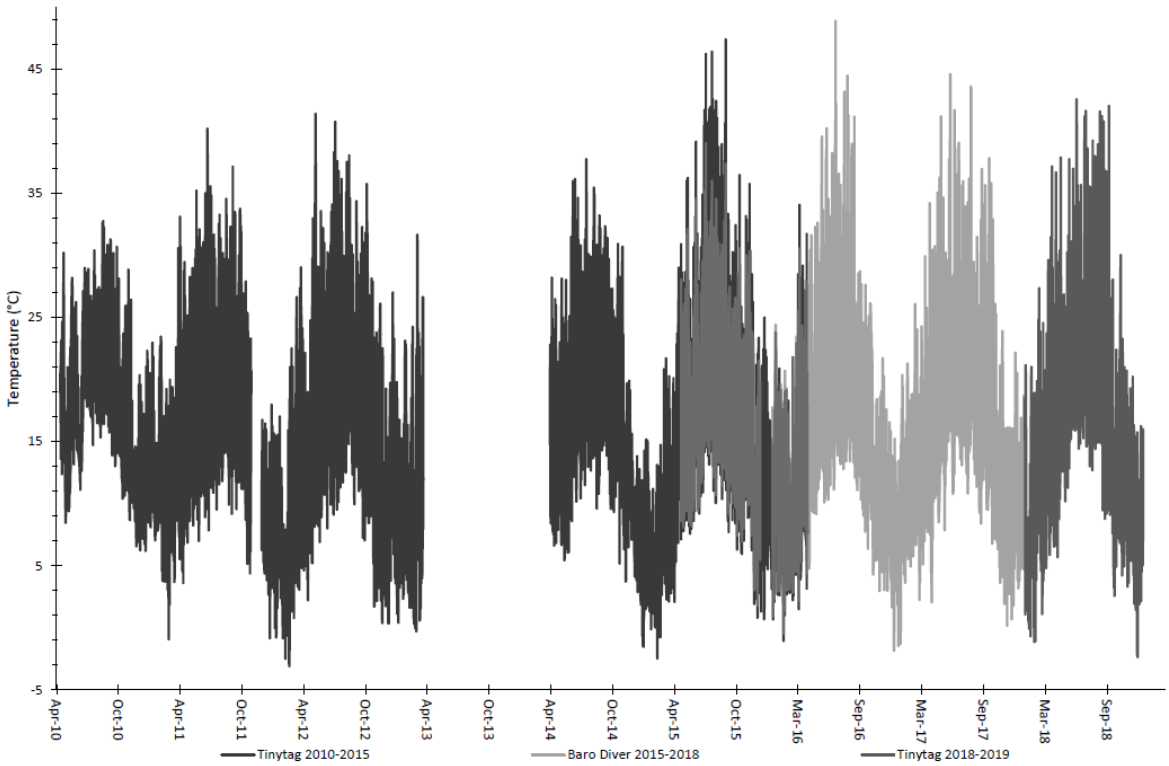

Figure 4.1 - External hourly average temperatures. External loggers were placed on the slope outside Cueva de las Perlas and Cueva de Asiul (43°19'00.1"N 003°35'40.1"W, 293m a.s.l). Data from 2010-2018 taken from Deeprose (2018).

Table 4.4 – Monthly temperatures from Jan-18 to Jan-19. Data averaged from hourly external temperature monitoring.

	MONTHLY AVERAGE (°C)	MONTHLY MIN (°C)	MONTHLY MAX (°C)	MONTHLY RANGE (°C)
JAN-18	9.1	1.1	21.1	20.1
FEB-18	6.4	-1.1	21.0	22.1
MAR-18	10.7	1.1	27.3	26.2
APR-18	13.9	5.5	37.2	31.6
MAY-18	15.8	5.7	37.9	32.2
JUN-18	20.2	11.3	42.6	31.3

JUL-18	21.2	14.4	41.6	27.2
AUG-18	20.3	12.7	39.2	26.6
SEP-18	18.8	8.8	41.6	32.8
OCT-18	13.2	2.6	42.0	39.5
NOV-18	11.8	3.3	30.0	26.7
DEC-18	8.0	-2.4	20.2	22.6
JAN-19	7.5	2.2	16.2	14.1

4.1.2. Cave Air Temperature

4.1.2.1. Results

The average temperature within Cueva-Cubío del Llanío was 12.6°C. The average temperature within the Entrance Shelter was 10.8°C, whilst the average temperature within the two cave chambers monitored was 13.2°C (High Hopes Chamber) and 13.8°C (Whoopee Hall). All temperatures within the cave were lower than that of the external average temperature (14.4°C).

Throughout the annual cycle, in-cave temperatures display periods of both stability and instability. Stable temperatures typically pervade during the summer months of Jun-18 and Sep-18 (Figure 4.2). However, periods of instability extend throughout the autumn until spring of the following year, with this instability reducing as one moves further into the cave.

During periods of stability, cave air temperature in High Hopes Chamber became cooler than that of Whoopee Hall by approximately 2°C (Figure 4.2). During periods of instability, this reversed, with High Hopes Chamber cave air becoming warmer than Whoopee Hall cave air. It is also of note that Whoopee Hall cave air temperatures begin to break down into the unstable temperature regime earlier than that of High Hopes Chamber.

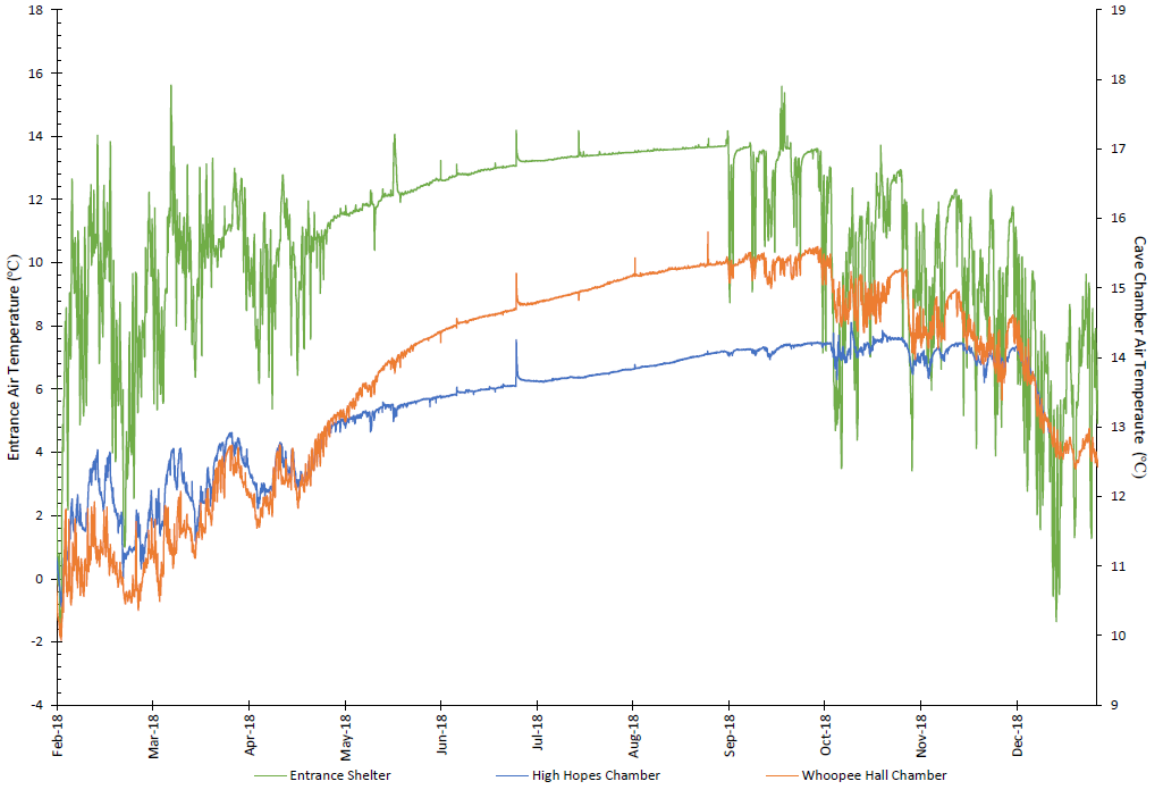

Figure 4.2 – Half hourly temperature in three areas of Cueva-Cubío del Llanío. Whoopee Hall and High Hopes Chamber have been plotted on a secondary axis to show the smaller variations in comparison to the noisier temperature signal of the Entrance Shelter.

Periods of stability and instability in cave air temperature occur concurrently with changes in external air temperature (Figure 4.3). Examining external air temperature against one of the internal cave air temperature loggers, it can be noted that the periods of instability that occur during the colder months coincide with periods when external air temperatures drop below that of cave air temperature (Figure 4.3). Equally, in Figure 4.3, the period of stable cave air temperature coincides with periods when external air temperature stops dropping below the internal cave air temperature.

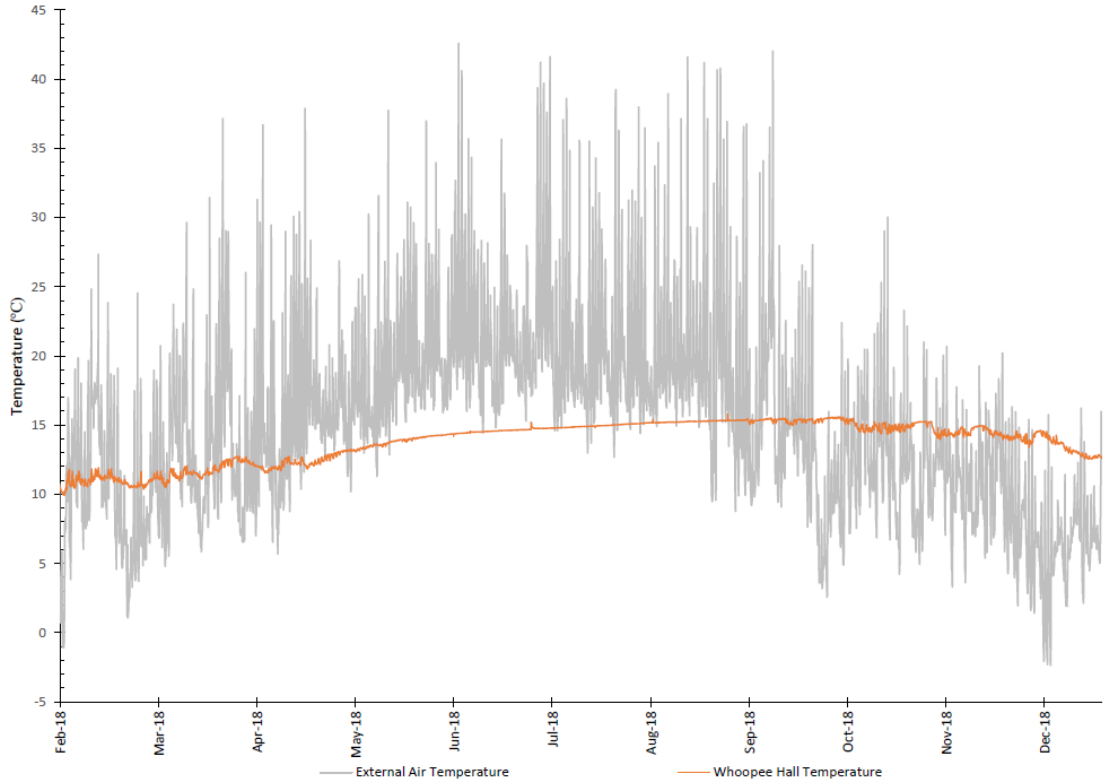

Figure 4.3 – Hourly external air temperatures and half-hourly cave air temperatures from Whoopee Hall.

4.1.2.2. Discussion

This cave displays a seasonal density-driven ventilation effect – during periods where cave air temperature remains above external temperature, cold dense air moves into the cave. This leads to continuous ventilation. Conversely during periods where cave air temperature is consistently lower than external air temperature, air is drawn out of the cave, thus leading to a more stable temperature regime.

Cave air temperature is also moderated by the specific heat capacity of the rock. Heat is exchanged between the cave air and rock surface, which is never in equilibrium with deeper layers of rock and never in equilibrium with cave air temperature (Badino, 2010). This continuous exchange helps to moderate cave air temperatures.

Whoopee Hall appears to be more connected to the density-driven seasonal ventilation regime than High Hopes – the fluctuations in temperature are greater for Whoopee Hall and Whoopee Hall enters the instable winter ventilation regime much earlier than High Hopes Chamber, suggesting High Hopes may be somewhat cut off from the main path of ventilation.

4.1.3. CO_2 Concentrations in Cave Air

4.1.3.1. Results

Carbon dioxide concentrations are plotted in Figure 4.4 and compared to trends in temperature recorded externally to the cave and within High Hopes Chamber. CO_2 records in Jan-Feb 2019 are substantially lower than in Apr-May 2019. During the Apr-19 monitoring period, external air temperature exceeds the internal cave air temperature in High Hope Chamber a greater number of times and at a higher frequency than during the Jan-19 monitoring period.

Instability in CO_2 concentrations is greater during the Apr-19 monitoring period. Toward the end of the Jan-19 monitoring period CO_2 concentrations are also beginning to become more unstable, as external air temperature first exceeds that of the cave air temperature.

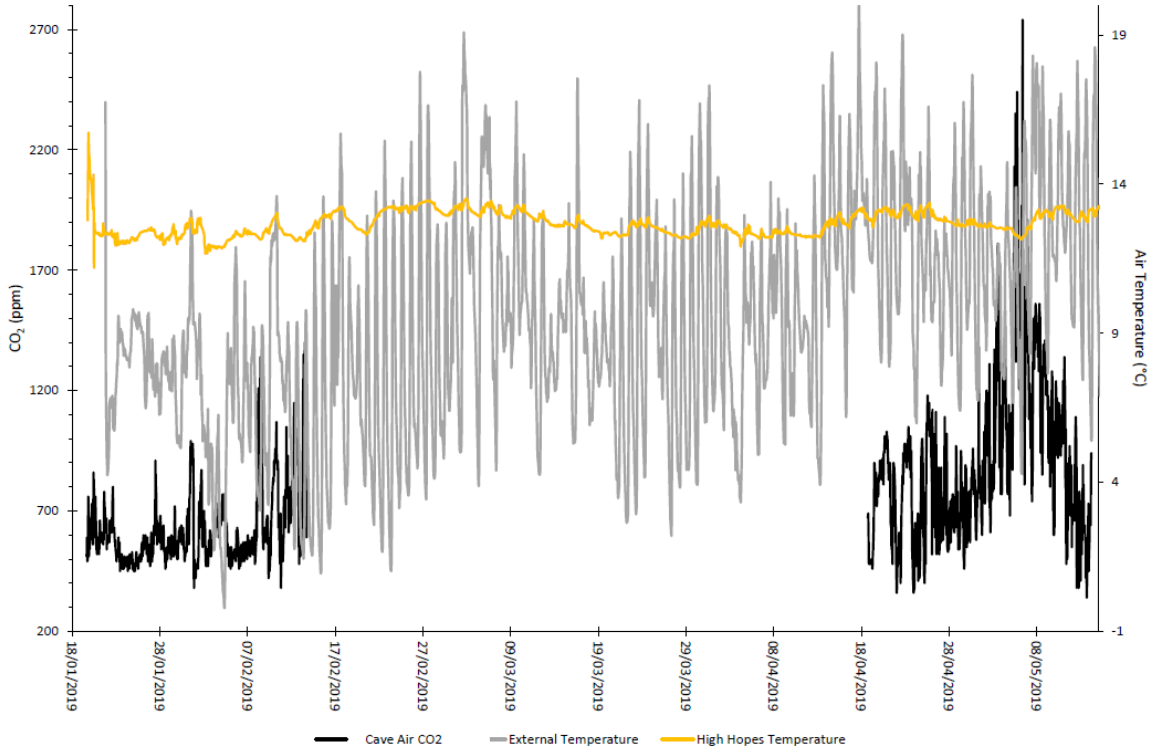

Figure 4.4: Jan-Feb and Apr-May 2019 CO_2 logging periods compared to the long-term temperature records.

In the Jan-19 to Feb-19 monitoring period, cave air CO_2 fluctuated between approximately 400ppm and 1400ppm (Figure 4.5). External air temperature did not exceed internal cave air temperature often – only two times during this month-long period. In all occasions where external air temperature was greater than internal cave air temperature, cave air CO_2 spiked notably.

On occasion CO_2 will rise as external temperature and cave air temperature falls. This is the opposite of the expected pattern – CO_2 is expected to rise with cave and external air temperatures. Some examples of this pattern can be seen in Figure 4.5 between 21-23rd Jan-19, 26-28th Jan-19, 1st-4th Feb-19 and 7th Feb-19.

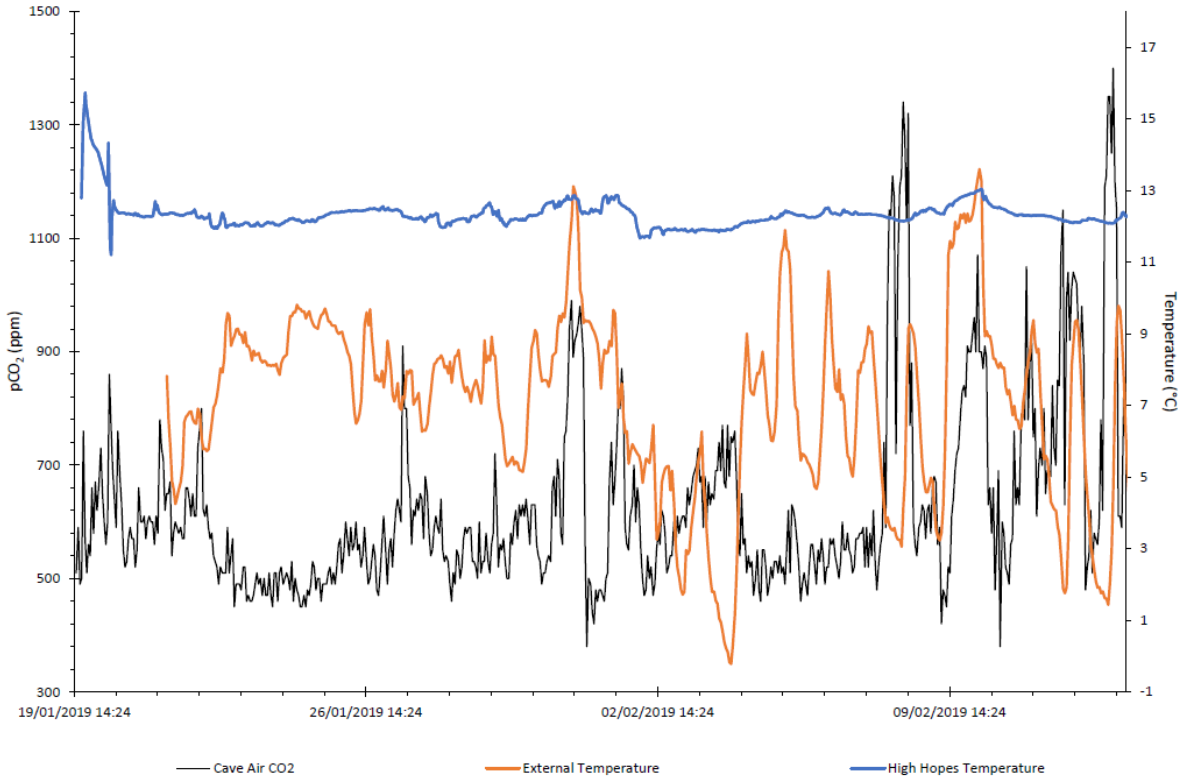

Figure 4.5: Jan-19 to Feb-19 CO_2 monitoring records with external air temperature and High Hopes chamber cave air temperature displayed.

In the Apr-19 to May-19 monitoring period shown in Figure 4.6, cave air pCO_2 fluctuated between approximately 500 and 2600ppm, with pCO_2 generally increasing during the month-long monitoring period until 5th May-19 and then falling again following the peak on 4-5th May-19. Unlike in the Jan-19 monitoring period, external temperature exceeded internal cave air temperature often during the Apr-19 monitoring period.

Cave air pCO_2 is more closely aligned with air temperature during this monitoring period, with fewer examples of the reversed relationship where CO_2 rises with falling air temperatures (and vice versa). There are still some examples of inverse temp-CO2 dynamics during the Apr-19 monitoring period however, (e.g. 28th Apr-19 to 2nd May-19 and 9-10th May-19), likely attributed to temperature differentials driving reverse ventilation dynamics through the cave system (Figure 4.6).

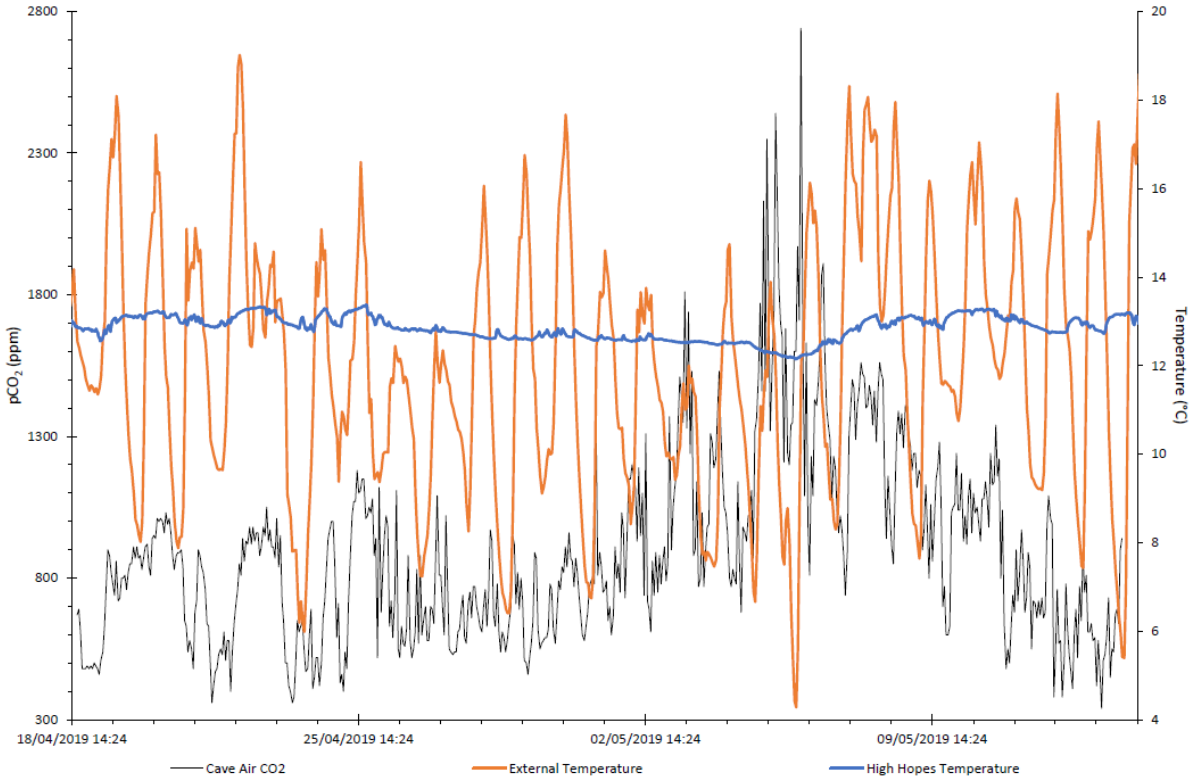

Figure 4.6: Apr-19 to May-19 CO_2 monitoring records with external air temperature and High Hopes cave air temperature displayed.

A diurnal pCO_2 fluctuation was also observed (Figure 4.7). Here it can be seen that during the day cave air generally rises (as external temperatures rise above internal cave air temperatures) and then fall rapidly in the night (as external air temperatures drop below internal cave air temperatures). This pattern is most clear during 23-Apr-19. In days where external air temperatures do not exceed internal cave air temperatures, CO2 can be seen to fluctuate greatly throughout the day (26-Apr-19 in Figure 4.7).

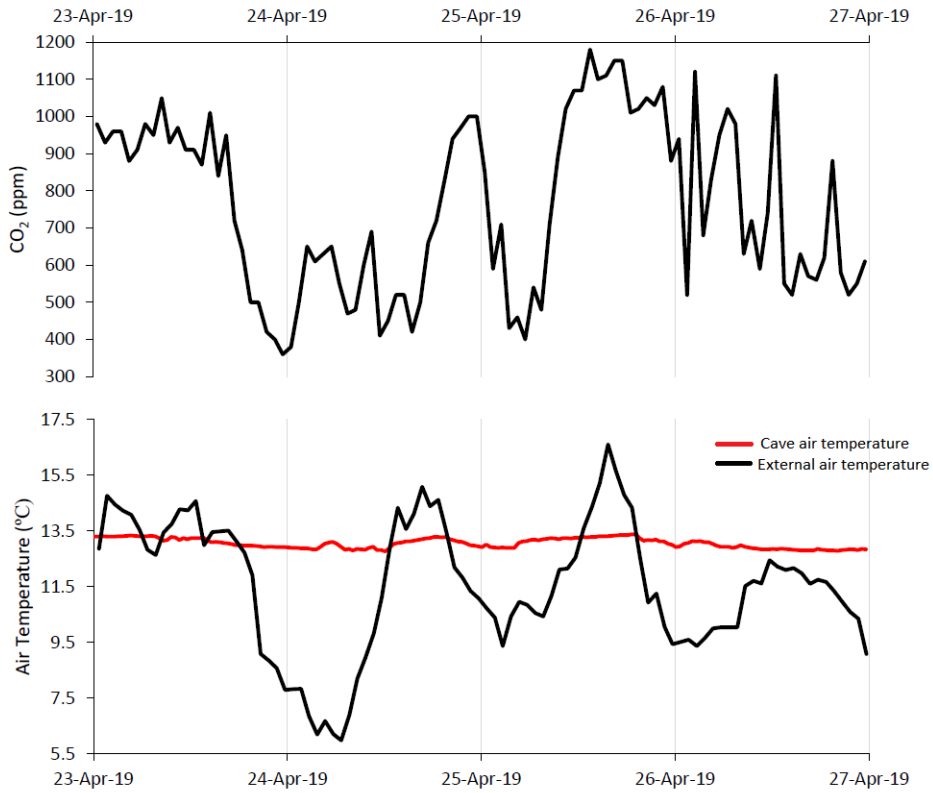

Figure 4.7: Diurnal CO_2 concentrations from 23-Apr-19 to 27-Apr-19 in High Hopes chamber, with High Hopes chamber cave air temperature contrasted against external air temperature.

4.1.3.2. Discussion

External air temperature has an influence on cave air pCO_2 in two differing patterns.

The first is that as external air temperature rises, so does cave air pCO_2. This pattern is due to the airflows that accompany a density driven ventilation regime in caves – when external air temperature rises above the internal cave air temperature, the external air mass is less dense than that within the cave, thus the external air mass rises and draws out of the cave. To accommodate for this, air is drawn into the cave through the soil and karst (and thus through the high pCO_2 ground air) and into cave chambers, leading to a build-up of CO_2 in the cave chambers. When external temperature drops, the external air mass is denser than that within the cave, thus external CO_2-poor air sinks into the cave and replaces the CO_2-rich internal air.

This density-driven ventilation dynamic and accompanying changes in pCO_2 can be seen whenever the external air temperature exceeds internal cave air temperature – such as 25-Apr-19 in Figure 4.7.. Here, external temperatures exceed internal values and CO_2 values begin to fluctuate to higher levels. This becomes more frequent with seasonal progression due to density-driven air circulation, which restricts the ingress of CO_2-poor external air to flush the cave. This can account for the increased pCO_2 in the cave during the Apr-19 logging period, as there is less ventilation to remove CO_2 from the cave air. However even though external air temperatures continued to surpass that of internal cave air temperatures, there was a clear reduction in cave air pCO_2 following a peak on 04/05/19 (Figure 4.6).

The second pattern is a reverse of the normal dynamic – here CO_2 rises as air temperatures fall. This is common during the Jan-19 logging period – see Figure 4.6. It is uncertain as to

why CO_2 occasionally rises as air temperature falls. A working theory is that due to the complexity of Cueva-Cubío del Llanío, which has multiple entrances and a complex series of caverns and passages beyond the study area, there may be areas deeper in the cave that are warmer than High Hopes Chamber and Whoopee Hall. Airflow from the external environment may be drawn deeper into the cave and effectively 'cut off' High Hopes Chamber from ventilation (Figure 4.8). There is limited evidence to support this theoretical model of ventilation in Cueva-Cubío del Llanío - no cave air temperature record exists for deeper chambers as of writing. However, drip water temperatures taken from deeper within the cave – the Corner Bottom, Corner Top and Aven samples – all are roughly a degree warmer than the water samples taken in High Hopes Chamber and Whoopee Hall (Figure 4.8).

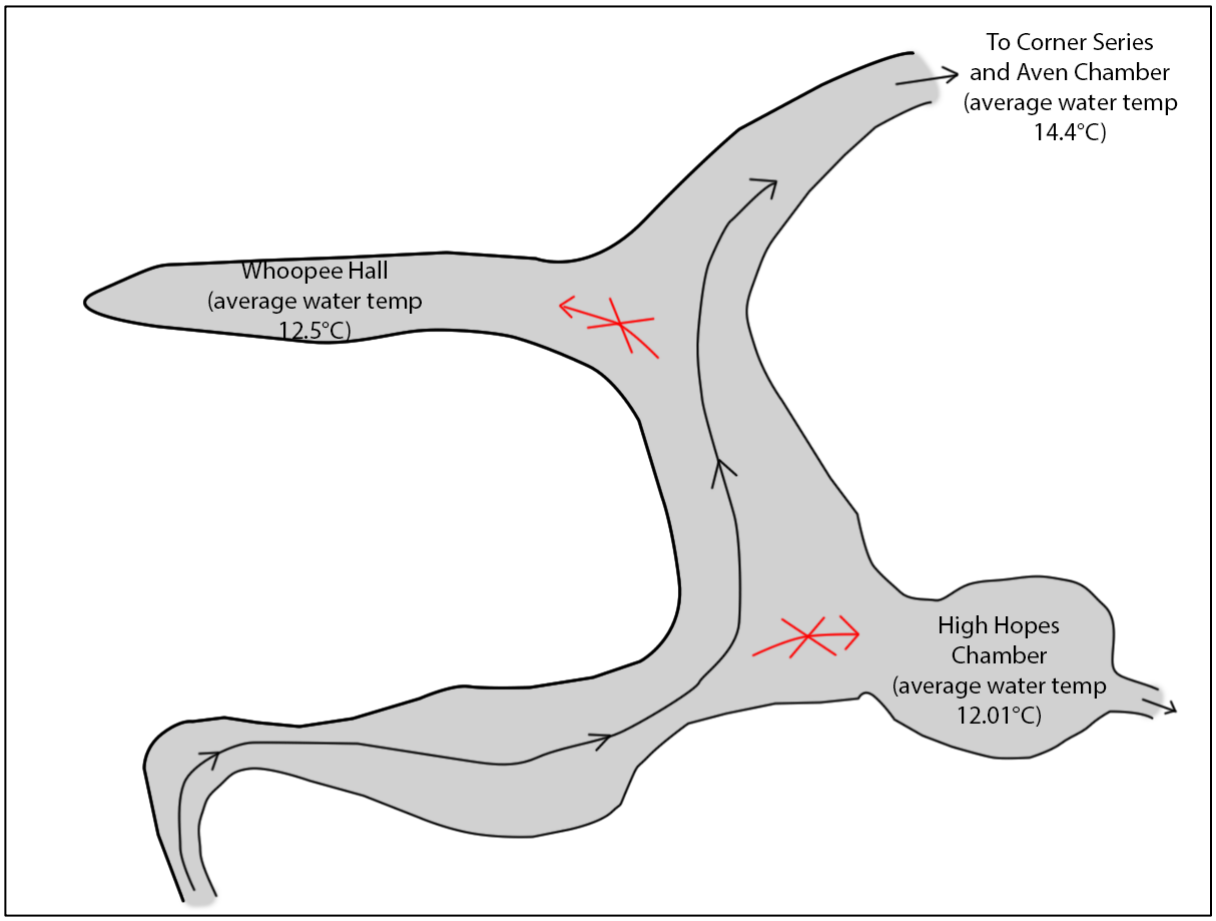

Figure 4.8: A diagram of the theoretical model of cave ventilation in Cueva-Cubío del Llanío with average drip water temperatures added to demonstrate the likely difference in chamber temperatures between High Hopes and Whoopee Hall and deeper cave sites.

4.1.4. Ventilation Dynamics in Cueva-Cubío del Llanío

Cueva-Cubío del Llanío displays a typical seasonal ventilation regime when excluding High Hopes Chamber. During winter months, a density-driven ventilation regime is established as external temperature remains below internal cave temperature, leading to an influx of cool, CO_2-poor, dense air into the cave. During summer months, this density-driven ventilation regime breaks down as external temperatures exceed internal cave air temperatures, leading to a build-up of CO_2 due to the stagnation of the air mass within the cave.

There is an exception in High Hopes Chamber to this regime. On occasion, it appears as though cave ventilation will flow past shallower chambers (e.g. Whoopee Hall and High Hopes). Theoretically it may be drawn more strongly into warmer, deeper chambers within the cave (Figure 4.7), thus shallower chambers will not be flushed with external CO_2-poor air, leading to a build-up in CO_2 concentrations in these chambers even as the cave chamber air temperature falls. High Hopes appears to be a side chamber that contains a stagnant air pocket, its temperature and pCO_2 are controlled by multiple temperature variations throughout the cave system.

4.2. Rainfall

4.2.1. Results

The Matienzo rainfall record shown in Figure 4.9 demonstrates that the region in which Cueva-Cubío del Llanío sits primarily receives the largest input of rainfall during the winter months, with summer months tending to be drier with less intense periods of rainfall if there is any rainfall at all. 2012 was a particularly wet year compared to the rest of the record.

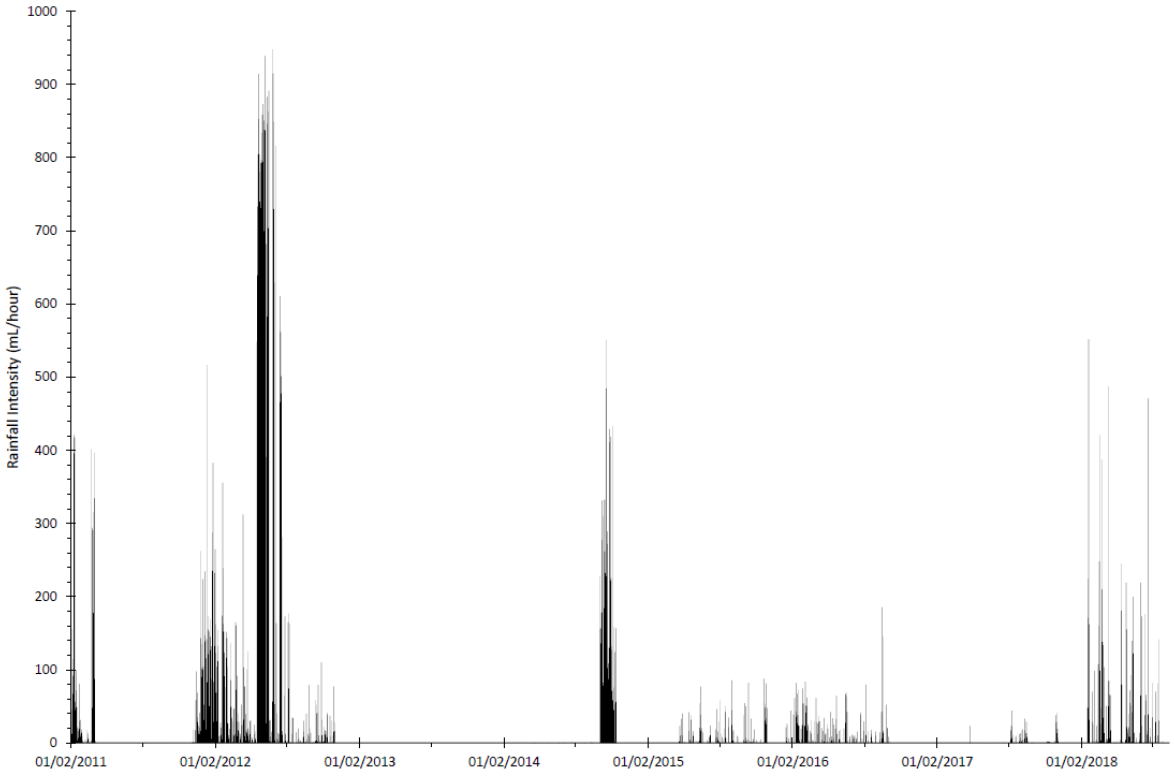

Figure 4.9 – An extended rainfall intensity record, with further data taken from Deeprose (2018). Note there is a hiatus in the data in 2013/2014.

The wettest month over the logging period (Feb-18 to Aug-18) was March, with an average of 74.3 mm (Table 4.2) of rain falling each day. The most intense rainfall event occurred in February, where 552 mL (Table 4.2) of rain fell in a single day. The driest month was August, which had the least rain on average (11.7 mL/day, Table 4.2).

Not only was March the wettest month on average, it also contained the fewest days with no rainfall (4 days without rainfall), whilst August contained the most days with no rainfall (21 days) (Table 4.2).

Rainfall in the area appears to be intense but short, with rainfall events lasting no more than a few days at most (with an exception being found in the latter half of Mar-18 where there were two periods of consecutive and intense week-long rainfall events) – Figure 4.10 displays this short intense rainfall pattern.

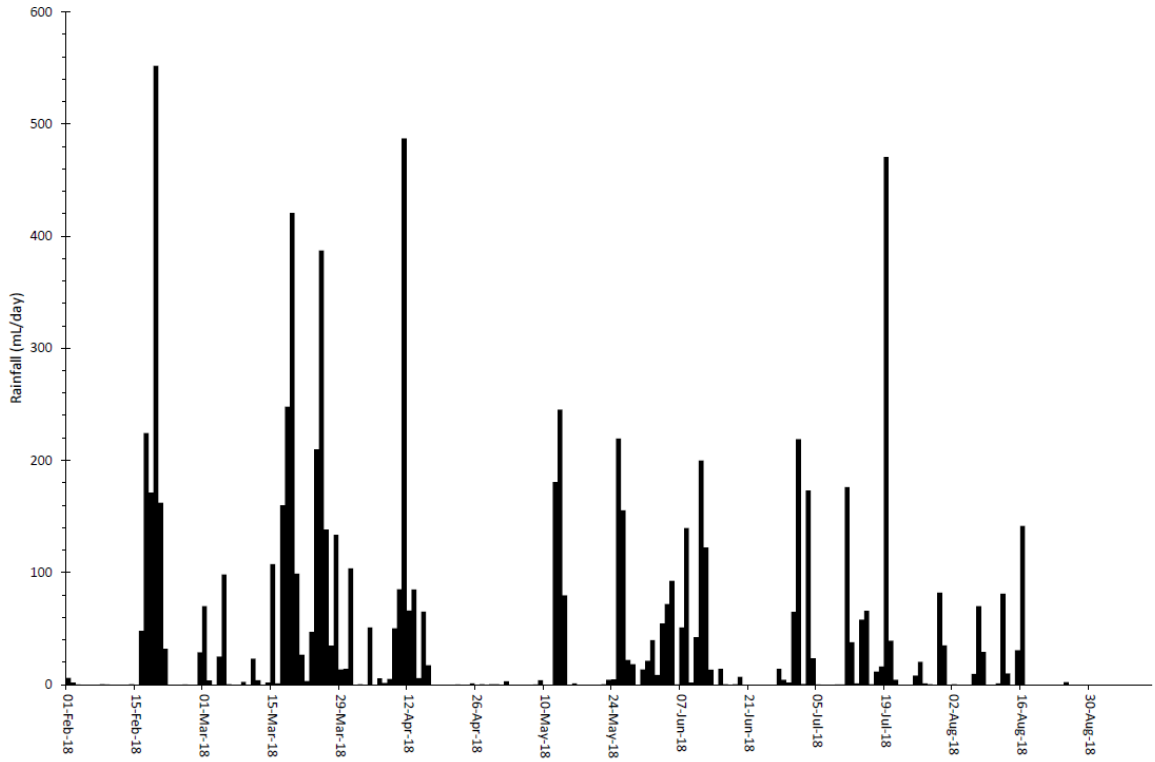

Figure 4.10 – Rainfall data from Feb-18 to Aug-18. Pluvimate was placed within Matienzo village, roughly 4.4km from the entrance to Cueva-Cubío del Llanío.

Table 4.5 – Monthly rainfall from Feb-18 to Aug-18. Data average from daily rainfall monitoring.

	AVERAGE RAINFALL (mL)	MAXIMUM RAINFALL (mL)	NUMBER OF DAYS WITHOUT RAINFALL
FEB-18	42.3	552	14
MAR-18	74.3	420.6	4
APR-18	29.9	487.3	12
MAY-18	30.4	245.3	15
JUN-18	30.4	199.9	9
JUL-18	45.1	470.7	7
AUG-18	11.7	141.5	21

4.3. Drip rate Response to Rainfall Events

4.3.1. Results

Drip rates for both loggers was plotted against rainfall data in Figure 4.11. Overall Whoopee 1 had a more stable drip rate than that of Hope 3. Whoopee 1 also had the higher average drip rate, with an average of 3410.6 drips/day over the monitoring period, compared to Hope 3 which had 1986 drips/day. Hope 3 had the highest drip count for a single day (a maximum of 5977 drips/day), despite having the lowest average drip rate.

Whoopee 1 remained at a relatively constant drip rate over the monitoring period until Jul-18, when it began to fall quite rapidly over the next two months (Figure 4.11), reaching 0 drips/day on 07-Sep-18 and remaining at 0 until the end of the logging period. Longer periods of rainfall, especially those with longer periods of greater intensity, lead to peaks in the drip rate of Whoopee 1. This is clearest during the spring months (Feb-18 to May-18, Figure 4.11).

Overall, the drip rate at Hope 3 follows the same seasonal pattern as Whoopee 1, with higher drip rates in the winter months that then reduce during the summer months (though do not stop completely, unlikely Whoopee 1). Variability is greatest during the winter months – in Figure 4.11 a maximum of ~6000 drips/day is followed a few weeks later by a minimum of ~1000 drips/day – indicating that drip rate sensitivity to rainfall events during the winter season is much greater than during the summer season.

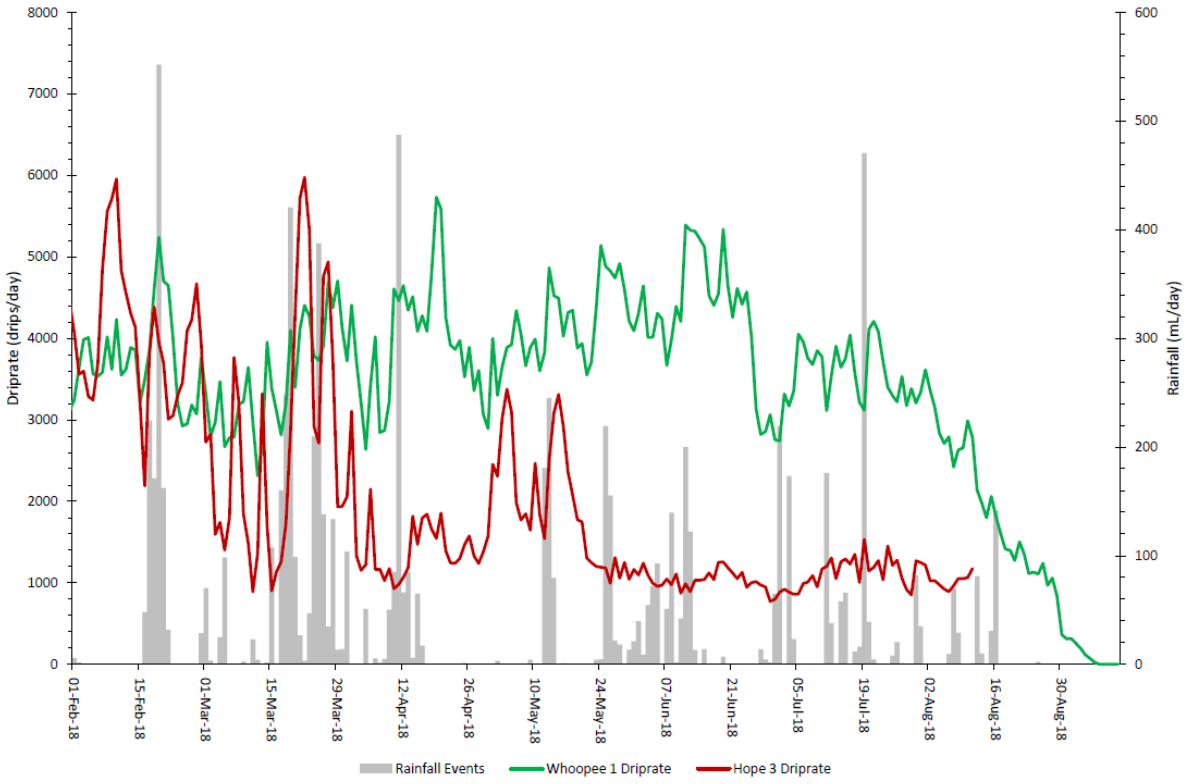

Figure 4.11 – Daily drip rate for all loggers in Cueva-Cubío del Llanío, contrasted against rainfall events. As each logger hit maximum data capacity at different times, the data for each drip ends at a different time.

Observing drip responses from a particular rainfall event, there is often a short time lag between peak rainfall intensity and peak drip rate, as can be seen in Figure 4.12. Here, a large rainfall event on 19/02/2018 leads to peaks in the drip rate for both Whoopee 1 and Hope 3. Hope 3 reached peak drip rate within a day of the greatest rainfall intensity with drip rates falling quickly following this peak and then returning to a steady decrease. Whoopee 1 demonstrated an almost immediate response with a long tail of increased drip rates following the rainfall event.

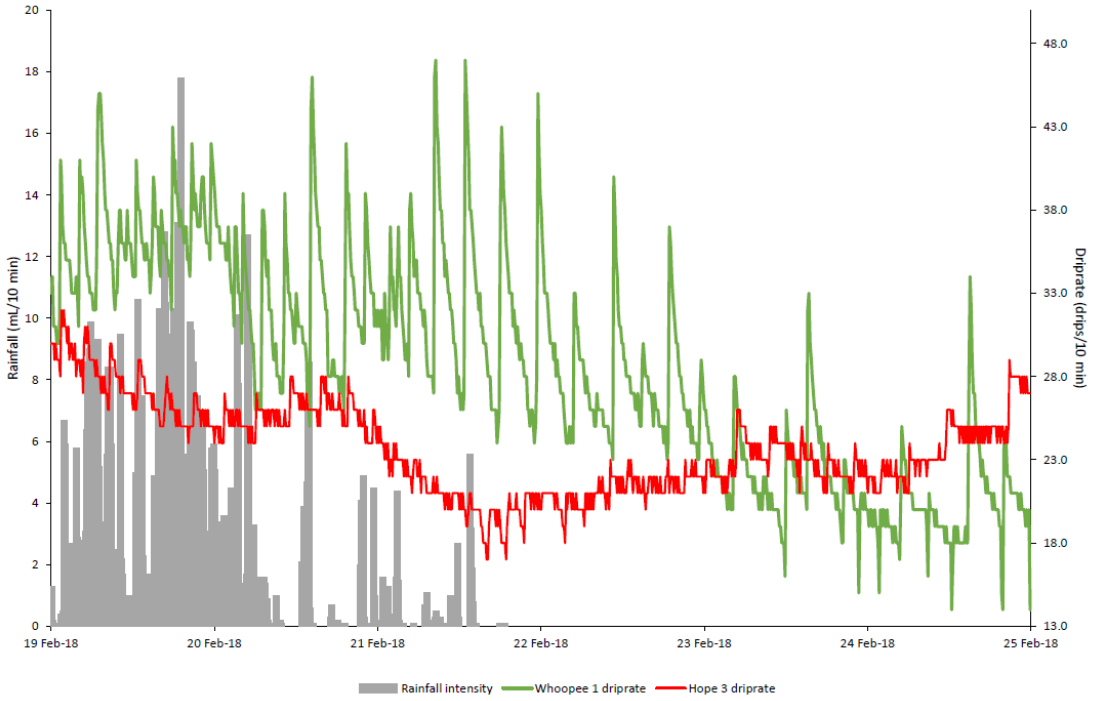

Figure 4.12 – Drip rate response to a large rainfall event beginning 19/02/2018. Rainfall and drips recorded per 10 minutes to show more detailed response.

4.3.2. Discussion

Whoopee 1 drip has an event response on top of a baseline drip rate, explaining the greater stability of the long term drip rate record (Figure 4.11), though in the short term there is more variability in the drip rate (Figure 4.12), likely due to the shallower depth of this drip. This indicates that this drip is both aquifer and event fed. It is evident that Whoopee 1 may dry up in the later months of summer, likely for roughly 1-2 months, as indicated by the drip rate reaching 0 in Figure 4.11.

In contrast, the drip at Hope 3 is more indicative of a changing aquifer response to antecedent conditions. During summer the amplitude of the drip response is reduced, reaching a base level of ~1000 drips/day with little evidence of fracture flow dynamics. During winter the matrix-fed baseflow peaks in February with larger amplitude variation in response to key rainfall events, implying a fracture flow fed dynamic.

4.4. Drip rate influence on cave air pCO_2

Drip waters can be source of CO_2 ingress into caves. Figure 4.13 presents the Apr/May-19 CO_2 record alongside the drip rate and internal and external air temperature records during this period. The red dashed line in Figure 4.13 highlights a particular rise in drip rate that occurs approximately a day prior to a large peak in the Apr/May-19 CO_2 record. This rise in drip rate remains over the period of elevated pCO_2. However, this CO_2 peak also coincides with a general rise in external air temperature. It is likely that the elevated drip rate present in Figure 4.13, alongside a general trend toward higher external air temperatures, contributed to this peak in CO_2 on 06-May-19. In a large and complex cave system such as Cueva-Cubío del Llanío, it is highly likely that there is an interaction between multiple influences on cave ventilation dynamics and accompanying values.

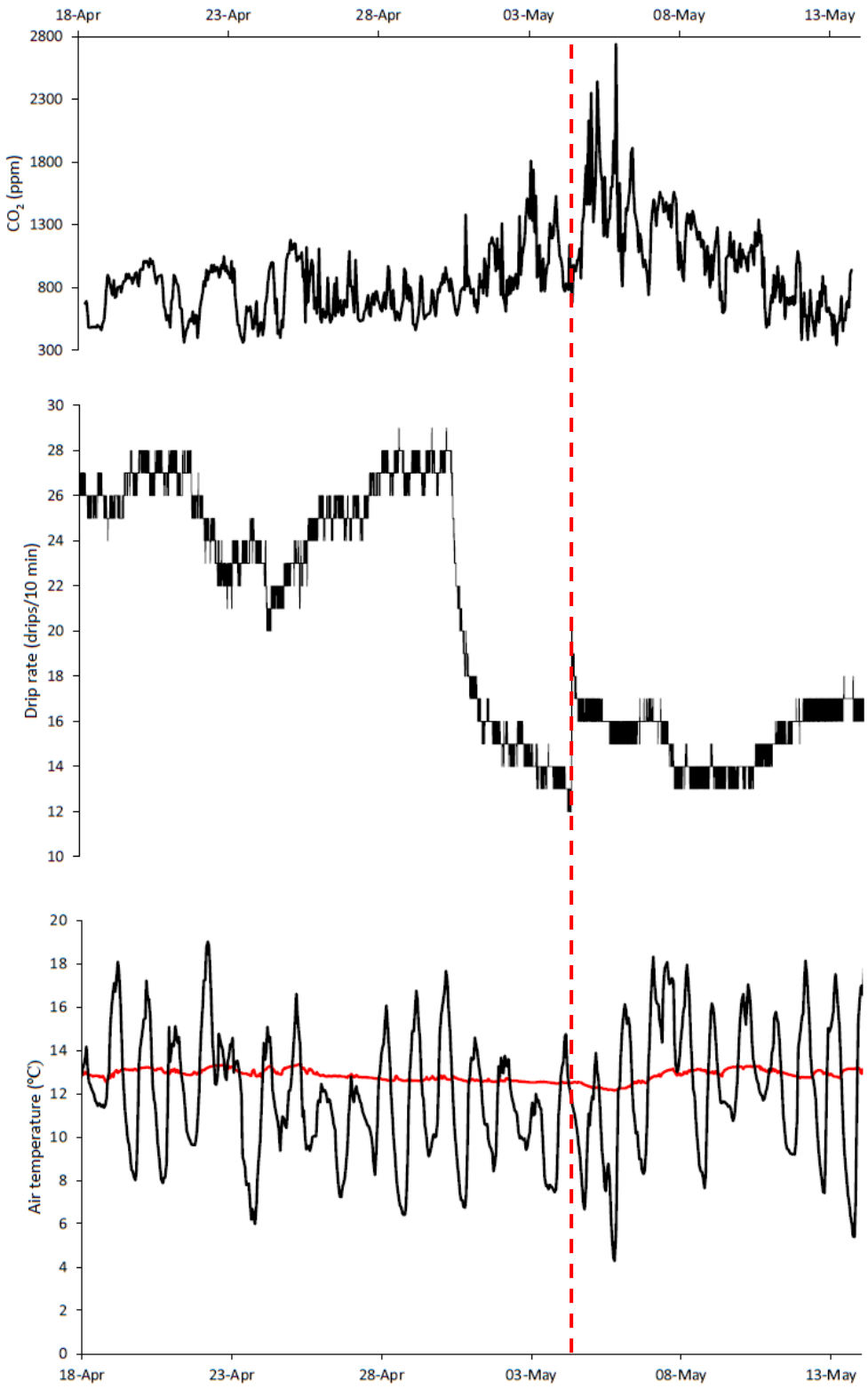

Figure 4.13: Examining the Apr/May-19 CO_2 record alongside the drip rate and air temperature records for the same time period in High Hopes chamber. Red dashed line demonstrates an increased drip rate event that occurs prior to a rapid increase In cave air pCO_2.

4.5. Hydrological Regime

The drip waters in Cueva-Cubío del Llanío display both matrix-fed and fracture flow-fed dynamics, with a baseline drip rate established by the matrix flow and a flashy high amplitude response to rainfall characteristic of fracture flow dynamics. There is a seasonal element to this – in summer the baseline drip rate is reduced for Hope 3 and cuts out altogether for Whoopee 1 – and both drips display reduced fracture flow dynamics in the summer months.

Whoopee 1 does demonstrate a dry period (Figure 4.11) but from observations this dry period had ended by Sep-19 (Whoopee 1 was observed to be dripping during the Sep-19 visit to Cueva-Cubío del Llanío) thus showing that this dry period is fairly short. Hope 3 generally has a flashier response to rainfall events and then returns to a baseline drip rate quickly (within a few days), whereas Whoopee 1 both a more immediate response followed by a slower return to baseline drip rate. The quick return to a baseline drip rate for Hope 3 indicates that the fracture flow dynamic in Hope 3 is stronger than in Whoopee 1, which returns to a baseline more slowly despite a swifter initial response to a given rainfall event due to the shallower depth of the drip.

4.6. Water Chemistry

4.6.1. Physicochemical Properties

Water samples were analysed in the field for pH, EC and water temperature – full results can be found in Table 4.3.

4.6.1.1. Results

Cave waters had an average temperature of 12.4°C. Some samples had a noticeably higher water temperature, such as the Aven Drip, both Corner Drips, Hope Long Drop and Gour Pool, which all were above 13°C. Corner Drip Top was the warmest water sample, whilst Entrance Pool was the coolest. On average the Aven Chamber had the warmest water samples, whilst High Hopes Chamber had the coolest.

Average pH in the cave water samples was 7.9. The minimum pH was 6.82 (Fast Drip 1, Jan-18) and the maximum was 8.2 (Whoopee 1, Jan-18). Whoopee Hall had waters of the highest pH whilst Aven Chamber had waters of the lowest pH. The majority of the water samples were close to a neutral pH or slightly alkaline, however there were some drips that measured slightly acidic when retested for pH in the lab – both Fast Drip 1 and 2 Jan-18 water samples had pH levels below 7 in their lab pH, but not in their field pH. This may be due to the time between retrieving the samples and taking them to the lab to be tested, as this lower pH is not observed in the Jan-19 field pH values.

Average EC in the cave water samples was 415.5 µS/cm. Maximum EC was found at Corner Drip Top (the warmest water sample), whilst minimum EC was found at Raft Pool in Jan-19. The Aven Chamber had the highest average EC, whilst Whoopee Chamber had the lowest average EC.

Table 4.6: Physicochemical data from water sampling at Cueva-Cubío del Llanío. Orange represents samples taken from High Hopes Chamber, red from Whoopee Hall, green from Aven and Corner series and blue from precipitation.

Water Sample	Date	Day	pH (lab)	pH (field)	Electrical Conductivity (µS/cm)	Water Temp (°C)
Fast Drip 1	Jan-18		6.82	7.14	395	13
	Jan-19		-	7.778	384	12.5
Fast Drip 2	Jan-18		6.83	-	-	-
	Jan-19		-	7.85	384	12.7
Hope 2	Jan-18		8.09	-	479	-
	Jan-19	20th	-	8.155	449	11.6
		21st	-	8.036	435	11.4
Hope 2A	Jan-19	21st	-	7.951	444	11.8
Hope 3	Jan-18		8.05	-	461	-
Hope 4	Jan-19	20th	-	8.142	440	11.8
		21st	-	8.104	435	11.5
Hope 6	Jan-19	21st	-	8.11	417	12.1
Hope Long Drop	Jan-19	19th	-	7.81	388	12.8
Entrance Pool	Jan-19	19th	-	8.146	356	11.4
Hope 1 Pool	Jan-19	19th	-	8.177	363	11.5
Raft Pool	Jan-18		7.02	-	380	11.8
	Jan-19	19th		8.198	344	11.4
Gour Pool	Jan-19	19th	-	7.874	382	13
Waste Water Pool Drip	Jan-19	21st	-	7.955	442	11.9
Whoopee 1	Jan-18		8.2	-	413	-
	Jan-19		-	8.166	359	11.7
Whoopee 2	Jan-19	21st	-	8.07	367	12.6
Corner Drip Top	Jan-19	19th	-	7.898	521	14.7
Corner Drip Bottom	Jan-19	19th	-	7.865	441	14
Aven Drip	Jan-19	19th	-	7.763	492	14.4
Llanío Precipitation 20th	Jan-19	20th	7.272	-	33.4	-
Llanío Precipitation 20-21st	Jan-19	21st	7.888	-	28	7.7

4.5.1.2. Discussion

Drips that are suspected to be fed from fracture flow through the karst generally displayed lower EC values – here the water has less time to sit within the aquifer and so contains fewer trace elements than that of water that has entered the cave through slower matrix flow. For most drip sites in Cueva-Cubío del Llanío this seems to be the case with the exception of the Aven drip and both Corner Drips, which display much higher EC values despite being fast dripping and warmer drips which can indicate a drip fed through fracture flow. A potential lack of prior calcite precipitation (PCP) could explain this trend – there is little time for trace elements to be precipitated out of the water - EC values tend to be higher when PCP is low.

4.6.2. Bicarbonate (HCO_3) and SI_{CC}

Water samples retrieved during Jan-18 and Jan-19 were titrated in the field. Using titration results, water temperature, pH, and, calcium and magnesium concentrations for Jan-19 water samples (water samples from Jan-18 were not analysed for Ca and Mg concentrations); saturation index for calcite (SI_{CC}, see Equation 4.1) and alkalinity was calculated using MIX4 speciation software.

Equation 4.17: Saturation index for calcite (SI_{CC}). Taken from Fairchild et al. (2007).

$$SI_{CC} = \log(\frac{IAP}{K_S})$$

Where:

IAP (Ionic Activity Product) = $(Ca^{2+})(CO_3^{-})$ in a given solution
K_S is the solubility product

Titrations were only performed on water samples where enough water had been collected – slower drips where water did not collect in a timely manner did not allow for enough water to be collected for all analyses to be done. Equally, only some locations produced enough water for Ca and Mg concentrations to be measured. Thus, SI_{CC} was not calculated for all samples.

SI_{CC} <0 indicates that a water sample is supersaturated with regards to calcite, and all calculated SI_{CC} values are over 0, indicating supersaturation in all samples, with an average SI_{CC} of 0.47 (Table 4.5). This indicates that calcite deposition is occurring for all drips. 21/01/19 Hope 4 had an anomalously high SI_{CC} value of 0.81, an effect of the anomalously high calcium concentration in this drip water sample.

Alkalinity for Jan-18 samples was only derived from field titration (Table 4.4), whilst Jan-19 samples were both titrated and had magnesium and calcium concentrations measured, thus allowing for two measures of alkalinity (Table 4.5). Alkalinity within the cave had an average of 171 mg/l $CaCO_3$ with notable examples being that of Hope 2 (Jan-19) with an alkalinity of 240 mg/l $CaCO_3$ (Table 4.5) and Fast Drip 2 (Jan-18) with an alkalinity of 124 mg/l $CaCO_3$ (Table 4.4). With these maximum and minimum alkalinity values as an exception, the other values were closer to the average. Alkalinity measured via titration was always be higher than that calculated using calcium and magnesium concentrations for each water sample – a graphical comparison is plotted in Figure 4.14.

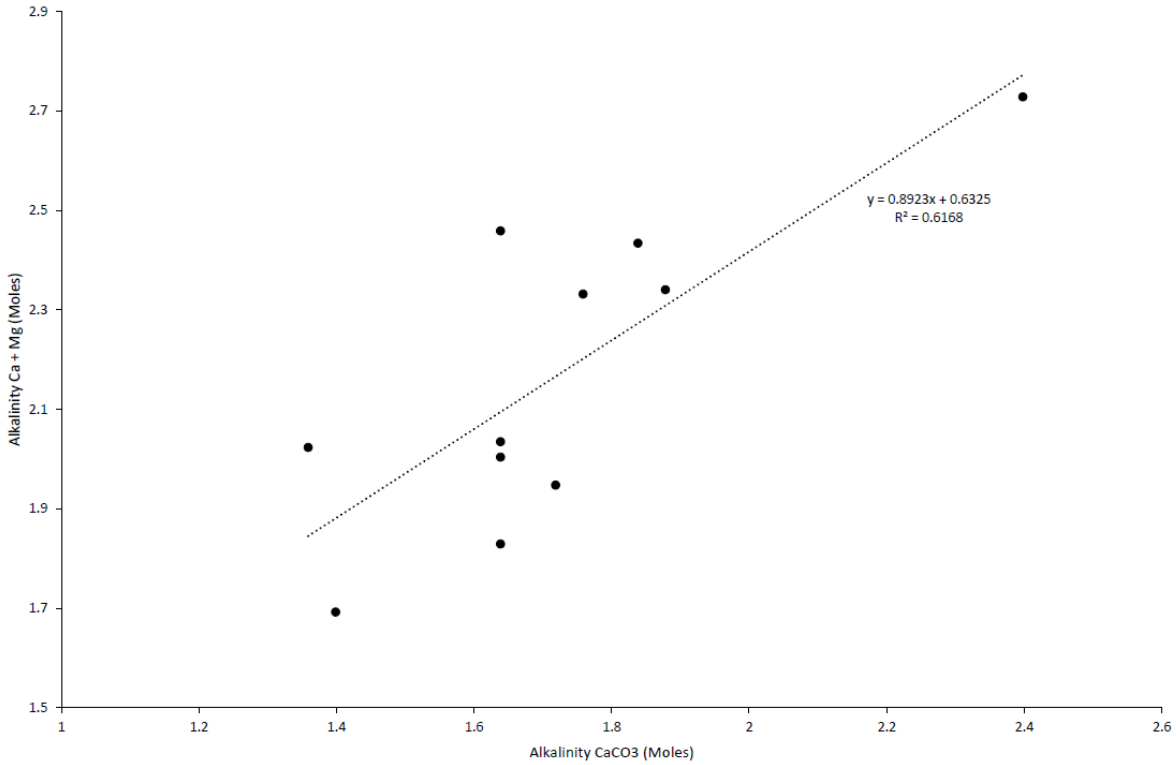

Figure 4.14 – Linear regression between both alkalinity values calculated for water samples.

Table 4.7: Alkalinity values for cave water samples from Jan-18.

Cave Chamber	**Water Sample**	**Titrated Alkalinity (mg/l $CaCO_3$)**
High Hopes	Fast Drip 2	124
	Hope 2	164
	Hope 3	148
	Raft Pool	182
Whoopee Hall	Whoopee 1	166

Table 4.8: Titrated and Ca + Mg Alkalinity and SI_{CC} values for cave water samples from Jan-19.

Cave Chamber	Water Sample	Titrated Alkalinity (mg/L $CaCO_3$)	Alkalinity from Ca/Mg Concentrations (mg/L $CaCO_3$)	SI_{CC}
High Hopes	Fast Drip 1	180	-	0.24
	Fast Drip 2	176	-	0.24
	Hope Long Drop	172	-	-
	Entrance Pool	164	78.74	0.55
	Hope 1 Pool	172	76.52	0.59
	Raft Pool	164	71.83	0.57
	Gour Pool	164	79.96	0.3
	Hope 2 20/01/19	240	100.62	0.75
	Hope 2 21/01/19	176	84.75	0.43
	Hope 2A	184	88.71	0.38
	Hope 4 20/01/19	188	85.17	0.57
	Hope 4 21/01/19	188	174.04	0.81
	Waste Water Pool Drip	164	87.82	0.32
Whoopee Hall	Whoopee Pool	136	79.79	0.45
	Whoopee 1	140	65.37	0.32
Corner and Aven	Corner Drip Bottom	188	-	-
	Corner Drip Top	204	-	-
	Aven	144	-	-

4.6.3. Drip water Oxygen Isotope Chemistry

Water oxygen isotope values are shown against historic rainfall data and Global and Local Meteoric Water Lines (GMWL and LMWL – see Equations 4.2 and 4.3) in Figure 4.15. Jan-19 cave water samples cluster around a point on the LMWL, whilst cave water samples taken over a longer period of monitoring in nearby caves (Cueva de Asiul and Cueva de las Perlas) spread further along the LMWL but still remain somewhat clustered. Matienzo rainfall oxygen isotope values do not cluster in the same manner as the cave waters but follow the LMWL in their distribution.

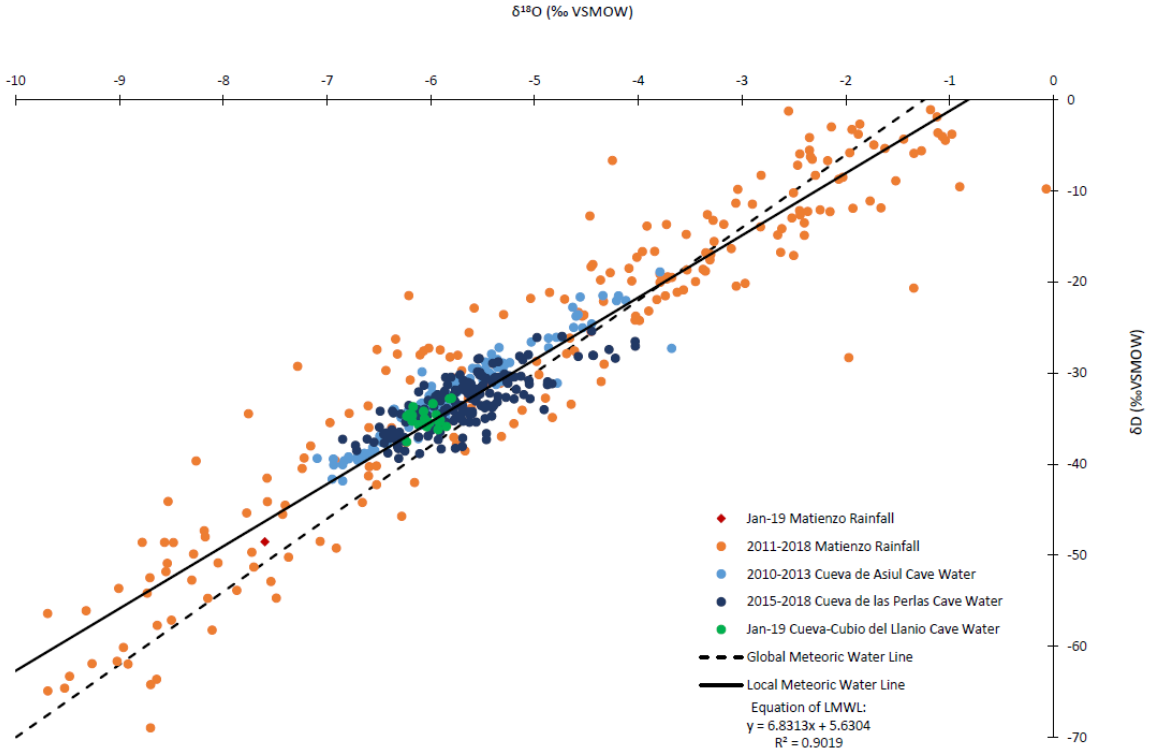

Figure 4.15: Rainfall and cave water data with Local Meteoric Water Line (Equation 3) and Global Mean Water Line (Equation 2). Further cave water data taken from Smith et al. (2016) for Cueva del Asiul and Deeprose (2018) for Cueva de las Perlas. 2011-2018 Matienzo rainfall data collated from both Smith et al. (2016) and Deeprose (2018).

Equation 4.18: Global Meteoric Water Line (GMWL), from Craig (1961). Both δ values in per mille.

$$\delta D = 8\,\delta^{18}O + 10$$

Equation 4.19: Local Meteoric Water Line (LMWL) for Matienzo precipitation, calculated from rainfall data from Deeprose (2018) and Smith et al. (2016).

$$\delta\mathrm{D} = 6.8313\,\delta^{18}O + 5.6304$$

The clustering of cave waters implies that the cave waters are well-mixed in the aquifer above before entering the cave system. The location of the cluster of the Jan-19 Cueva-Cubío del Llanío cave water samples is skewed toward winter rainfall values in relation to the LMWL plotted in Figure 4.15, thus implying the majority of the cave water collected in Cueva-Cubío del Llanío during Jan-19 is sourced from winter rainfall. This agrees with

findings from Smith *et al*. (2016), which found that Matienzo region cave waters generally skew toward the winter values in relation to LMWL.

4.6.4. Trace Element Concentrations

Water samples were analysed for calcium and magnesium (Table 4.6) where possible.

4.6.4.1. Calcium

The average calcium concentration in cave waters during Jan-19 was 80.38ppm, with a standard deviation of 22.75. It should be noted that the calcium concentration for 21/01/19 Hope 4 (highlighted in red in Table 4.6) is anomalously high, both in comparison to the other cave water calcium concentrations and to the calcium concentration for a water sample taken from the same drip the day before. Removing this anomalous concentration corrects the average calcium concentration to 74.69ppm and the standard deviation to 5.76ppm.

The average calcium concentration in precipitation during Jan-19 was 6 ppm.

4.6.4.2. Magnesium

The average magnesium concentration in cave waters during Jan-19 was 7.85ppm with a standard deviation of 5.94. Magnesium concentrations generally cluster into two distinct groups – one with concentrations between approximately 2-3 ppm and one with concentrations between approximately 13-14 ppm. Most drips in High Hopes have the higher concentration whilst the pools have the lower concentrations. Despite this, Fast Drip 1 and 2 have low magnesium concentrations compared to other drips in the same chamber. In Whoopee Hall, both the pool and drip water samples are lower in magnesium concentration. It is likely that those drips with a lower magnesium concentration are fed through faster water pathways than those with higher magnesium concentrations – the greater rock-water contact time will allow a greater amount of the dolomitic bedrock to be dissolved and thus lead to a higher Mg concentration.

The average magnesium concentration in precipitation during Jan-19 was 0.67 ppm.

Table 4.9: Cation and anion concentrations for water samples taken during Jan-19. The Hope 4 calcium concentration measurement from 21/01/2019 has been displayed in red as it is considered to be an anomalous result.

Date	Sample Name	Chamber	Ca (ppm)	Mg (ppm)
19/01/2019	Fast Drip 1	High Hopes	78.25	2.48
	Fast Drip 2	High Hopes	75.47	2.49
	Entrance Pool	High Hopes	76.31	2.43
	Hope 1 Pool	High Hopes	74.16	2.36
	Raft Pool	High Hopes	69.54	2.29
	Gour Pool	High Hopes	77.49	2.47
20/01/2019	Whoopee Pool	Whoopee Hall	77.76	2.03
	Hope 2	High Hopes	87.17	13.45
	Hope 4	High Hopes	71.86	13.31
	Llanío Precipitation 20th	n/a	4.04	0.60
	Llanío Precipitation 20-21st	n/a	7.97	0.74
21/01/2019	Hope 2	High Hopes	71.35	13.41
	Hope 6	High Hopes	78.33	13.22
	Hope 4	High Hopes	160.13	13.91
	Hope 2A	High Hopes	75.07	13.64
	Whoopee 1	Whoopee Hall	61.60	3.77
	Waste Water Pool Drip	High Hopes	71.28	16.54

4.7. Calculated Speleothem Growth Rates

Speleothem growth rates were calculated using two methods, deriving growth rates from water chemistry or calcite plate weights.

Theoretical speleothem growth was calculated using Equation 4.4, taken from Baldini (2010) and derived from Dreybrodt (1999).

Equation 4.20: Theoretical speleothem growth, taken from Baldini (2010).

$$R_o = 1.174 * 10^3 (Ca - Ca_{eq}) * (\delta * \Delta T - 1)[1 - e^{(-\alpha * \Delta T * \delta^{-1})}]$$

Where:

R_o is speleothem extension rate in mm/yr
$1.174*10^3$ is a conversion constant that converts molecular accumulation ($mmol/mm^2/s$) into growth rate in mm/yr
Ca_{eq} is drip water Ca^{2+} at equilibrium with a stated atmospheric CO_2 (see Equation 4.5)
δ is thin film thickness (mm), this study uses 0.1mm
ΔT is time between successive drips (s)
α is a kinetic constant (mm/s), dependent upon δ and temperature (10°C) – derived from Equation 4.6.

Equation 4.21: equation for the calculation of Ca_{eq}.

$$Ca_{eq} = 7.611 * {pCO_2}^{0.275}$$

Equation 4.22: equation for the calculation of α.

$$\alpha = 8.5 * 10^{-4} * \beta$$

Where β is a term derived from Dreybrodt (1999) that encapsulates the effect of temperature and thin film thickness. Dreybrodt (1999) provides values of β at varying temperatures and film thicknesses; using the value given at 10°C and 0.1mm an α value of 0.000128 is calculated.

Using conditions averaged from the relevant chamber (Table 4.7), theoretical growth rates were calculated for a selection of Jan-19 drip water samples. All speleothems display positive growth rates of between 100-200 microns/year.

Table 4.10: components of theoretical speleothem growth rate calculations. All speleothems show a positive growth rate.

Date	Sample	Ca (mmol /L)	pCO2 (atm)	Ca_{eq}	Thin film thickness (mm)	Average time between drips (s)	α	β	Growth Rate (mm/yr)
19/01/19	Fast Drip 1	1.95	0.0007	1.0145	0.1	35	0.000128	0.024	0.137
	Fast Drip 2	1.88	0.0007	1.0145	0.1	35	0.000128	0.024	0.127
20/01/19	Hope 2	2.16	0.0007	1.0145	0.1	33	0.000128	0.024	0.170
	Hope 4	1.79	0.0007	1.0145	0.1	35	0.000128	0.024	0.114
21/01/19	Hope 2	1.78	0.0007	1.0145	0.1	33	0.000128	0.024	0.112
	Hope 6	1.95	0.0007	1.0145	0.1	35	0.000128	0.024	0.138
	Hope 2A	1.87	0.0007	1.0145	0.1	35	0.000128	0.024	0.126
	Waste Water Pool Drip	1.78	0.0007	1.0145	0.1	35	0.000128	0.024	0.112
	Whoopee 1	1.54	0.0007	1.0145	0.1	42	0.000128	0.024	0.076

4.8. Conclusion

Cueva-Cubío del Llanío is a cave with a complex ventilation regime – there is evidence of a classic density driven ventilation regime but this does not extend to all chambers – High Hopes appears to be an offshoot chamber with its own isolated pocket of air that is only partly influenced by the main ventilation of the cave. Both temperature and CO_2 records support this theory, as High Hopes chamber reverts to the instable ventilation regime later

in the year than other chambers in the cave and displays an odd inverse CO_2-temperature dynamic.

Hydrology in the cave indicates drips fed both through matrix and fracture flow – with a baseflow fed by matrix flow and a flashier drip response fed by fracture flow. Water chemistry indicates that the bedrock above the cave is dolomitic in nature due to the split clustering of magnesium concentrations. Where water is likely fed through faster pathways through the rock, magnesium concentrations are lower as there is not enough rock-water contact time for the dolomitic bedrock to be dissolved by the water. Conversely, in waters likely fed by slower pathways magnesium concentrations are higher due to the increased contact time between the water and bedrock.

5. The Biogeochemical Cycling of N in Cueva-Cubío del Llanío

5.1. Introduction

N is cycled through the environment in the N biogeochemical cycle – atmospheric N is fixed by plants into organic-N, which is then deposited into the soil organic matter pool and assimilated by plants or denitrified back to atmospheric N (Jaffe, 1992). When considering underlying cave systems, further components of this cycle are considered – drip waters, bedrock and speleothem material. All of the key components of the cycle, with regards to their interaction with cave systems, will be discussed below.

Rainfall forms an atmospheric end member of the biogeochemical cycle, comprising inputs from atmospheric pollution, lightning and atmospheric ozone chemistry (He *et al*, 2011). Rainfall tends to have a low concentration of N in comparison to other members in the cycle (Decina *et al.,* 2018).

Soil-N comprises inputs from wet and dry atmospheric deposition of N, conversion of bedrock to soil, decomposing vegetative matter and anthropogenic inputs of fertiliser/manure N (Butterbach-Bahl and Gundersen, 2011). Outputs from soil-N include assimilation by vegetation, volatilisation and leaching by both atmospheric rainfall and anthropogenic irrigation. Vegetation-N and Soil-N are constantly exchanging N between themselves. Vegetation comprises inputs from assimilation of soil-N and fixation of atmospheric N, organic-N in vegetation is lost by decomposition of vegetation into soil-N pool (Butterbach-Bahl and Gundersen, 2011).

Drip water comprises of leached N from the soil-N reservoir above and bedrock-N from dissolution of the bedrock due to the dual porosity of the karst bedrock (Ford and Williams, 2007). The bedrock itself is a small reservoir of inorganic N with a millennia-long residence time (Holloway and Dahlgren. 2002). Bedrock- N contributes to soil-N as it is converted to soil and to drip water-N as it is dissolved by slightly acidic rainwater that has infiltrated through the soil.

Finally, there are two end members of the N biogeochemical cycle within the cave system itself. Both cave sediments and speleothem deposits represent end members for the N biogeochemical cycle.

Cave sediments can be endogenic or exogenetic in origin – originating from within or outside the cave respectively – but tend to be a mixture of both endogenic and exogenetic material (Ones, 1978). Bedrock-N is the major contributor to the N found in endogenetic sediments, whilst in-washed soil-N is the major contributor to exogenetic sediment-N.

Speleothem-N is wholly controlled by drip water-N and is determined by a partition coefficient – only some of the N within the drip waters is incorporated into the speleothem record. Due to the similarity in size between nitrate and carbonate ions (Jenkins and Thakur, 1979), it is theorised that there will minimum lattice distortion during incorporation (Kontrec *et al.*, 2014) but a full understanding of the mechanism was not feasible for this project.

With the key components of the N biogeochemical cycle discussed, it is important to also discuss the key processes by which N is moved between these components of the N biogeochemical cycle. Fixation is the process by which plants fix atmospheric N into organic-N. Organic-N in plants is also produced by assimilation, in which plants take up N from the soil-N pool. When plants die, the organic-N is returned to the soil-N pool via mineralisation – a two-step process in which organic-N is first converted to NH_4^+ (ammonification) and then oxidised to NO_3^- (nitrification). Soil-N can be lost via volatilisation - a chemical process at the soil surface in which NH_4^+ is converted to ammonia gas at high pH. When rainwater passes through the soil system is becomes slightly acidic due to uptake of CO_2 in soil pores - dissolution is the process by which carbonate bedrock is dissolved by this weak acidic rainwater.

These processes are drawn together into the hypothetical model in Figure 5.1 and use the N concentrations and isotopic compositions discussed through Chapters 5 and 6 to verify these processes with regards to their operation within and above Cueva-Cubío del Llanío.

At Cueva-Cubío del Llanío, samples of all the major components (rainwater, soil, vegetation, bedrock, drip water, cave sediment, speleothem material) were taken and analysed for N concentration to quantify the biogeochemical cycling of N in the system present at this location.

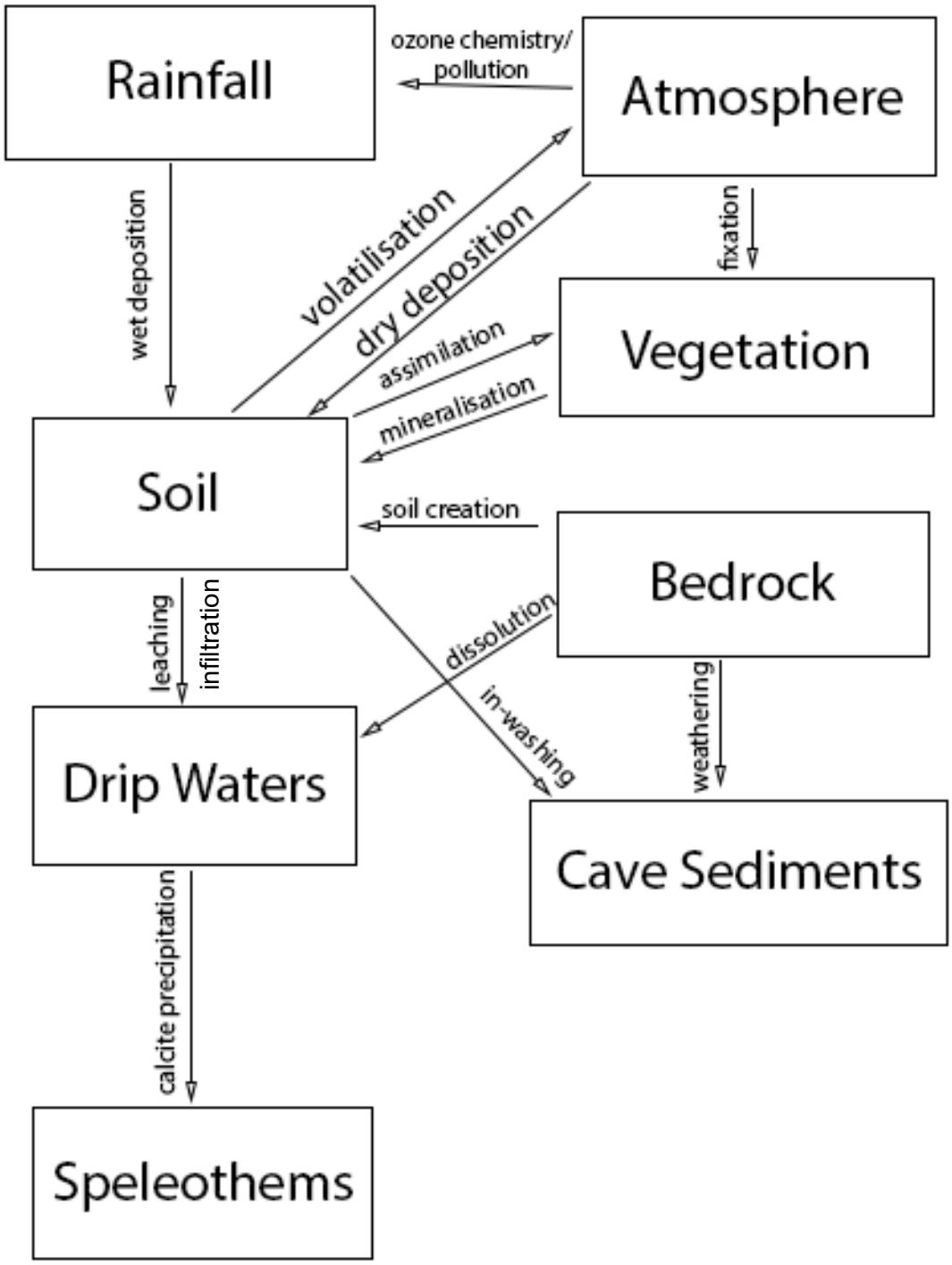

Figure 5.1 – Conceptual model of the N biogeochemical cycle present at Cueva-Cubío del Llanío.

5.2. Results

5.2.1. Rainfall

From the concentrations recorded at Cueva-Cubío del Llanío, rainfall appears to contribute only a small input of N into the system. The average nitrate-N concentration of 0.115 ppm (see Table 5.1). Nitrate-N concentrations are thus low but total flux to the cave system is unknown – rainfall amount data was not collected to quantify this flux.

Table 5.1 – Nitrate-N concentrations for precipitation collected close to Cueva-Cubío del Llanío.

Month	Sample Name	Nitrate-N (ppm)
Jan-19	Llanío Precipitation 20th	0.1215
	Llanío Precipitation 20-21st	0.204
	Ppt Jan-19	0.048
Feb-19	Ppt Feb-19	0.182
Mar-19	Ppt Mar-19	0.008
Apr-19	Ppt Apr-19	0.004
Sep-19	Ppt Sep-19	0.236

5.2.2. Soil and Vegetation

Vegetation hosts concentrations of organic-N which range between 26,350 to 52,600 ppm with an average organic-N of 32,863 ppm. In contrast, the soil reservoir has much lower concentrations of total N, ranging between 4950 to 5200 ppm, with an average total N of 5050 ppm (Figure 5.2). In this instance, it would appear assimilation of N from soil to plant and fixation of N into the biomass outweighs the return flow of N into the soil via mineralisation. This has elevated the vegetation N composition above that found in the soil.

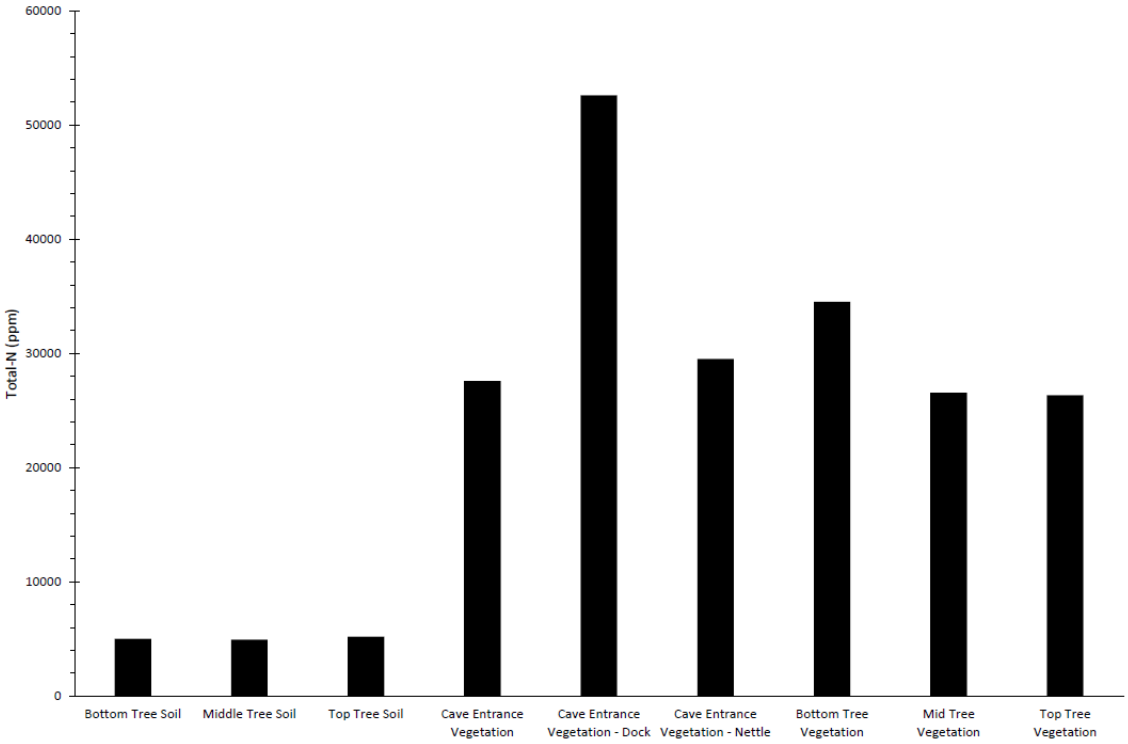

Figure 5.2 – Soil and vegetation total-N concentrations.

5.2.3. Bedrock

The bedrock above Cueva-Cubío del Llanío is likely a contributor to the N that enters the cave system. The two bedrock samples taken from Cueva-Cubío del Llanío had the NO_3-N concentrations 6.70 mg ppm and 13.2 ppm respectively.

Bedrock dissolution can therefore feasibly contribute N to the drip water composition. This can be calculated according to Equation 5.1.

Equation 5.1: calculating percentage contribution of bedrock N to drip water N

$$\%\text{bedrock N} = [1/(\text{bedrock Ca} + \text{Mg: NO}_3/\text{drip water Ca} + \text{Mg})/\text{drip water NO}_3] * 100$$

Assuming the bedrock is pure $CaMg(CO_3)_2$ with a Ca+Mg concentration of 349,000 ppm, there is 0.08-0.27% bedrock contribution to the N in the drip waters at Cueva-Cubío del Llanío, as calculated by Equation 5.1.

5.2.4. Cave waters

On average, drip waters had a nitrate-N concentration of 1.929 ppm. The highest recorded drip water nitrate-N concentration was 12.095 ppm, recorded at the Aven Drip during the Jan-19 sample collection, whilst the lowest was 0.0547 ppm and recorded at Hope 1 during the Feb-18 sample collection. These are all well below the 50 mg/L limit set out by the Nitrates Directive and Drinking Water Directive published by the EU (Council Directive 91/676/EEC, 1991 and Council Directive 98/83/EC, 1998 respectively) The full report of cave water nitrate-N concentrations can be found in Table 5.2.

Table 5.11 -Nitrate-N concentrations for cave waters collected within Cueva-Cubío del Llanío.

Month	Date	Sample Site	Nitrate-N (ppm)
Jan-18		Fast Drip 1	3.266
		Fast Drip 2	3.236
		Hope 1	1.452
		Hope 2	
		Hope 3	1.49
		Raft Pool	3.16
		Whoopee 1	2.321
Feb-18		Fast Drip 1	1.014
		Fast Drip 2	0.7591
		Hope 1	0.0547
Aug-18		Fast Drip 1	0.773
		Fast Drip 2	0.7525
Jan-19	19th	Fast Drip 1	2.453
		Fast Drip 2	2.328
		Hope 1	1.71
		Hope Long Drop	2.467
		Entrance Pool	2.646
		Hope 1 Pool	2.533
		Raft Pool	2.507
		Gour Pool	2.39
		Corner Drip Bottom	1.767
		Corner Drip Top	4.808
		Aven Drip	12.095
	20th	Whoopee Pool	3.227
		Hope 2	1.306
		Hope 4	1.347
	21st	Hope 2	1.263
		Hope 5	1.257
		Whoopee 2	6.162
		Hope 6	1.383
		Hope 4	1.274
		Hope 2A	1.285
		Whoopee 1	1.984
		Waste Water Pool Drip	1.104
Apr-19		Fast Drip 1	0.7005
		Gour Pool	0.804
Aug-19		Hope 1	1.723
		Hope 2	1.113
		Hope 2A	1.096
		Hope 3	1.104
		Hope 4	1.007
		Hope 5	1.073

Month	Date	Sample Site	Nitrate-N (ppm)
		Hope 6	1.189
		Whoopee Pool	0.831
		Whoopee Speleo Pool	2.298
Sep-19		Hope 1	1.812
		Hope 2	1.108
		Hope 3	1.076
		Hope 4	1.173
		Hope 5	1.125
		Hope 6	1.356
		Whoopee Pool	1.318
		Whoopee Speleo Pool	0.833

Figure 5.3 shows how nitrate-N concentrations change with time within various cave water samples. There appears to be a winter high and as summer low across two annual cycles, indicating that there may be seasonality to the nitrate-N composition of the drip waters in Cueva-Cubío del Llanío.

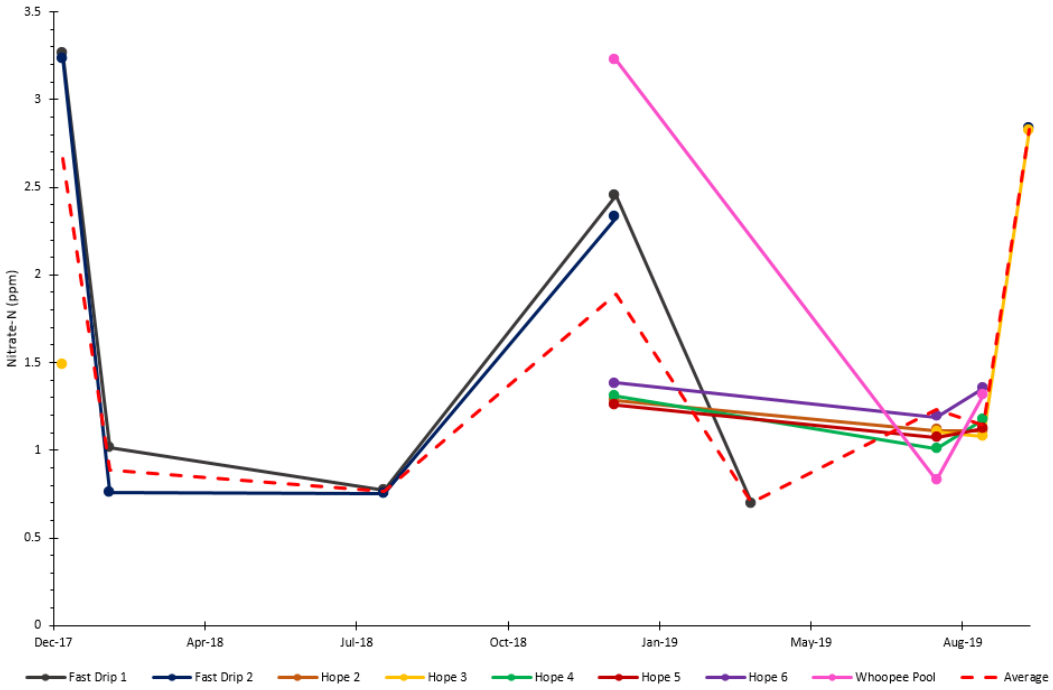

Figure 5.3 – Changing nitrate-N concentrations over time in cave waters from Cueva-Cubío del Llanío.

It is likely that N is gained as rainwater moves through the system from point of entry at the ground surface to appearance in the cave as a drip and pool waters and whilst it is not possible to demonstrate that the concentration increases between rainfall and drip water are not due to evaporation due to lack of chlorine trace element concentration data, drip water N is in part generally influenced in the most part by soil-N and bedrock inputs, with the majority of N sourced from the soil-N pool and 0.35% from bedrock-N.

5.2.5. Cave Sediments

Cave sediments in Cueva-Cubío del Llanío have lower total-N concentrations than the soil and vegetation samples taken from above the cave (see Figure 5.4) but lower than vegetation or soil NO_3-N concentrations. Overall sediments have an average total-N of 1070 ppm. Most sediments are similar in total-N composition to one another with a range of 400 ppm between minimum and maximum values when discounting S3, which has a notably higher total-N composition. When discounting the S3 total-N value, average total-N composition for sediments is 662 ppm.

S3 has a total-N composition of 2700 ppm, a value 1700 ppm higher than the next nearest sediment total-N value. This may in part be due to the difference in sampling characteristics between S3 and the other sediment samples. S1, 2 and 4 were dry sediments scraped from the floor of the cave passage, whilst S3 was in the bottom of a gour pool below a largely fracture flow fed drip. S5 was a morphologically distinct layer of mud that could be peeled away from sub-deposits. The distinctively high S3 total-N value may be influenced by this difference in sample characteristics and associated links (or lack of links) to surface activity, though this will be expanded upon in the discussion.

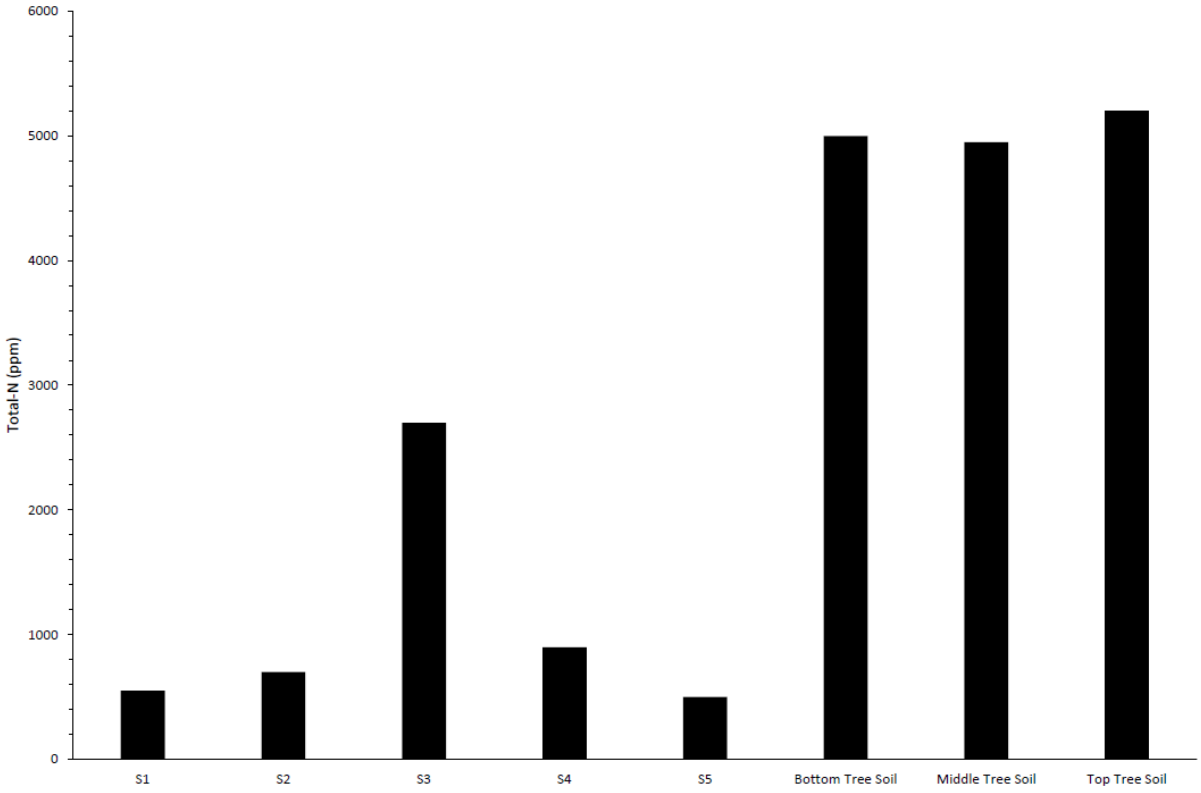

Figure 5.4 – Cave sediment total-N concentrations contrasted with soil total-N.

5.2.6. Speleothems

NO_3-N concentrations in speleothem calcite in Cueva-Cubío del Llanío have an average of 2.44 ppm with the Stalagmate logger left on Whoopee 1 from Jan-19 to Aug-19 had the highest concentration at 5.35 ppm (see Table 5.3) – though it is important to note that there is a risk of contamination with all Stalagmate logger scrape samples.

Table 5.12 – Speleothem sample NO_3-N concentrations from Cueva-Cubío del Llanío.

Sample Name	NO_3-N in solid (ppm)
Whoopee 1 Stalagmate Calcite Jan-19	1.85
Hope 3 Stalagmate Calcite Jan-19	1.61
Whoopee 1 Stalagmate Plate Jan-19 to Aug-19	5.35
Hope 2 Stalagmate Plate Jan-19 to Aug-19	1.44
Hope 3 Calcite Plate	2.78
Hope 4 Calcite Plate	3.21
Hope 6 Calcite Plate	2.49

Whoopee 1 stalagmite was removed from Cueva-Cubío del Llanío and samples were taken from the centre of the speleothem every 2.5mm to create a time series of changing NO_3-N concentration – Figure 5.5. There is a clear upward trend in NO_3-N concentrations with decreasing depth, indicating that over time the amount of N entering the cave system has likely increased.

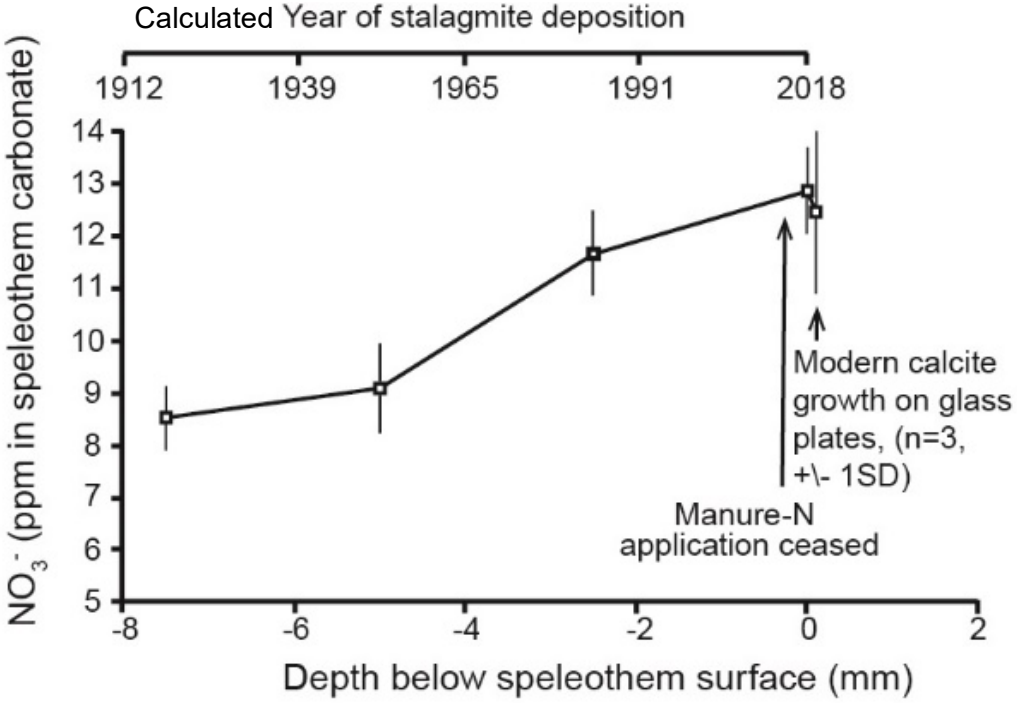

Figure 5.5 – Changing nitrate-N concentrations with depth in Whoopee 1 stalagmite. Error bar for most recent data point is 1SD of the three glass calcite growth plates, other points have errors related to replication of standards by the AQ2 SEAL discrete analyser used for concentration analysis on speleothem samples. Year of deposition was based on calculated theoretical growth rate based on Ca concentrations of the accompanying drip waters, as derived from Dreybrodt (1999) and Baldini (2010), with further details of these calculations found in Section 4.7.

Other speleothem samples from caves around the world were also analysed for nitrate-N, with full results found in Table 5.4. It is clear that these samples all contain some amount of nitrate-N – there is an average NO_3-N concentration in these samples of 15.54 ppm. As there is no accompanying water samples no partitioning can be calculated, but it is clear that some of the nitrate-N that enters a cave system via drip waters is preserved in the speleothem record in systems other than Cueva-Cubío del Llanío.

Table 5.13 – Speleothem sample NO_3-N concentrations for calcite samples taken from speleothems from other cave sites. Note that concentrations highlighted in yellow are calculated from mass spectrometer area due to issues with AQ2 SEAL data and thus are more unreliable.

Sample Name	NO_3-N in solid (ppm)
SOPELH	1.64
BFM 96-2 (1)	2.21
BFM 96-2 (2)	2.12
MERC-1 (1)	55.16
MERC-2 (2)	54.18
CC-Bil (1)	4.57
CC-Bil (2)	2.16
Yorkshire Dales	2.30

5.3. Discussion

The biogeochemical cycling at Cueva-Cubío del Llanío follows the conceptual model detailed in Figure 5.1. Rainfall samples had low concentrations but flux was unable to be calculated for this project, so though concentrations were comparatively low, it is not possible to quantify the amount of rainfall entering the system and thus the total N input into the system from rainfall is not quantified. Another smaller contribution to the system is the contribution by the bedrock N pool to the drip water N pool, calculated by Equation 5.1 to be 0.35%.

Observing the differences in Total-N concentrations between the vegetation and soil samples taken above Cueva-Cubío del Llanío, there is a larger amount of N within the vegetation-N pool when compared to the soil-N pool. This would imply that at this site, assimilation of N from the soil-N pool to the plant-N pool and the fixation of N by vegetation greatly outweighs the return flow of N into the soil via mineralisation. This would explain the greater total-N concentration within the vegetation N pool. As the samples were taken in Jan-18, just before the beginning of the 2019 growing season, it is likely that this reflects the reduction in total soil ammonifying bacteria and fungi at the end of the dormant season (Isobe *et al*., 2018), thus reflecting the reduced potential mineralisation in the soil pool. Thus assimilation and fixation of N by vegetation during this period outweighs the return flow of N via mineralisation.

From the drip water N content, there is a seasonal signal of high N concentration in the winter months and low N content in the summer months. This cannot be a dilution factor, as the higher N concentration is present in the wetter winter months where concentrations would be expected to be lower if a dilution factor was present due to the increased input of water into the karst system. Again, due to the presence of the higher concentrations in the cooler winter months, this increased concentration signal cannot be due to evaporation as evaporation is lower in the colder winter months. The oxygen isotopes in the water samples taken in the winter (D/O isotopic composition) are lighter (see Chapter 4) – if there was an evaporative effect in the winter months oxygen isotopes would be heavier during the winter. This higher concentration can also not be explained by an increased residence time in the aquifer as the drip rates detailed in Chapter 4 are higher in the winter months and drips in Cueva-Cubío del Llanío have been observed to dry up in the summer months – if residence times were high in the winter months then the drip rates would behave differently.

It is thus likely that this seasonal drip water N concentration signature is from the seasonal changing balance between vegetation and soil N pools above the cave. It is likely that during the winter months, when deciduous plants shed foliage and exhibit reduced growth rates, the mineralisation of plant-N to soil-N is greater, thus increasing amount of N in the soil-N pool. This is then reflected in the drip water N signature, with a higher N concentration in the drips in the winter. In the summer months, when plant growth rates are increased, assimilation and fixation outweigh the mineralisation and thus the soil-N pool is reduced. This is again reflected in the drip water N signature with a summer N concentration that is lower.

Sediments within the cave reflect a changing surface environment. The S3 sediment sample is likely younger and exogenetic. S3 was mud taken at the bottom of a gour pool fed by a largely fracture flow fed drip. With this collection site characteristic, it is likely that S3 is comprised of in-washed material from the soil system above and thus reflects the modern anthropogenic reactive N input into the soil system. Older endogenetic sediments, taken as dry sediments taken from the cave floor (e.g. S1, 2 and 4), likely reflect a N composition that is of a less polluted origin.

Therefore, it seems that the biogeochemical cycle at Cueva-Cubío del Llanío has inputs from rainfall and fixation of atmospheric N by plants, which are cycled by the soil and vegetation N pools according to seasonality, which then enters the cave system via drip waters which then deliver this seasonal signal into the speleothem record.

The speleothem sampling methodology used for this project is too low to see this seasonal signal delivered. However, this seasonality may be apparent if it can be analysed at a high enough resolution, such as by Synchrotron radiation.

5.4. Conclusion

In Cueva-Cubío del Llanío, the various inputs at varying concentrations enter into the N biogeochemical cycle.

The relative concentrations of N within the system present at Cueva-Cubío del Llanío are presented in Figure 5.6, with arrows representing the movement of N between the reservoirs. Beginning in the atmosphere, which contains the greatest reservoir of N, N is transferred into the vegetation-N pool via fixation (as in Figure 5.1). N passes between the soil-N and vegetation-N pools back and forth via assimilation and mineralisation (Fig. 5.1), though through the results presented in Chapter 5, there is a greater concentration of N within the vegetation-N pool above Cueva-Cubío del Llanío. Another source of N into the soil-N pool is rainfall, which has a relatively low concentration of N in comparison to the other reservoirs and inputs into the system. Bedrock-N contributes to the soil-N pool via soil creation (Fig 5.1) and in this system represents a small reservoir of inorganic N. As slightly acidic rainwater infiltrates through the soil and karst, it becomes more concentrated in N as N is transferred from both the soil-N and bedrock-N pools into the infiltrating rainwater (Fig. 5.1). This manifests within the cave as dripwater-N, which is then transferred to speleothems via calcite precipitation (Fig 5.1). The dripwater-N contains a lower concentration of N compared to the soil-N and bedrock-N pools, and the speleothem-N pool contains a lower N concentration compared to that of the dripwater-N pool, though both contain a greater concentration of N than the original rainwater-N pool.

N is cycled seasonally in the overlying environment due to changes in the balance between the soil and vegetation N pools above the cave system. This is reflected in the N composition of the drip waters entering the cave. Sediments, according to their age and origin, display a modern anthropogenic reactive N signal or a less polluted pre-industrial N signal. Sampling resolution of speleothem material is not at a fine enough resolution in this project to show this seasonal signal that is present in the drip waters. Further work at a high enough resolution may show that a historical seasonal changing signal of N is present in speleothem deposits.

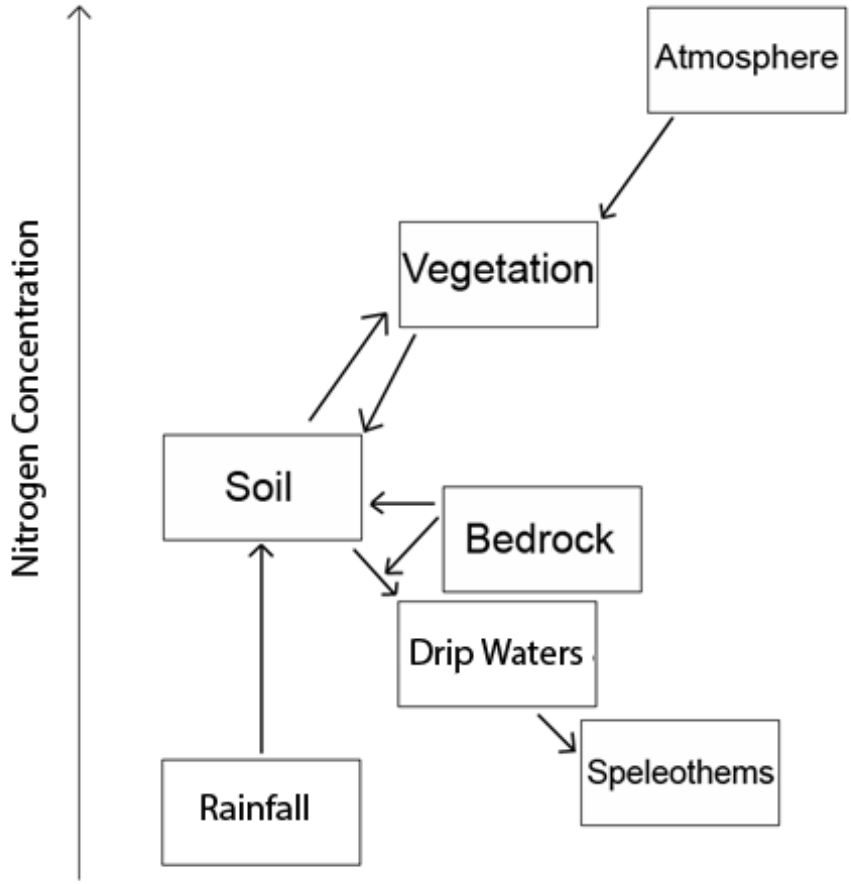

Figure 5.6 – A conceptual diagram illustrating the relative N concentrations between different reservoirs in the biogeochemical cycle at Cueva-Cubío del Llanío, based off nitrate-N concentrations presented in Chapter 5. Arrows represent the flow of N between reservoirs. Not to scale.

6. Nitrate Isotopes in Cueva-Cubío del Llanío

6.1. Introduction

The N biogeochemical cycle involves the movement of N through the environment (Figure 6.1). Various inputs into the cycle have their own isotopic signature – distinctive $\delta^{15}N\text{-}NO_3$ and $\delta^{18}O\text{-}NO_3$ ratios. As N passes through various components of the cycle via the processes in Figure 5.1, fractionation occurs.

Differing sources of anthropogenic reactive N have clear isotopic signatures that can be recognised in plots such as Figure 2.2. There is a large overlap between many of the potential sources in terms of the $\delta^{15}N\text{-}NO_3$ value, so where possible $\delta^{18}O\text{-}NO_3$ is also analysed. In general terms, the heavier the $\delta^{15}N\text{-}NO_3$ value, the greater proportion of the

source of the nitrate is organic waste. A lighter $\delta^{18}O\text{-}NO_3$ value is indicative of N fixed from the atmosphere – either in rainfall or from the Haber-Bosch process.

The main three processes within the N biogeochemical cycle that have the greatest effect on the isotopic signature are denitrification, nitrification and assimilation. Nitrification depletes $\delta^{15}N$ by 5-35‰ (Nikolenko *et al*., 2018). Oxygen composition of the nitrate is dependent on the $\delta^{18}O$ of the water and atmosphere, as nitrification takes one third of the oxygen from atmospheric oxygen and two-thirds from surrounding water, though the $\delta^{18}O\text{-}NO_3$ value for nitrate that has undergone nitrification is generally -10‰ to +10‰ as reported by Zhang *et al*. (2019).

Denitrification enriches $\delta^{15}N$ by -40 to - 5‰ and $\delta^{18}O$ by -18 to -8‰ (Zhang *et al*., 2019). Zhang *et* al. also state that denitrification leads to a negative correlation between $\delta^{15}N$ and nitrate concentration. Assimilation results in an extensive isotopic fractionation of both $\delta^{15}N$ and $\delta^{18}O$ (-27‰ to 0‰), with an expected fractionation ratio of $\delta^{15}N$ and $\delta^{18}O$ of 1:1 (Zhang *et al*., 2019).

At Cueva-Cubío del Llanío, vegetation, soil and cave sediments were analysed for $\delta^{15}N$ and rainwaters, bedrock, drip waters and speleothem material were analysed for $\delta^{15}N\text{-}NO_3$ and $\delta^{18}O\text{-}NO_3$ with an aim to examine the sources and fractionations of N in the N biogeochemical cycle present at the cave site. Further speleothem material from other cave sites around the world were also analysed for $\delta^{15}N\text{-}NO_3$ and $\delta^{18}O\text{-}NO_3$ to further the exploration of the method

6.2. Biogeochemical Cycling

6.2.1. Results

6.2.1.1. Rainfall to Drip Waters

The data range for the drip water samples is between +1.98 to +6.95‰ for $\delta^{15}N$ and -2.49 to 6.04‰ for $\delta^{18}O$. Within this isotope space, two distinct clusters of data can be observed (Figure 6.1) – the cluster for Whoopee Hall drip waters and the cluster for High Hopes chamber drip waters.

Whoopee Hall drip waters display a general trend toward lighter $\delta^{15}N\text{-}NO_3$ values, with a range of +1.98 to +6.36‰ and a mean of +3.345‰, clustering within the range typical for nitrate sourced from soil N or manure N. $\delta^{18}O\text{-}NO_3$ values are also generally isotopically light – Whoopee Hall $\delta^{18}O\text{-}NO_3$ values range from -2.49 to + 6.04‰ with a mean of +1.34‰. This indicates that the source of nitrate for Whoopee Hall drip waters is not atmospheric in origin.

High Hopes chamber drip waters have a heavier $\delta^{15}N\text{-}NO_3$ signature than that of Whoopee Hall, with a range of +4.48 to +6.95‰ and a mean of +5.95‰. Soil sources of N represent an average of all sources (e.g. atmospheric deposition, fixation, manure and inorganic fertiliser). At Whoopee Hall, where $\delta^{15}N\text{-}NO_3$ values in drip waters are isotopically lighter, the overlying environment is a low-grade hillslope with little agricultural development and thus will have very low inputs to no inputs of manure N. It is likely there is a greater input of N via atmospheric fixation compared to the input of manure N over Whoopee Hall. At High Hopes, which is located under agricultural pasture, there will still be a high degree of atmospheric fixation (perhaps more than above Whoopee Hall due to the clover-rich nature of the pasture) yet the drip water $\delta^{15}N\text{-}NO_3$ values are heavier than those of Whoopee Hall. Considering that any other input into the soil N pool would make the isotopic signature

lighter or not change the signature at all (as the soil N pool represents an average of the sources of N) it has to be concluded that the nitrate source above High Hopes chamber is a combination of soil N with an input of manure N.

$\delta^{18}O\text{-}NO_3$ values for High Hopes chamber drip waters skew toward being isotopically heavier than those in Whoopee Hall, with a range of -1.48 to +4.87‰ and a mean of +2.92‰.

Aven and corner series drip water isotope values blend between the two clusters of drip water isotope values. $\delta^{15}N\text{-}NO_3$ values range between +3.71 to +5‰ with a mean of +4.33‰, whilst $\delta^{18}O\text{-}NO_3$ values range between -0.05 to 2.58‰ with a mean of +1.13‰.

Rainfall $\delta^{15}N\text{-}NO_3$ values range from -1.32 to +2.96‰ with a mean of 1‰, whilst $\delta^{18}O\text{-}NO_3$ values range from +62.27 to +71.86‰ with a mean of +66.48‰. As such, both $\delta^{15}N\text{-}NO_3$ and $\delta^{18}O\text{-}NO_3$ values of the drip waters are different from those in the rainfall source waters. $\delta^{15}N\text{-}NO_3$ is enriched by 2.98 to 5.8‰ in High Hopes samples, and less so (3.3 to 3.4‰) in Whoopee Hall samples. The $\delta^{18}O\text{-}NO_3$ is distinctly offset by approximately 63.75 to 66.99‰ for High Hopes samples and 64.76 to 65.82‰ for Whoopee Hall samples.

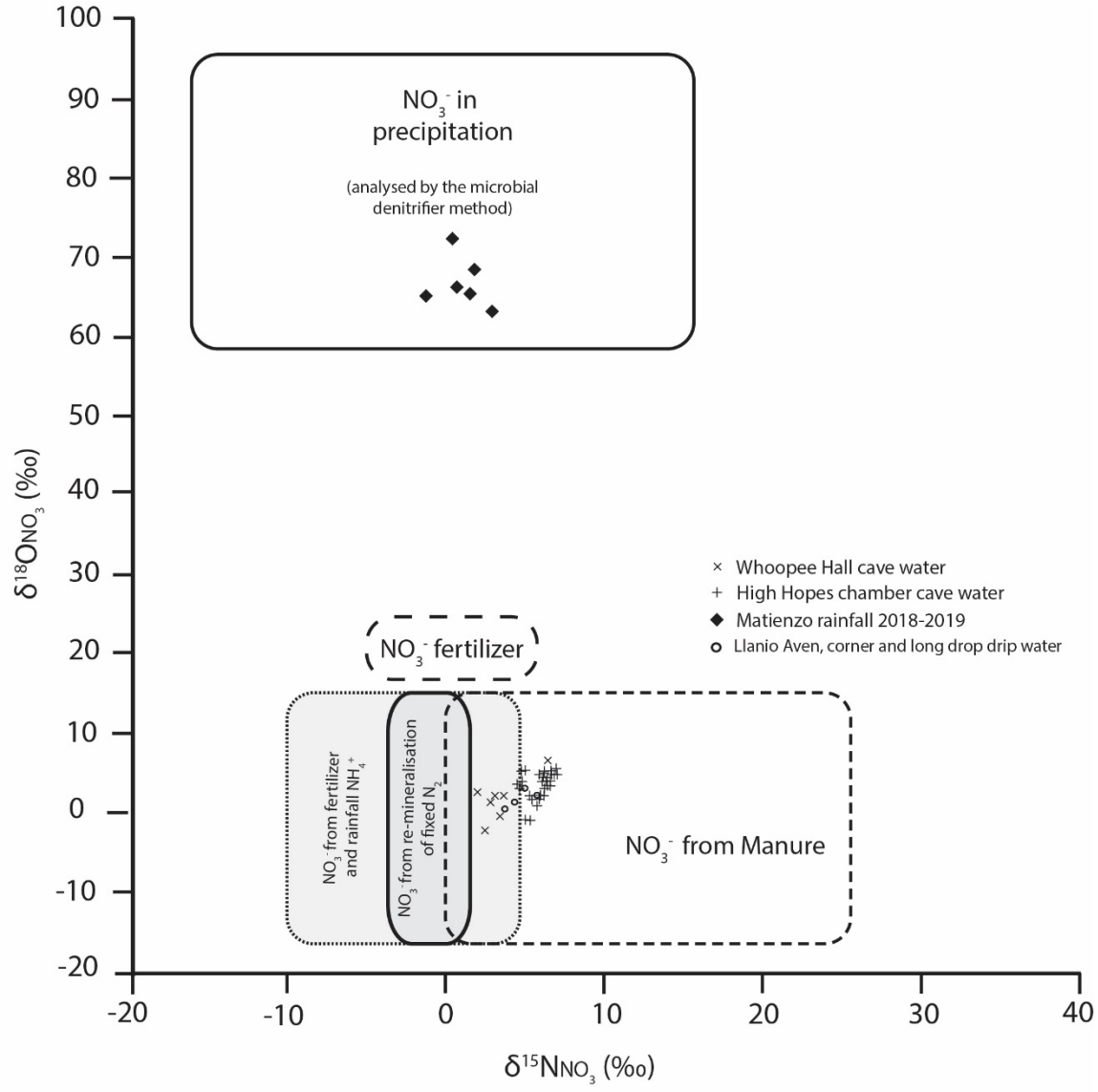

Figure 6.1 – Nitrate isotope ratios for cave waters collected from Cueva-Cubío del Llanío as compared to rainwater samples.

There is little to no observable seasonality to the $\delta^{15}N\text{-}NO_3$ values in the drip waters, as can be seen in Figure 6.2.

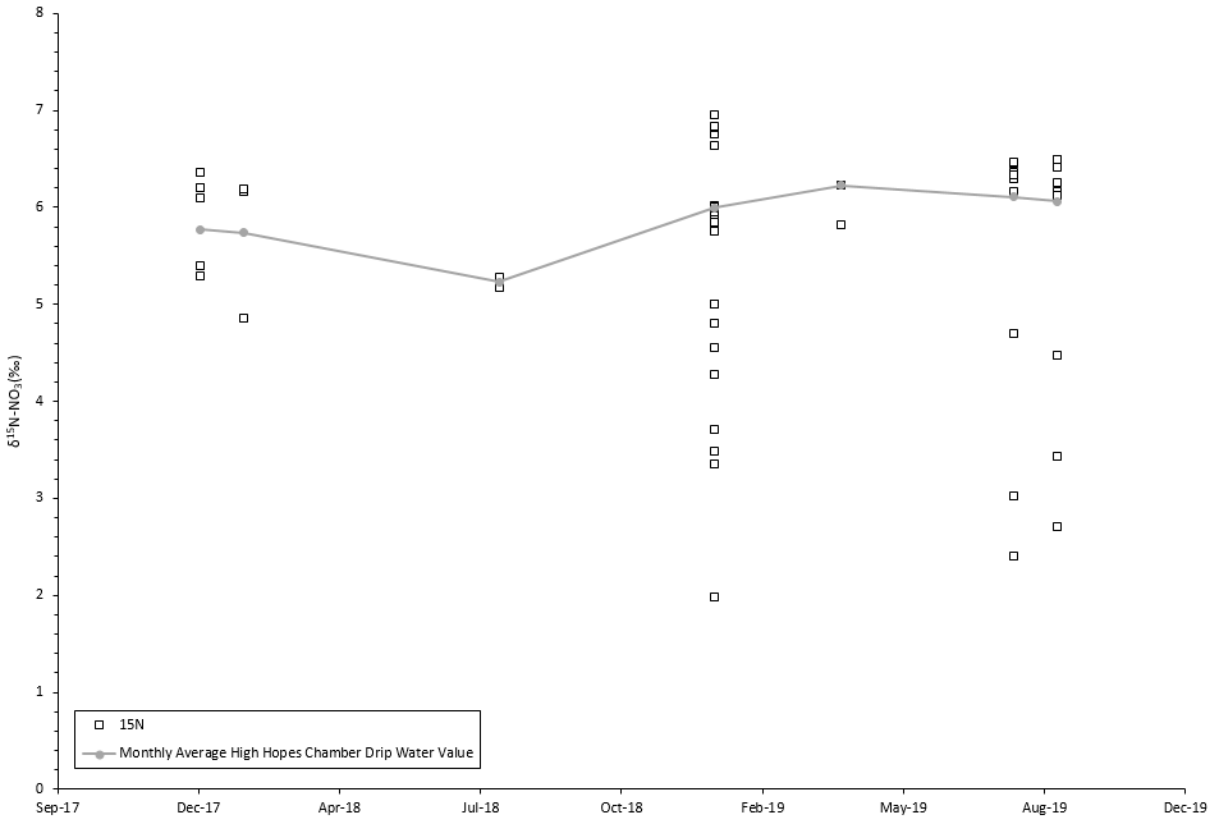

Figure 6.2: Drip water $\delta^{15}N\text{-}NO_3$ values over time, with the average 'monthly' (restricted to every month that samples were collected) $\delta^{15}N\text{-}NO_3$ value from High Hopes chambers superimposed.

There is little to no seasonality in the drip water $\delta^{18}O\text{-}NO_3$ values – Figure 6.3 - though the nitrate oxygen isotope values are not as stable as the nitrate N isotope values.

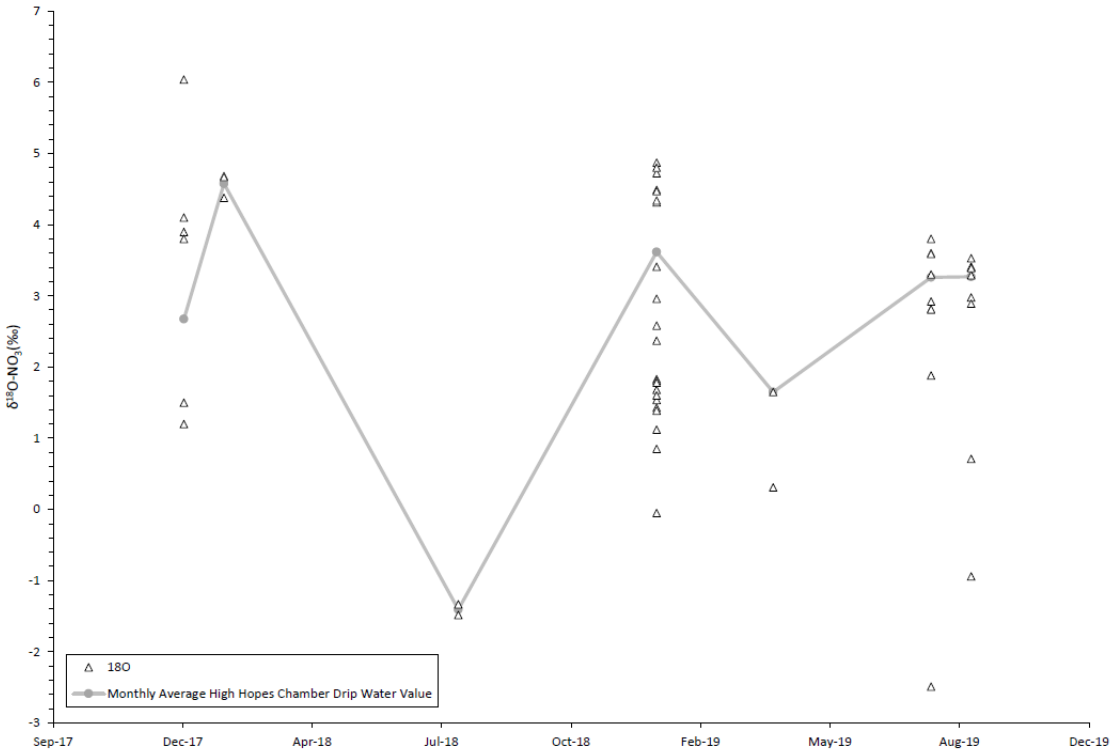

Figure 6.3: Drip water $\delta^{18}O\text{-}NO_3$ values over time, with the average 'monthly' (restricted to every month that samples were collected) $\delta^{18}O\text{-}NO_3$ value from High Hopes chamber drip waters superimposed.

6.2.1.2. Between Rainfall and Drip Waters

There is a clear difference between the rainfall and drip water N isotopes, thus it is important to look at the stores of N between the two to understand the sources of N between rainfall and drip water. Stores of N between rainfall and drip waters comprise of soil, vegetation, bedrock and cave sediments. These can be characterised isotopically, as detailed below.

6.2.1.2.1. Soil and Vegetation

Vegetation samples had lower $\delta^{15}N$ values than soil samples (Figure 6.4), with vegetation sample $\delta^{15}N$ ranging from -1.13 to +2.27‰ with a mean of 0.84‰ and soil sample $\delta^{15}N$ ranging from +5.42 to +6.67‰ with a mean of +5.91‰.

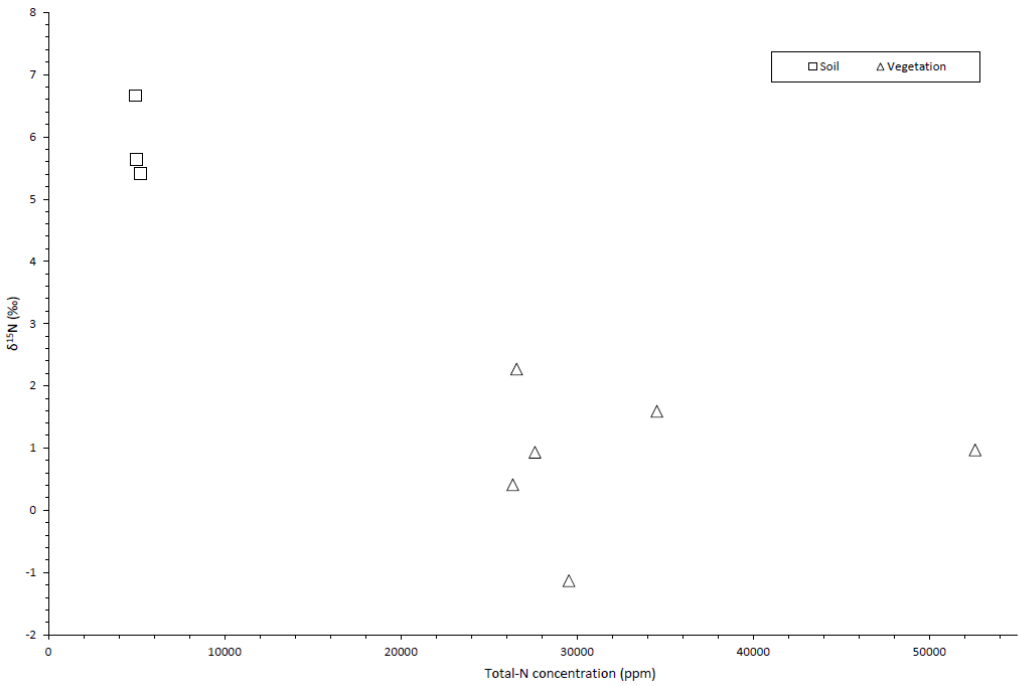

Figure 6.4: Comparing isotopic composition of soil samples versus vegetation samples.

6.2.1.2.2. Bedrock

Bedrock samples had similar $\delta^{15}N\text{-}NO_3$ values to drip waters but with $\delta^{18}O\text{-}NO_3$ values a little heavier than that of the drip water $\delta^{18}O\text{-}NO_3$ values (Table 6.1).

Table 6.1: NO_3 isotopic ratios for bedrock samples taken from Cueva-Cubío del Llanío.

Sample Name	**$\delta^{15}N\text{-}NO_3$ (‰)**	**$\delta^{18}O\text{-}NO_3$ (‰)**	**NO_3-N concentration (ppm)**
Llanío Bedrock 1	+4.19	+5.42	13.2
Llanío Bedrock 2	+4.71	+16.2	6.7

6.2.1.2.3. Cave Sediments

Cave sediments were collected from locations provided on Figure 3.10 (Chapter 3). $\delta^{15}N$ values ranged from +2.29 to +8.01‰ with a mean of +5.12‰. Figure 6.6 provides an overview of sediment $\delta^{15}N$ values contrasted with total-N concentration.

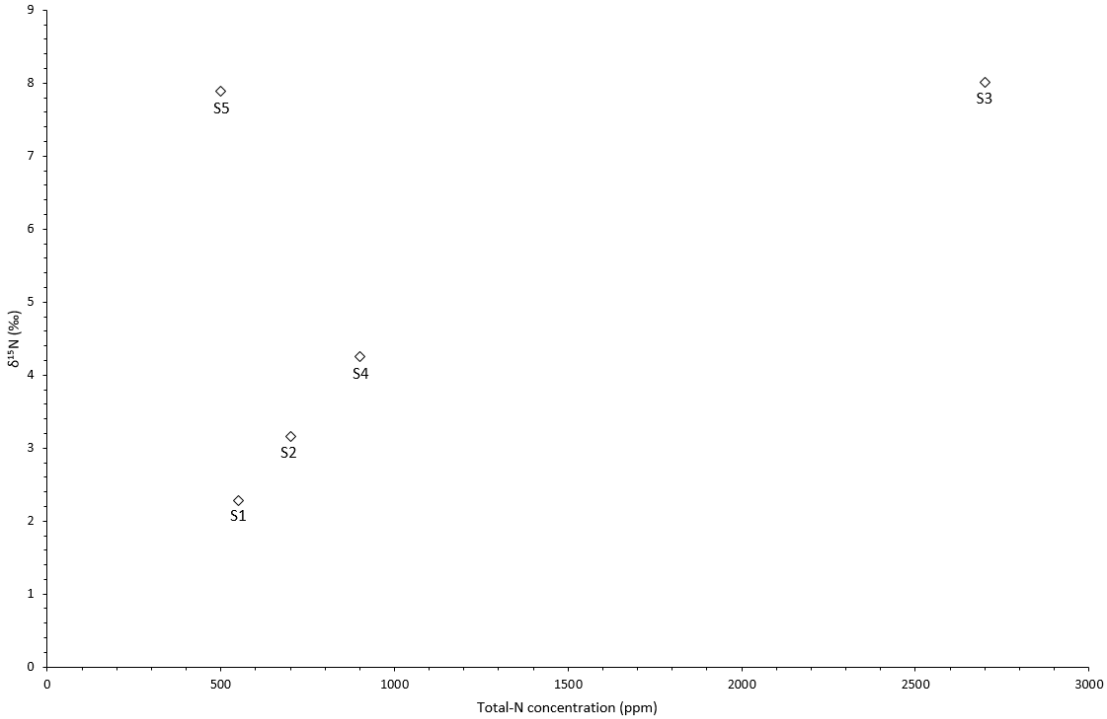

Figure 6.5 – $\delta^{15}N$ values for cave sediments taken from Cueva-Cubío del Llanío, contrasted with total-N concentration.

6.2.2. Discussion

6.2.2.1. Drip Waters

Surface environments above the chambers likely contribute to the differing NO_3 isotopic signatures present in each. Whoopee Hall is located underneath a steep grass slope with small rocky outcrops, High Hopes chamber under flat pasture land with some tree cover. Aven and Corner series is located under a steep grassy slope similar to the environment above Whoopee Hall, but within the boundaries of a small farmstead. The lighter isotopic ratio of nitrate-N in Whoopee Hall is likely a reflection of this overlying environment – the steep slope is unattractive for manure spreading and likely reduces the infiltration of rainwater through the soil and epikarst into the cave chamber below. In contrast, the pasture above High Hopes chamber has historically been used for grazing cattle and has an observed history of muckspreading to aid grass growth, thus it is likely a higher proportion of the nitrate-N present in the drip waters originated as manure-N. The nitrate-N isotope values found in the drip waters in the Aven and Corner series bridge the two clusters of drip waters from High Hopes chamber and Whoopee Hall. Two of the data points sit within the Whoopee Hall cluster and two within the High Hopes cluster, suggesting a mixture of the two land uses outlined above for Whoopee Hall and High Hopes' overlying environments.

6.2.2.2. Lack of seasonality in drip water nitrate isotopes

There is no observable seasonality in the drip water isotopes, despite the definite seasonal changes in nitrate-N concentrations described in chapter 5. This indicates that whatever causes the high winter and low summer nitrate-N concentrations, the process is not fractionating. The conclusion reached in Chapter 5, in which the seasonally shifting balance between assimilation and mineralisation in the soil-N pool is attributed to seasonality may still apply.

In a karst system such as the one found above Cueva-Cubío del Llaníο, where there is a history of agricultural land use, it can be assumed that the system is replete in N. It can also be considered an open system as soil N supply continuously exceeds demand due to the addition of fertiliser or manure. In such a system, the potential for fixation and assimilation to isotopically fractionate the soil N pool is low. Fixation causes very limited isotopic fractionation (-2 to +2 ‰) (Casciotti, 2009). Assimilation generates a residual soil pool deplete in ^{15}N (Liu *et al.*, 2014), however the impact of assimilation and its kinetic fractionation upon the soil N pool is dependent on whether the soil system is representative of an open or closed system. In a soil system such as that above Cueva-Cubío del Llaníο, where soil N supply likely continuously exceeds N demand, there will be an offset between plant and soil, though this will not be reflected in a change of soil isotopic composition over time. Mineralisation rarely causes fractionation in the soil N pool (Möbius et al., 2013).

Thus, both assimilation, fixation and mineralisation are processes that, in a karst system supporting agricultural land use are replete in N and likely follows an open system in regards to N cycling, have little effect upon soil-N isotopic status. Therefore, this shifting balance is the cause of the seasonality of the drip water nitrate-N concentration, it is unlikely that this seasonality would be present in the isotope data.

6.2.2.3. Soil and Vegetation

The soil N pool represents the fractionating effects of many processes. Wet deposition by rainfall is isotopically light. Mineralisation fractionates against the heavier isotope, thus the isotopes returned to the soil from the soil are isotopically lighter. Conversely volatilisation and assimilation cause heavier isotopes to accumulate in the soil. The isotopically heavy nature of the soil likely represents a preference in the Cueva-Cubío del Llaníο system for assimilation over mineralisation, rather than a preference for mineralisation or a balance between the two processes. This preference for assimilation is also reflected through the lighter vegetation isotopes, as vegetation has preferentially taken up isotopically lighter soil-N.

The similarity between the soil-N and drip water N isotopic values suggests that the soil-N pool is a source for cave water N, with little contribution being made through epikarst processes below the soil layer such as the dissolution of karst bedrock, the addition of stored water or denitrification.

6.2.2.4. Cave Sediments

Samples S1, 2, and 4 were dry sediments collected from the cave chamber floor and likely represent a mixture of endogenetic materials (cave aerosols, dust and rock spalling) and exogenous in-wash material from when the cave system was phreatic. Samples S3 and S5 were both unique sediment coatings, deposited in a gour pool system in High Hopes chamber and on the calcite floor within the Hub respectively. These deposits were wet when collected and seem to present spatially restricted materials related to fracture flow events. These sediment samples are therefore possibly younger in origin and likely consist of a greater proportion of exogenous material, thus have a heavier N isotope value.

6.3. Speleothem carbonate capture of drip water nitrate isotopes

A spatial and contemporary approach was taken to investigate the speleothem capture of N isotopic composition. Glass plates and the surface of Stalagmate loggers were used to collect contemporary calcite which was then scraped off and analysed.

6.3.1. Results

Speleothem material from Cueva-Cubío del Llanío had δ^{15}N-NO_3 values that ranged between +1.6 to +6.41‰ with a mean of +4.44‰ and δ^{18}O-NO_3 values that ranged between +12.32 to +32.34‰ with a mean of +22.31‰ (Figure 6.7).

Both cave chambers display similar speleothem material δ^{15}N-NO_3 values – Whoopee Hall has an average δ^{15}N-NO_3 of +3.36‰ and High Hopes chamber has an average of +4.87‰. The major difference between the two is the δ^{18}O-NO_3 values – Whoopee has a much lighter average δ^{18}O-NO_3 ratio of +14.74‰ compared to the average of +25.34‰ for High Hopes chamber.

Comparing these values to that of the drip waters in Cueva-Cubío del Llanío, it is clear that speleothem δ^{15}N-NO_3 displays a minimal depletion from the δ^{15}N-NO_3 present in the drip waters. For Whoopee Hall this is a depletion of 0.38 - 1.25‰, for High Hopes 0.54 - 1.21‰. In contrast, the difference in δ^{18}O-NO_3 values between speleothem and drip waters is notable. For Whoopee Hall, δ^{18}O-NO_3 values displayed an enrichment of 11.12 - 14.81‰ between drip waters and speleothem values, High Hopes displayed an enrichment of 20.37 - 27.47‰ between drip waters and speleothems.

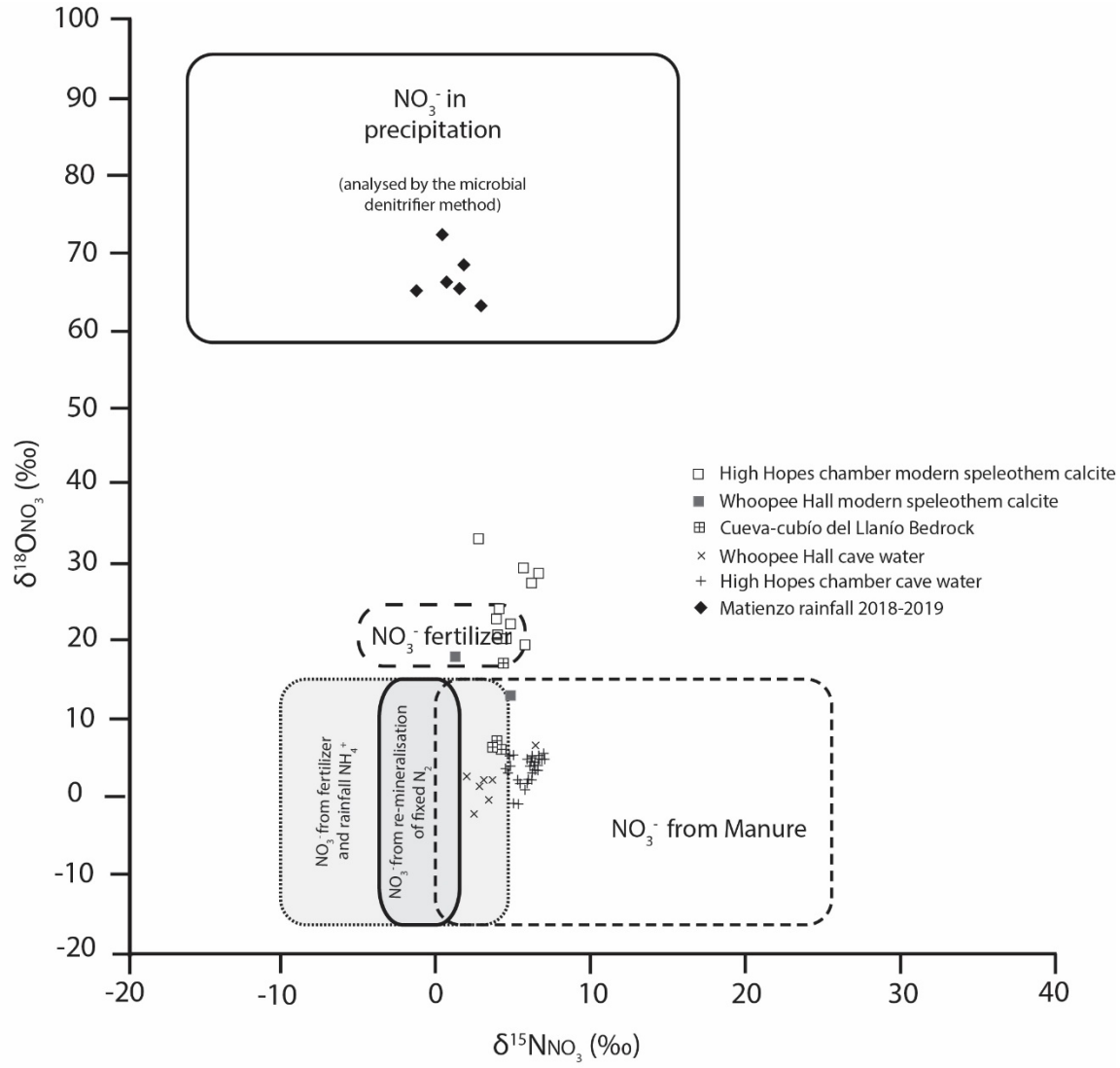

Figure 6.6: Nitrate isotopes in Cueva-Cubío del Llanío, comparing drip and rainwaters to speleothem values.

Further speleothem samples from around the world were also analysed for nitrate isotopic composition (Figure 6.8). Speleothem δ^{15}N-NO_3 values ranged from +3.49 to 5.95‰ with a mean of 4.77‰. Speleothem δ^{18}O-NO_3 values ranged from +5.96 to +57.3‰ with a mean of +25.66‰.

The greater range of speleothem δ^{18}O-NO_3 is of note, as the oxygen isotope value differs depending on the speleothem sample location. The speleothem material from the Yorkshire Dales has a very heavy δ^{18}O-NO_3 (~+57‰) compared to all the other speleothem samples, which generally cluster around the +20 to +30‰ range. MERC-1 material from Rukiesa Cave in Ethiopia has a lighter δ^{18}O-NO_3 value compared to the bulk of the speleothem samples with values ranging from +5.96 to +14.1‰ – a large range for samples taken from one stalagmite.

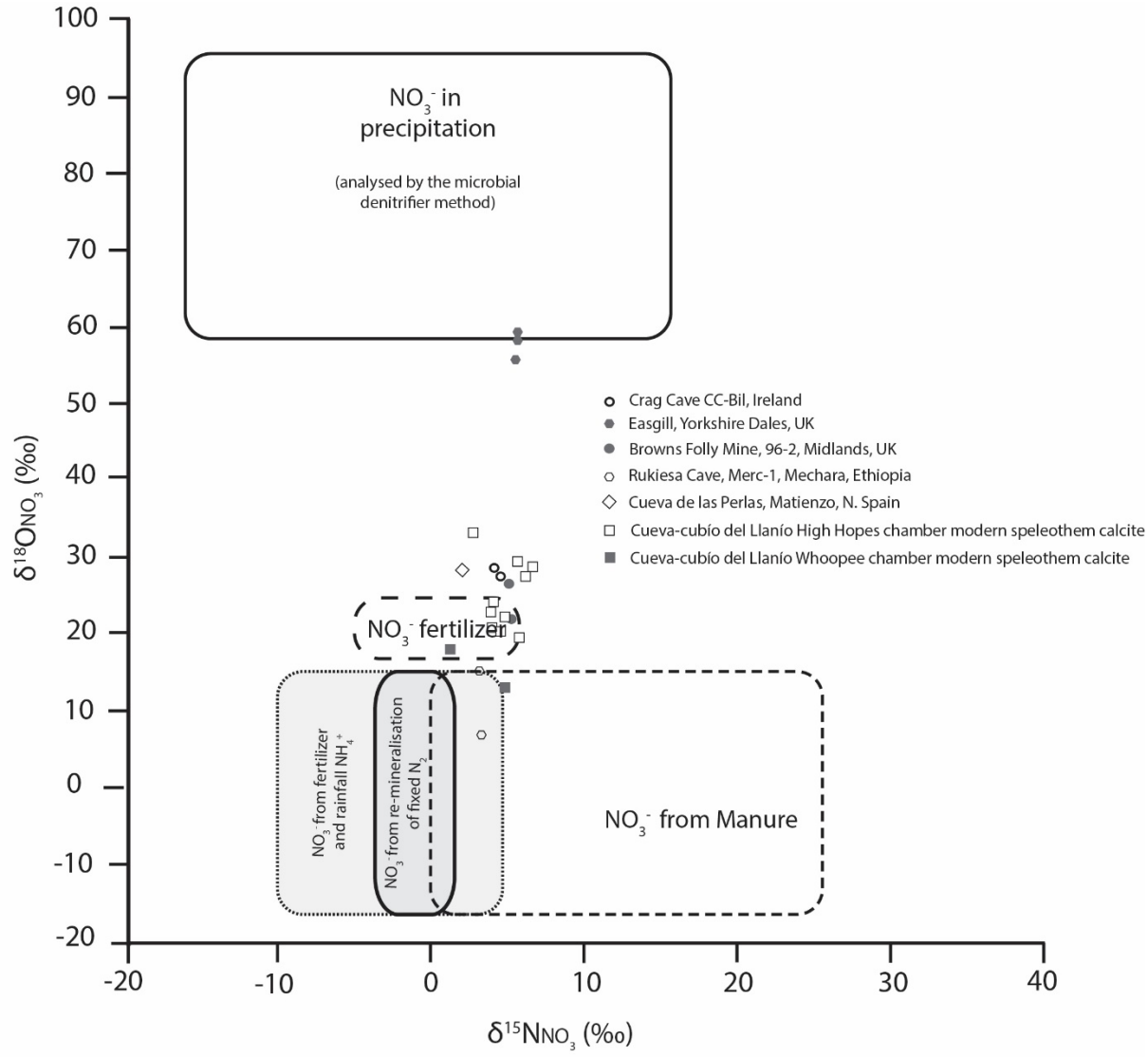

Figure 6.7: All speleothem nitrate isotope values from speleothems taken from cave sites around the world.

6.3.2. Discussion

6.3.2.1. δ^{18}O-NO_3 enrichment between drip waters and speleothems

The δ^{18}O values found within the speleothem calcite nitrate are not as expected – it was expected that the δ^{18}O values should be similar to the drip that feeds the speleothem. Instead δ^{18}O values are intermediate to the drip water and incoming rainfall.

One reason for this is that the speleothem calcite likely represents a 6-month integrated signal, as compared to the 24-hour signal encapsulated in the drip water sample. The differing resolutions between the two different sample types may be the cause of the intermediate $\delta^{18}O$ value. The speleothem calcite likely represents a weighted average signal of N.

Another possible explanation for this $\delta^{18}O$ signal is that fractionation may be occurring in the laboratory. Kaneko and Poulson (2013) reported that under low pH and high temperatures (i.e. pH <1, temperature >50°C) nitrate oxygen exchange may occur, though concluded that under natural conditions (e.g. 25°C. pH 7) the exchange rate was exceedingly slow. It is extremely unlikely that the digestion of the speleothem powders in hydrochloric acid could have led to this nitrate oxygen isotope exchange, as the temperature was ~20°C and the reaction went to neutral following the full digestion of speleothem material.

A final possible explanation is that there may be bacterial assimilation of the drip water nitrate occurring on the speleothem surface within the cave. Legatzki *et al.* (2011) provide evidence of speleothem-specific bacterial and archaeal colonies and Ortiz *et al*. (2014) indicates that speleothem-based microbiological colonies likely utilise a N-based primary production strategy. However, this enrichment pathway is unlikely – if bacterial fixation was occurring within Cueva-Cubío del Llanío it would be expected that the $\delta^{18}O$ values taken from pools within the cave would be similar to those displayed by the speleothem material, as pool water sits in the cave for long periods (and pools are fed by the same drips as the speleothems) and should show the same evidence of bacterial activity if it was occurring. Further tests to disprove this theory could include collecting thin film water samples from the stalagmites (though this would be incredibly difficult to do) or to conduct RNA screening. RNA screening would be the easier of the two tests, but it would be difficult to ascertain whether the screening would show only bacteria active on the stalagmite – it is likely some bacteria are washed into the cave from the soil system above through fracture flow similar to the way some sediments are washed into the cave from the soil above.

6.3.2.2. $\delta^{18}O$-NO_3 values in further speleothem samples

6.3.2.2.1. Browns Folley Mine 96-2, Midlands, UK

$\delta^{18}O$-NO_3 values for BFM 96-2 are indicative of nitrate of an atmospheric or nitrate-fertiliser origin. As the overlying environment above Browns Folley Mine is mixed deciduous woodland developed over the past 100 years, the presence of nitrate fertiliser can be discounted. Previous work on this speleothem by Wynn *et al*. (2008) investigated the origin of sulphate in BFM speleothems, where it was discovered that the sulphate present was of atmospheric origin, entering the mine directly through fractures and fissures and thus omitting any biogeochemical processing. It is likely that nitrate follows a similar hydrological pathway as the sulphate, with a $\delta^{18}O$-NO_3 signature indicative of atmospheric N pollution unmodified by biogeochemical cycling.

6.3.2.2.2. Easegill-1, Yorkshire Dales, UK

Easegill-1 has a presumed age of several thousand years – whilst the speleothem itself is undated, samples were drilled from the base of a fossil formation. This age precludes the invention of inorganic fertilisers. The $\delta^{18}O$-NO_3 signature indicates that the origin of the nitrate in Easegill-1 is atmospheric deposition.

6.3.2.2.3. MERC-1, Rukiesa Cave, Mechara, Ethiopia

The two samples taken from MERC-1 have $\delta^{18}O\text{-}NO_3$ values that differ from another notably. The lighter sample $\delta^{18}O\text{-}NO_3$ value suggests a large component of biogeochemical cycling (mineralisation to nitrate), whilst the heavier sample $\delta^{18}O\text{-}NO_3$ value suggests an origin of inorganic fertiliser. The area above the cave is intensively cultivated, which suggests an inorganic origin of N for both samples (ammonia and nitrate fertiliser respectively) with the lighter sample N having been mineralised prior to incorporation into the speleothem calcite. It is also possible that the two samples drilled from MERC-1 may represent different ages – whilst they were drilled from the same place, the second sample was drilled at a greater depth into the speleothem.

6.3.2.2.4. CC-Bil, Crag Cave, Ireland

Based on the $\delta^{18}O\text{-}NO_3$ and $\delta^{15}N\text{-}NO_3$ values for CC-Bil speleothem nitrate, it would be expected that there is minimal biogeochemical cycling above the cave as the nitrate isotopic signatures suggest direct incorporation of rainfall nitrate into speleothem calcite. This is unexpected, as work by Wynn *et al*. (2008) on speleothem sulphate suggested an extensive amount of sulphate reduction at Crag Cave on the basis of $\delta^{18}O\text{-}SO_4$ values. If sulphate reduction was extensive, nitrate concentrations would be expected to be minimal – though this is not the case as nitrate concentrations from CC-Bil calcite samples were 2.16 and 4.57 ppm (concentrations differ due to differences in method used to calculate nitrate-N concentration). Equally nitrate isotopes should follow the denitrification trajectory if sulphate reduction was extensive above the cave. It may be that the methodology of Wynn *et al*. (2008) did not account for the presence of nitrate, thus the heavy sulphate isotope values reported by Wynn *et* al. were influenced by contamination of product barium sulphate by speleothem nitrate, and thus it may be that the nitrate isotope values are the truer indication of the environment above the cave.

6.4. Conclusion

Examining the major components of the N biogeochemical cycle at Cueva-Cubío del Llanío, it can be suggested that the majority of the N in the drip waters is sourced from the soil N pool. It can be inferred from the soil and vegetation N isotopes that there is a preference for assimilation over mineralisation in the overlying environment above Cueva-Cubío del Llanío and though the total-N concentration data suggests that this signal is transferred to the drip waters, there is no isotopic evidence of this in the drip waters themselves. The drip water nitrate isotopes themselves are spatially distinct from one another, likely influenced by the differing land use above the chambers sampled.

This project represents the first successful extraction of N isotopes from speleothem material and thus proves that N isotopic signatures can be extracted from speleothem material. Observed speleothem $\delta^{15}N\text{-}NO_3$ values display little fractionation from drip water $\delta^{15}N\text{-}NO_3$, whilst speleothem $\delta^{18}O\text{-}NO_3$ values show an enrichment between drip water $\delta^{18}O\text{-}NO_3$ and speleothem values. This may be due to a difference in sampling resolutions between drip waters and speleothem materials or possibly due to microbiological activity on the speleothem surface but there is insufficient evidence to conclusively explain this isotopic enrichment at this time.

Further work in this area should include extracting a time series of changing N isotope composition, using growth rates and/or absolute dating techniques to create a historic record of changing N sources and fractionations over time; and the further investigation of

the non-fractionating process that causes the seasonality in the nitrate-N concentrations in the drip waters, likely using chlorine trace element concentrations to quantify the evaporation effect in the epikarst and further investigation into the hydrological regime above the cave to quantify the effects of residence time on drip water nitrate chemistry.

7. Conclusions and suggestions for further research

This dissertation is the first comprehensive cave monitoring study of Cueva-Cubío del Llanío and represents the first successful extraction of nitrate isotopes from speleothem calcite. The following sections will summarise key findings and highlight areas for further research.

7.1. Cave monitoring

Cave air temperatures display a seasonal density-driven ventilation regime, induced by the differences in temperature between the internal and external environments. This ventilation is moderated by the specific heat capacity of the rock. The seasonal patterns of cave air temperature (temperature stability in the summer, and instability in the winter) and the correspondence of these patterns to external air temperatures suggest a density-driven ventilation regime common in many cave systems around the world. Cave chambers within Cueva-Cubío del Llanío display differing connectivity to the overall density-driven ventilation regime that is further confirmed from observing the pCO_2 dynamics in the different cave chambers. An inverse temperature-CO_2 dynamic exists with High Hopes chamber, where pCO_2 rises as cave air temperatures fall. It is theorised that un-monitored chambers deeper within the cave system are warmer, thus strongly draw ventilation down deeper into the cave, bypassing the side-chambers of High Hopes and Whoopee Hall which leads to these chambers' air pockets stagnating due to lack of ventilation.

Stable isotope analyses of cave waters found that $\delta^{18}O$ and δD values lie clustered toward the winter end of the Local Meteoric Water Line, suggesting a homogenised aquifer primarily recharged during the winter months. From modern trace element analysis, it can be suggested that Mg concentrations reflect both water pathway and the dolomitic nature of the bedrock. Drips considered to be mostly fracture-fed contained lower Mg concentrations, suggesting a reduced rock-water contact time when compared with more matrix-fed drips.

Hydrological dynamics were determined through drip response to rainfall events. Two drip responses were recorded over the monitoring period. The first indicated an event-based response on top of a baseline drip rate, the second a drip that reflected a changing aquifer response to antecedent seasonal conditions with a further fracture-flow fed dynamic superimposed on top of a matrix-fed baseflow. These differing dynamics characterised the two monitored chambers – with Whoopee Hall exhibiting the more stable baseline drip rate + event response dynamic and High Hopes chamber reflecting a changing aquifer response.

A theoretical speleothem growth rate was established for drips within Cueva-Cubío del Llanío using a combination of monitoring data. Reported growth rates were ~0.1 mm/yr.

7.2. N Biogeochemical Cycling at Cueva-Cubío del Llanío

N concentrations from the main components of the N biogeochemical cycle showed that N followed the expected dynamics outlined in the hypothetical model of N biogeochemical cycling presented in Figure 5.1, with a low concentration input of rainfall followed by cycling

of N by vegetation and soil processes. N entered the cave system via drip waters and in-washing of external materials.

A preference for assimilation and fixation of N by plants over mineralisation of organic-N back to the soil was inferred through the larger concentration of N within the vegetation pool. A seasonal signal of N in the drip waters, with a winter high and summer low, was recorded. Dilution, evaporation and residence time were discounted due the winter timing of the high concentration signal combined with the D/O stable isotope signature of the drip waters. The seasonal signal was thus attributed to the changing seasonal balance of assimilation/fixation versus mineralisation in the overlying environment.

Speleothem sampling showed a general increase in speleothem nitrate concentrations with decreasing sampling depth in the Whoopee 1 stalagmite – indicating that there has been an increase in the input of reactive N into the system at Cueva-Cubío del Llanío over time. This follows the observed history of muck-spreading for grass growth at the site, though the expected reduction in reactive N that follows the cessation of this practice is not currently contained within the speleothem archive.

7.3. N isotopes in Cueva-Cubío del Llanío

Isotopic analysis of the components of the N biogeochemical cycle at Cueva-Cubío del Llanío displayed that surface environment has an observable impact on nitrate isotope composition in the cave drip waters below. Curiously, no seasonal signal was observed in the nitrate isotopes of the drip waters despite the seasonal signal found in the N concentrations. It was concluded that whatever caused the seasonality in concentration must be non-fractionating.

The isotopically heavy $\delta^{15}N$ values of the soil samples collected above the cave were attributed to the preference in the system for assimilation over mineralisation. The similarity between soil N isotopes and drip water N isotopes was taken as proof that cave water N was primarily sourced from the soil-N pool, as expected based on the predictions presented by Figure 5.1.

Comparison of drip water nitrate isotopes to speleothem nitrate isotopes showed little fractionation between drip water and speleothem $\delta^{15}N\text{-}NO_3$. However, it was found that $\delta^{18}O\text{-}NO_3$ values were enriched between drip water and speleothem values. The most plausible explanation for this is that it reflects the difference in resolutions between the two sample types, as drip water represent a 24-hr integration of the signal versus the longer 6-month integration present in speleothem calcite.

Further speleothems from a selection of cave sites around the world were analysed for their nitrate isotope compositions. Whilst $\delta^{15}N\text{-}NO_3$ values did not range greatly, each speleothem had a distinct $\delta^{18}O\text{-}NO_3$ signature. This nitrate oxygen isotope signature was taken as a reflection of the biogeochemical cycling and land use above the relevant cave site.

7.4. Potential avenues for further research

Exploring the potential for speleothems as an historic archive of groundwater N dynamics is key to validating groundwater N models (Meter and Basu, 2015; Meter *et al.,* 2016; Ascott *et al.*, 2017) and thus quantifying legacy N.

Preliminary work on speleothem N archives presented in this project represent the first of their kind. The potential for an archive of groundwater N dynamics at a seasonal scale,

contained within speleothem calcite, is unprecedented. Further work using Synchotron radiation to investigate speleothem material at a far greater resolution would be invaluable in investigating the resolution at which speleothem carbonate captures N signals.

Further work in quantifying the processes that affect N between soil and cave would help further characterise the N dynamics at play within the epikarst – this project did not truly investigate the impact of processes such as evaporation and water residence time on N concentrations and isotopes. With further work, a full understanding of the interaction between epikarst and N could be gained.

7.5. Summary

This study represents the first efforts to monitor a portion of the Cueva-Cubío del Llanío cave. In light of this monitoring program, the dynamics of N biogeochemical cycling through the overlying environment and into the cave were investigated. With this understanding of the N biogeochemical cycle at Cueva-Cubío del Llanío, speleothem samples were taken from the cave. For the first time, nitrate isotope values were extracted from speleothem material. A changing N signal was present within a speleothem, suggesting that with further work an archive of groundwater N dynamics could be found in speleothems, with a resolution as good as seasonal.

8. Reference List

Aranburu, A., Arriolabengoa, M., Iriarte, E., Giralt, S., Yusta, I., Martínez-Pillado, V., Val, M., Moreno, J., and Jimenez-Sanchez, M. (2015). Karst landscape evolution in the littoral area of the Bay of Biscay (north Iberian Peninsula). *Quaternary Internation* 364, 217-230. Ascott, M. J., Gooddy, D. C., Wang, L., Stuart, M. E., Lewis, M. A., Ward, R. S., and Binley, A. M. (2017). Global patterns of nitrate storage in the vadose zone. *Nature Communications* 8, 1416.

Ascott, M. J., Gooddy, D. C., Wang, L., Stuart, M. E., Lewis, M. A., Ward, R. S., and Binley, A. M. (2017). Global patterns of nitrate storage in the vadose zone. *Nature Communications* 8, 1416.

Badino, G. (2010). Underground meteorology – "what's the weather underground?". *Acta Carsologica* 39, 427-448.

Baker, A. J., Mattey, D. P., and Baldini, J. U. L. (2014). Reconstructing modern stalagmite growth from cave monitoring, local meteorology, and experimental measurements of dripwater films. *Earth and Planetary Science Letters* 392, 239-249.

Baker, A., and Brunsdon, C. (2003). Non-linearities in drip water hydrology: an example from Stump Cross Caverns, Yorkshire. *Journal of Hydrology* 227, 151-163.

Baldini, J. U. L. (2010). Cave atmosphere controls on stalagmite growth rate and paleoclimate records. *Geological Society, London, Special Publications* 336, 283-294.

Baldini, J. U. L., McDermott, F., and Fairchild, I. J. (2002). Structure of the 8200-year cold event revealed by a speleothem trace element record. *Science* 296, 2203-2206.

Bar-Matthews, M., Ayalon, A., and Kaufman, A. (1997). Late Quaternary paleoclimate in the eastern Mediterranean region from stable isotope analysis of speleothems at Soreq Cave, Israel. *Quaternary Research* 47, 155-168.

Bedard-Haughn, A., van Groenigen, J. W., and van Kessel, C. (2003). Tracing ^{15}N through landscapes: potential uses and precautions. *Journal of Hydrology* 272, 175-190.

Borsato, A., Frisia, S., Wynn, P. M., Fairchild, I. J., and Miorandi, R. (2015). Sulphate concentration in cave dripwater and speleothems: long-term trends and overview of its significance as proxy or environmental processes and climate changes. *Quaternary Science Reviews* 127, 48-60.

Bradley, C., Baker, A., Jex, C. N., and Leng, M. J. (2010). Hydrological uncertainties in the modelling of cave drip-water delta O-18 and the implications for stalagmite paleoclimate reconstructions. *Quaternary Science Reviews* 29, 2201-2214.

Buckley, C. (2012). Implementation of the EU Nitrates Directive in the Republic of Ireland – a view from the farm. *Ecological Economics* 78, 29-36.

Burkart, M. R., and Stoner, J. D. (2008). 'Nitrogen in groundwater associated with agricultural systems' in Hatfield, J. L., and Follet, R. F. (eds.) *Nitrogen in the Environment: Sources, Problems and Management*. Amsterdam: Elsevier, pp. 177-202.

Butterbach-Bahl, K., and Gundersen, P. (2011). 'Nitrogen processes in terrestrial ecosystems', in: Sutton, M. A., Howard, C. M., Erisman, J. W., Billen, G., Bleeker, A., Grennfelt, P., van Grinsven, H., and Grizzetti, B. (eds.) *The European Nitrogen Assessment. Cambridge: Cambridge University Press,* pp. 99-125.

Cai, Y., Chang, S. X., and Cheng, Y. (2017). Greenhouse gas emissions from excreta patches of grazing animals and their mitigation strategies. *Earth-Science Reviews* 171, 44-57.

Carrasco, F., Aandreo, B., Liñan, C., and Mudry, J. (2006). Contribution of stable isotopes to the understanding of the unsaturated zone of a carbonate aquifer (Nerja Cave, southern Spain). *Comptes Rendus Geoscience* 338, 1203-1212.

Casciotti, K.L. (2009). Inverse kinetic isotope fractionation during bacterial nitrite oxidation. *Geochimica et Cosmochimica Acta*, 73, 2061- 2076.

Chen, J., Liu, J., Xie, C., Chen, G., Chen, J., Zhang, Z., Zhou, A., Rühland, K. M., Smol, J. P., and Chen, F. (2018). Biogeochemical responses to climate change and anthropogenic nitrogen deposition from a ~200-year record from Tianchi Lake, Chinese Loess Plateau. *Quaternary International* 493, 22-30.

Clarke, I., and Fritz, P. (1997). *Environmental Isotopes in Hydrogeology*. Boca Raton, USA: CRC Press.

Cobo, J. R. (n.d.). *The Matienzo Valley.* Date accessed: 08/01/2020. <http://matienzocaves.org.uk/science/web_matienzo/pdfs/Matienzo%20Environment.pdf>

Connor, D.J. (2018). Land required for legumes restricts the contribution of organic agriculture to global food security. *Outlook on Agriculture* 47, 277-282.

Corrin, J. (2018). 3234: Llanío, Cueva-Cubío del (Cold Store Cave). <http://matienzocaves.org.uk/surveys/3234-current.pdf>

Corrin, J. (2020). *Site 3234*. Date accessed 08/01/2020. <http://www.matienzocaves.org.uk/descrip/3234.htm>

'Council Directive 91/676/EEC concerning the protection of waters against the pollution caused by nitrates from agricultural sources' (1991). *Official Journal* L375, p. 1. Ascott, M. J., Gooddy, D. C., Wang, L., Stuart, M. E., Lewis, M. A., Ward, R. S., and Binley, A. M. (2017). Global patterns of nitrate storage in the vadose zone. *Nature Communications* 8, 1416.

'Council Directive 98/83/EC of 3 November 1998 on the quality of water intended for human consumption' (1998). *Official Journal* L330, p. 32-54.

Craig, H. (1961). Isotopic Variations in Meteoric Waters. *Science* 133, 1702-1703.

Cubas, M., Altuna, J., Álvarez-Fernández, E., Armendariz, A.,Fano, M. A., López-Dóriga, I. L., Mariezkurrena, K., Tapia, J., Teira, L. C., and Arias, P. (2016). Re-evaluating the Neolithic: the impact and the consolidation of farming practices in the Cantabrian region (northern Spain). *Journal of World Prehistory* 29, 79-116.

Dahlgren, R. A. (2006). Biogeochemical processes in soils and ecosystems: from landscape to molecular scale. *Journal of Geochemical Exploration* 88, 186-189.

Deeprose, L. (2018). *Speleothem climate capture of the Neanderthal demise*. PhD, Lancaster University.

Denniston, R. F., González, L. A., Asmerom, Y., Reagan, M. K., and Recelli-Snyder, H. (2000). Speleothem carbon isotopic records of Holocene environments in the Ozark Highlands, USA. *Quaternary International* 67, 21-27.

Dewitt, J., Foubert, S., Desouky, H. A., Muchez, P., Hunt, D., Vanhaecke, F., and Swennen, R. (2014). Characteristics, genesis and parameters controlling the development of a large stratabound HTD body at Matienzo (Ramales Platform, Basque-Cantabrian Basin, northern Spain). *Marine and Petroleum Geology* 55, 6-25.

Dreybrodt, W. (1999). Chemical kinetics, speleothem growth and climate. *Boreas* 28, 347-356.

Exner, M. E., Hirsh, A. J., and Spalding, R. F. (2014). Nebraska's groundwater legacy: nitrate contamination beneath irrigated cropland. *Water Resources Research* 50, 4474-4489.

Fairchild, I. J., and Baker, A. (2012). *Speleothem Science.* Wiley-Blackwell: Sussex, UK.

Fairchild, I. J., and Treble, P. C. (2009). Trace elements in speleothems as recorders of environmental change. *Quaternary Science Reviews* 28, 449-468.

Fairchild, I. J., Frisia, S., Borsato, A., and Tooth, A. F. (2007). Chapter 7: Speleothems. In: Nash, D.J., and McLaren, S. J. (eds.) *Geochemical Sediments and Landscapes.* Oxford: Blackwells.

Fairchild, I. J., Tuckwell, G. W., Baker, A., and Tooth, A. F. (2006). Modelling of dripwater hydrology and hydrochemistry in a weakly karstified aquifer (Bath, UK): implications for climate change studies. *Journal of Hydrology* 321, 213-231.

FAO (Food and Agriculture Organisation of the United Nations) (2015). *World Fertiliser Trends and Outlook to 2018*. Food and Agriculture Organisation of the United Nations: Rome.

Ford, D. C. and Williams, P. (2007). *Karst Hydrogeology and Geomorphology*. GB: Wiley.

Fowler, D., Coyle, M., Skiba, U., Sutton, M.A. *et al.* (2013). The global nitrogen cycle in the twenty-first century. *Philosophical Transactions of the Royal Society London B: Biological Sciences* 368, 20130164.

Frumkin, A., and Stein, M. (2004). The Sahara-East Mediterranean dust and climate connection revealed by strontium and uranium isotopes in a Jerusalem speleothem. *Earth and Planetary Science Letters* 217, 451-464.

Gao, Y., Yu, G., Luo, C., and Zhou, P. (2012). Groundwater nitrogen pollution and assessment of its health risks: a case study of a typical village in rural-urban continuum, China. *PLoS ONE* 7, e33983.

Goodchild, R. G. (1998). EU policies for the reduction of nitrogen in water: the example of the Nitrates Directive. *Environmental Pollution* 102, 737-740.

Gutiérrez, J. (2010). Geological map of Matienzo, Arredondo, Ogarrio and surroundings. *In:* Corrin, J., and Smith, P. (eds.) *Matienzo 50 years of speleology.* Bacup: Matienzo Caves.

Hansen, B., Thorling, L., Schullehner, J., Termansen, M., and Dalgaard, T. (2017). Groundwater nitrate response to sustainable nitrogen management. *Scientific Reports* 7, 8566.

Harter, T., Lund, J. R., Darby, J., Fogg, G. E. *et al.* (2012). *Addressing nitrate in California's drinking water with a focus on Tulare Lake Basin and Salinas Valley Groundwater*. Available at: <http://watermanagement.ucdavis.edu/files/2214/5886/6964/Harter_et_al._2012_Addressing_Nitrate_in_CA_Drinking_Water.pdf>

Hartsough, P., Tyler, S. W., Sterling, J., and Walvoord, M. (2001). A 14.6 kyr record of nitrogen flux from desert soil profiles as inferred from vadose zone pore waters. *Geophysical Research Letters* 28, 2955-2958.

He, J., Balasubramanian, R., Burger, D. F., Hicks, K., Kuylenstierna, J. C. I., and Palani, S. (2011). Dry and wet atmospheric deposition of nitrogen and phosphorus in Singapore. *Atmospheric Environment* 45, 2760-2768.

Heaton, T. H. E. (1986). Isotopic studies of nitrogen pollution in the hydrosphere and atmosphere: a review. *Chemical Geology (Isotope Geoscience Section)* 59, 87-102.

Holloway, J. M., and Dahlgren, R. A. (2002). Nitrogen in rock: occurrences and biogeochemical implications. *Global Biogeochemical Cycles* 16, 65-1-65-17.

Huang, P., Zhang, J., Ma, D., Wen, Z., Wu, S., Garland, G., Pereira, E. I. P., Zhu, A., Xin, X., and Zhang, C. (2016). Atmospheric deposition as an important nitrogen load to a typical agro-ecosystem in the Huang-Huai-Hai Plain. 2. Seasonal and inter-annual variations and their implications (2008-2012). *Atmospheric Environment* 129, 1-8.

Huebsch, M., Horan, B., Blum, P., Richards, K. G., Grant, J., and Fenton, O. (2013). Impact of agronomic practices of an intensive dairy farm on nitrogen concentrations in a karst aquifer in Ireland. *Agriculture, Ecosystems and Environment* 179, 187-199.

IARC (IARC Working Group on the Evaluation of Carcinogenic Risks to Humans). (2010). Ingested nitrate and nitrite, and cyanobacterial peptide toxins. *IARC monographs on the evaluation of carcinogenic risks to humans* 94, Lyon, France: IARC.

Isobe, K., Oka, H., Watanabe, T., Tateno, R., Urakawa, R., Liang, C., Senoo, K., and Shibata, H. (2018). High soil microbial activity in the winter season enhances nitrogen cycling in a cool-temperate deciduous forest. *Soil Biology and Biogeochemistry*, 124, 90-100.

James, E. W., Banner, J. L, and Hardt, B. (2015). A global model for cave ventilation and seasonal bias in speleothem paleoclimate records. *Geochemistry, Geophysics, Geosystems* 16, 1044-1051

James, J. M. (1977). Carbon dioxide in the cave atmosphere. *Transactions of the British Cave Research Association* 4, 417-429.

Jenkins, H. D. B. and Thakur, K. P. (1979). Reappraisal of thermochemical radii for complex ions. *Journal of Chemical Education* 56, 576-577.

Kaneko, M., and Poulson, S. R. (2013). The rate of oxygen isotope exchange between nitrate and water. *Geochimica et Cosmochimica Acta* 118, 148-156.

Katz, B. G., Chelette, A. R., and Pratt, T. R. (2004). Use of chemical and isotopic tracers to assess nitrate concentrations and ground-water age, Woodville Karst Plain, USA. *Journal of Hydrology* 289, 36-61.

Kendall, C. (1998). 'Tracing nitrogen sources and cycling in catchments', in Kendall, C., and McDonnell, J. J. (eds.) *Isotope Tracers in Catchment Hydrology*. Amsterdam: Elsevier, pp. 50-86.

Kendall, C. and Caldwell, E. A. (1998). 'Fundamentals of Isotope Geochemistry', in Kendall, C. and McDonnell, J. J. (eds.) *Isotope Tracers in Catchment Hydrology*. Amsterdam, Elsevier, pp. 50-86.

Kendall, C., Elliott, E. M., and Wankel, S. D. (2007). 'Tracing Anthropogenic Inputs of Nitrogen to Ecosystems', in Michener, R., and Lajtha, K. (eds.) *Stable Isotopes in Ecology and Environmental Science*. Malden, MA, USA: Blackwell Publishing, pp. 375-449.

Kontrec, J., Kralj, D., Brecevic, L., Falini, G., Fermani, S., Noethig-Laslo, V., and Mirosavljevic, K. (2004). Incorporation of inorganic anions in calcite. *European Journal of Inorganic Chemistry*, 4579-4585.

Kumar, S., Herrmann, M., Thamdrup, B., Schwab, V. F., Geesink, P., Trumbore, S. E., Totsche, K., and Küsel, K. (2017). Nitrogen loss from pristine carbonate-rock aquifers of the Hainich Critical Zone Exploratory (Germany) is primarily driven by chemolithoautotrophic anammox processes. *Frontiers in Microbiology* 8, 1961.

Lange, J., Arbel, Y., Grodek, T., and Greenbaum, N. (2010). Water percolation process studies in a Mediterranean karst area. *Hydrological Processes* 24, 1866-1879.

Le Quéré, C., Andrew, R.M., Friendlingstein, P. *et al.* (2018). Global carbon budget 2018. *Earth System Science Data* 10, 2141-2194.

Legatzki, A., Ortiz, M., Neilson, J. W., Dominguez, S., Andersen, G. L., Toomey, R. S., Pryor, B. M., Pierson, L. S., and Maier, R. M. (2011). Bacterial and archaeal community structure of two adjacent calcite speleothems in Kartchner Caverns, Arizona, USA. *Geomicrobiology Journal* 28, 99-117.

Liu, C., Li, S., Lang, Y., and Xiao, H. (2006). Using $\delta^{15}N$- and $\delta^{18}O$-values to identify nitrate sources in karst ground water, Guiyang, southwest China. *Environmental Science & Technology* 40, 6928-6933.

Liu, X., Zhang, Y., Han, W., Tang, A., Shen, J., Cui, Z., Vitousek, P., Erisman, J. W., Goulding, K., Christie, P., Fangmeier, A., and Zhang, F. (2013). Enhanced nitrogen deposition over China. *Nature* 494, 459–462.

Liu, X-Y., Koba, K., Makabe, A. and Liu, C-Q. (2014). Nitrate dynamics in natural plants: insights based on the concentration and natural isotope abundances of tissue nitrate. *Frontiers in Plant Science*, 5, article number 355.

Martens, D. A. (2005). 'Denitrification', in Hillel, D. (ed.) *Encyclopedia of Soils in the Environment.* Oxford: Elsevier, pp. 378-382.

Mattey. D. P., and Collister, C. (2008). Acoustic drip counters for environmental monitoring. *BCRA Cave Radio and Electronics Group* 70, 14-17.

McDonald, J., Drysdale, R., Hill, D., Chisari, R., and Wong, H. (2007). The hydrochemical response of cave drip waters to sub-annual and inter-annual climate variability, Wombeyan Caves, SE Australia. *Chemical Geology* 224, 605-623.

Minagawa, M., and Wada, E. (1984). Stepwise enrichment of ^{15}N along food chains: further evidence and the relation between $\delta^{15}N$ and animal age. *Geochimica et Cosmochimica Acta* 48, 1135-1140.

Miorandi, R., Borsato, A., Frisia, S., Fairchild, I. J., and Richter, D. K. (2010). Epikarst hydrology and implication for stalagmite capture of climate changes at Grotta di Ernesto (NE Italy): results from long-term monitoring. *Hydrological Processes* 24, 3101-3114.

Möbius, J., (2013). Isotope fractionation during nitrogen remineralization (ammonification): implications for nitrogen isotope biogeochemistry. *Geochimica et Cosmochimica Acta*, 105, 422–432.

Montross, G. G., McGlynn, B. L., Montross, S. N., and Gardner, K. K. (2013). Nitrogen production from geochemical weathering of rocks in southwest Montana, USA. *Journal of Geophysical Research: Biosciences* 118, 1068-1078.

Morellón, M., Aranbarri, J., Moreno, A., González-Sampériz, P., and Valero-Garcés, B. L. (2018). Early Holocene humidity patterns in the Iberian Peninsula reconstructed from lake, pollen and speleothem records. *Quaternary Science Reviews* 181, 1-18.

Morford, S.L., Houlton, B. Z., and Dahlgren, R. A. (2016). Direct quantification of long-term rock nitrogen inputs to temperate forest ecosystems. *ESA* 97, 54-64.

Mudarra, M., Andreo, B., Barberá, J. A., and Mudry, J. (2014). Hydrochemical dynamics of TOC and NO_3^- contents as natural tracers of infiltration in karst aquifers. *Environmental Earth Sciences* 71, 507-523.

Musgrove, M., Opsahl, S. P., Mahler, B. J., Herrington, C., Sample, T. L., and Banta, J. R. (2016). Source, variability, and transformation of nitrate in a regional karst aquifer: Edwards aquifer, central Texas. *Science of the Total Environment* 568, 457-469.

Newton, K. E., Fairchild, I. J., and Gunn, J. (2015). Rates of calcite precipitation from hyperalkaline waters, Poole's Cavern, Derbyshire, UK. *Cave and Karst Science* 42. 116-124.

Nikolenko, O., Jurado, A., Borges, A. V., Knöller, K., and Brouyère S. (2018). Isotopic nitrogen species in groundwater under agricultural areas: a review. *Science of the Total Environment* 621, 1415-1432.

Ones, B. (1978). 'Cave Sediments', in Middleton, G. V., Church, M. J., Coniglio, M., Hardie, L. A., and Longstaffe, F. J. (eds.) *Encyclopedia of Sediments and Sedimentary Rocks. Encylopedia of Earth Sciences Series.* Dordrecht: Springer. Ascott, M. J., Gooddy, D. C., Wang, L., Stuart, M. E., Lewis, M. A., Ward, R. S., and Binley, A. M. (2017). Global patterns of nitrate storage in the vadose zone. *Nature Communications* 8, 1416.

Opsahl, S. P., Musgrove, M., and Slattery, R. N. (2017). New insights into nitrate dynamics in a karst groundwater system gained from in situ high-frequency optical sensor measurements. *Journal of Hydrology* 546, 179-188.

Ortiz, M., Legatzki, A., Neilson, J. W., Fryslie, B., Nelson, W. M., Wing, R. A., Soderlund, C. A., Pryor, B. M., and Maier, R. M. (2014). Making a living while starving in the dark: metagenomics insights into the energy dynamics of a carbonate cave. *The ISME Journal* 8, 478-491.

Palmer, A. N. (2010). Understanding the hydrology of karst. *Geologica Croatia* 63, 143-148.

Pretty, J. N., Brett, C., Gee, D., Hine, R. E., Mason, C. F., Morison, J. I. L., Raven, H., Rayment, M. D., and van der Bijl, G. (2000). An assessment of the total external costs of UK agriculture. *Agricultural Systems* 65, 113-136.

Prosser, J. I. (2005). 'Nitrogen in Soils | Nitrification', in Hillel, D. (ed.) *Encyclopedia of Soils in the Environment*. Oxford: Elsevier, pp. 31-39.

Quin, A. (2010). Matienzo Geomorphology. *In*: Corrin, J. and Smith, P. (eds.) *Matienzo 50 years of speleology.* Bacup: Matienzo Caves.

Rivett, M. O., Buss, S. R., Morgan, P., Smith, J. W. N. S., and Bemment, C. D. (2008). Nitrate attenuation in groundwater: a review of biogeochemical controlling processes. *Water Research* 42, 4215-4232.

Robertson, W. D., Moore, T. A., Spoelstra, J., Li, L., Elgood, R. J., Clark, I. D., Schiff, S. L., Aravena, R., and Neufeld, J.D. (2012). Natural attenuation of septic system nitrogen by anammox. *Groundwater* 50, 541-553.

Sebilo, M., Mayer, B., Nicolardot, B., Pinay, G., and Mariotti, A. (2013). Long-term fate of nitrate fertilizer in agricultural soils. *PNAS* 110, 18185-18189.

Shukla, S., and Saxena, A. (2018). 'Global status of nitrate contamination in groundwater: its occurrence, health impacts, and mitigation measures', in Hussain, C. (ed.) *Handbook of Environmental Materials Management*. Cham: Springer, pp. 1-21.

Sigman, D. M., Casciotti, K. L., Andreani, M., Barford, C., Galanter, M., and Böhlke, J. K. (2001). A bacterial method for the nitrogen isotopic analysis for nitrate in seawater and freshwater. *Analytical Chemistry* 73, 4145-4153.

Smart, P. L., and Friedrich, H. (1987). Water movement and storage in the unsaturated zone of a maturely karstified aquifer, Mendip Hills, England. Conference on Environmental Problems in Karst Terrains and their Solution, Bowling Green, Kentucky. National Water Well Association, 57-87.

Smith, A. (2014). *Speleothem Climate Capture – A Holocene Reconstruction of Northern Iberian Climate and Environmental Change*. PhD, Lancaster University.

Smith, A. C., Wynn, P. M., and Barker, P. A. (2013). Natural and anthropogenic factors which influence aerosol distribution in Ingleborough Show Cave, UK. *International Journal of Speleology* 42, 49-56.

Smith, A. C., Wynn, P. M., Barker, P. A., and Leng, M. J. (2015). Drip water electrical conductivity as an indicator of cave ventilation at the event scale. *Science of the Total Environment* 532, 517-527.

Smith, A. C., Wynn, P. M., Barker, P. A., and Leng, M. J. (2015). Drip water electrical conductivity as an indicator of cave ventilation at the event scale. *Science of the Total Environment* 532, 517-527.

Smith, A. C., Wynn, P. M., Barker, P. A., Leng, M. J., Noble, S. R., and Stott, A. (2018). Cave monitoring and the potential for paleoclimate reconstruction from Cueva de Asiul, Cantabria (N. Spain). *International Journal of Speleology,* 45, 1-9.

Spötl, C., Fairchild, I. J., and Tooth, A. F. (2005). Cave air control on dripwater geochemistry, Obir Caves (Austria): implications for speleothem deposition in dynamically ventilated caves. *Geochimica et Cosmochimica Acta* 69, 2451-2468.

Stenstrom, M. K. and Poduska, R. A. (1980). The effect of dissolved oxygen concentration on nitrification. *Water Research* 14, 643-649.

Stigter, T. Y., Carvalho Dill, A. M. M., and Ribiero, L. (2011). Major issues regarding the efficiency of monitoring programs for nitrate contaminated groundwater. *Environmental Science and Technology* 45, 8674-8682.

Stuart, M. E., and Lapworth, D. J. (2016). Macronutrient status of UK groundwater: nitrogen, phosphorus and organic carbon. *Science of the Total Environment* 572, 1543-1560.

Sun, W., Shen, J., Zhang, E., Hasebe, N., Kashiwaya, K., Chen, R.,and Itono, T. (2016). Stable nitrogen isotope record of lacustrine sediments in Lake Onuma (Northern Japan) indicates regional hydrological variability during the past four centuries. *Quaternary International* 397, 307-316.

Talbot, M. R., and Johannessen, T. (1992). A high resolution paleoclimatic record for the last 27,500 years in tropical West Africa from the carbon and nitrogen isotopic composition of lacustrine organic matter. *Earth and Planetary Science Letters* 110, 23-37.

Ti, C., Gao, B., Luo, Y., Wang, S., Chang, S. X., and Yan, X. (2018). Dry deposition of N has a major impact on surface water quality in the Taihu Lake region in southeast China. *Atmospheric Environment* 190, 1-9.

Tiwari, M., Singh, A. K., and Sinha, D. K. (2015). 'Chapter 3 – Stable Isotopes: Tools for Understanding Past Climatic Conditions and Their Applications in Chemostratigraphy', in Ramkumar, M. (ed.) *Chemostratigraphy: Concepts, Techniques, and Applications*. Amsterdam: Elsevier, pp. 65-92.

Treble, P., Shelley, J. M. G., and Chappell, J. (2003). Comparison of high resolution sub-annual records of trace elements in a modern (1911-1992) speleothem with instrumental climate data from southwest Australia. *Earth and Planetary Science Letters* 216, 141-153.

U.S. Geological Survey (2016). Mineral commodity summaries 2016. *U.S. Geological Survey* 202, 118-119.

van den Berg, E.M., Rombouts, J. L., Kuenen, J. G., Kleerebezem, R., and van Loosdrecht, M. C. M. (2017). Role of nitrite in the competition between denitrification and DNRA in a chemostat enrichment culture. *AMB Express* 7, 1-7.

Van Meter, K. J., and Basu, N. B. (2015). Catchment legacies and time lags: a parsimonious watershed model to predict the effects of legacy storage on nitrogen export*. PLoS ONE* 10, e0125971.

Van Meter, K. J., Basu, N. B., Veenstra, J. J., and Burras, C. L. (2016). The nitrogen legacy: emerging evidence of nitrogen accumulation in anthropogenic landscapes. *Environmental Research Letters* 11, 035014.

Verheyden, S., Keppens, E., Fairchild, I. J., McDermott, F., and Weis, D. (2000). Mg, Sr and Sr isotope geochemistry of a Belgian Holocene speleothem: implications for paleoclimae reconstructions. *Chemical Geology* 169, 131-144.

Vieten, R., Winter, A., Warken, S. F., Schröder-Ritzrau, A., Miller, T. E., and Scholz, D. (2016). Seasonal temperature variations controlling cave ventilation processes in Cueva Larga, Puerto Rico. *International Journal of Speleology* 45, 259-273.

Waltham, A. (1981). The karstic evolution of the Matienzo depression, Spain. *Zeitschrift fur Geomorphologie* 25, 300-312.

Wang, L., and Burke, S. P. (2017). A catchment-scale method to simulating the impact of historical nitrate loading from agricultural land on the nitrate-concentration trends in the sandstone aquifers in the Eden Valley, UK. *Science of the Total Environment* 579, 133-148.

White, W. B. (2002). Karst hydrology: recent developments and open questions. *Engineering Geology* 65, 85-105.

WHO (World Health Organisation). (2011). *Nitrate and nitrite in drinking-water*. Geneva: WHO Press.

WWAP (United Nations World Water Assessment Programme). (2015). *The United Nations World Water Development Report 2015: Water for a Sustainable World*. Paris: UNESCO.

Wynn, P. M., Fairchild, I. J., Baker, A., Baldini, J. U. L., and McDermott, F. (2008). Isotopic archives of sulphate in speleothems. *Geochimica et Cosmochimica Acta* 72, 2465-2477.

Wynn, P. M., Fairchild, I. J., Spötl, C., Hartland, A., Mattey, D., Fayard, B., and Cotte, M. (2014). Synchrotron X-ray distinction of seasonal hydrological and temperature patterns in speleothem carbonate. *Environmental Chemistry* 11, 28-36.

Zhang, Y., Shi, P., Song, J., and Li, Q. (2019). Application of nitrogen and oxygen isotopes for source and fate identification of nitrate pollution in surface water: a review. *Applied Sciences* 9, 18.